An investigation of the ambient temperature field and thermal response of the Calgary Airport Trail Tunnel

by

Lomere Mori

A thesis submitted in partial fulfillment of the requirements for the degree of

Master of Science

in

Structural Engineering

Department of Civil and Environmental Engineering

University of Alberta

Abstract

Thermal loads must be considered in the design of many types of structures including buildings, dams, bridges, and tunnels. In some cases, thermal loads may have the same order of magnitude as dead and live loads. Determining the thermal load is a complex problem since it depends on several variables such as structural material, geometry of the structure, and the environment the structure is exposed to. The thermal response of the structure, which includes stresses and displacements, is also equally complex. There is currently a lack of design provisions in structural codes and literature that address design temperatures and the location of movement joints in tunnel structures. In this context, the main focus of this thesis is to study the temperature distribution and thermal response in concrete road tunnels due to ambient temperature using a case study. The main body of this thesis is comprised of two parts. The first part involves the study of temperature distributions and the resulting thermal response in the tunnel structure using numerical modelling. The second part involves the analysis of long term temperature and displacement sensor monitoring data collected from the Airport Trail Tunnel in Calgary, Alberta, which is a case study for this thesis. The aim of the study is to evaluate findings from the numerical analysis and sensor data with current structural code provisions that address design temperature and the location of movement joints. From the investigation, it was determined that the design temperature range was within CSA S6, however CSA S6 underestimates the temperature gradient effect in the walls and slabs of the tunnel. Recommendations and future work are addressed to conclude the thesis.

Acknowledgements

First of all, I would like to thank my supervisors, Dr. Gul and Dr. Cheng, for their encouragement, support, and time.

Special thanks to Dr. Ved Sharma from the City of Calgary who drove the initial idea for the basis of this thesis. His support and interest in this research project was instrumental for its completion. I would also like to thank Nathan Murdoch and Dr. Azita Azarnejad from CH2M Hill for their willingness to help me in understanding the technical aspects and general information regarding the Airport Trail Tunnel project.

Thanks to my colleagues in the structural health monitoring group for creating great memories and friendships.

Lastly, my friends and family are a continual source of encouragement and I could not thank them enough.

The temperature and displacement monitoring raw data from the Airport Trail Tunnel was provided by the City of Calgary. Any further analysis and opinions belong to the authors and may not necessarily represent the City's position.

Table of Contents

List of Tables

List of Figures

List of Symbols

∇	Gradient operator
$\propto_{solar}$	Solar radiation absorptivity coefficient
μ	Mean
c	Specific heat capacity
E	Modulus of Elasticity
I_{solar}	Solar radiation at Earth's surface
h	Convection coefficient
k	Thermal conductivity coefficient
q	Heat flux
Q	Internal heat generated
T	Temperature
t	Time
v_{wind}	Wind velocity
α	Linear coefficient of thermal expansion
Δ	Change in value i.e. temperature differential
E	Long wave radiation emissivity coefficient
ρ	Material density
σ	Stefan-Boltzmann constant (in context of long wave radiation)
σ	Standard deviation (in context of statistical distributions)

Chapter 1: Introduction

1.1 Introduction to Temperature Design and Effects in Tunnels

Thermal loads are considered in the design of many types of structures including buildings, dams, bridges, and tunnels. Determining the thermal load is a complex problem since it depends on several variables such as structural material, geometry of the structure, and the environment the structure is in. For instance, steel has a higher thermal conductivity compared to concrete resulting in lower temperature gradients through steel members under transient conditions; concrete members with large thicknesses have the tendency to form high gradients near the surface under transient conditions since the surface is more susceptible to temperature variation; and in bridges one of the major factors that affects temperature distribution is solar radiation. There are also several forms of thermal loads such as heat of hydration during concrete curing, ambient temperature, thermal load based on function (i.e. cooling pipes or heating lamps), and fire (Priestley 1984 and Vecchio 1993). The thermal response of the structure is equally complex since it is highly dependent on the amount of restrain developed due to the temperature distribution caused by the variables mentioned above as well as the type of thermal load the structure is subject to.

Tunnels are buried structures that typically underlie soil and/or water, where only the portals, i.e. entrances and exits, of the tunnel are exposed to an ambient environment, which includes wind, solar radiation, and temperature. Another important design consideration for tunnel design is the fire load which is a major safety concern due to the enclosed environment of the tunnel. In turn, these factors affect the temperature distribution of the tunnel.

The main focus of this thesis is to study the temperature distribution and thermal response in concrete road tunnels due to ambient temperature as knowledge in these areas is lacking in literature and current design codes. Evaluation of current design practices is important to determine if the code is conservative or non-conservative in regards to the design. The study will utilize numerical modelling as well as long term temperature and

displacement sensor data collected from the Airport Trail Tunnel in Calgary, Alberta, Canada.

1.2 Objectives and Scope

The purpose of the thesis is to investigate the design temperatures and gradient effects in road tunnels such that recommendations regarding temperature loads can be made in the future. In Canada, the current method for design temperature in tunnels considers provisions from the CSA S6 Canadian Highway Bridge Design Code (CHBDC). However, these provisions may not necessarily be applicable to tunnels since the thermal environment of bridges differs from tunnels since bridges they are exposed structures. In several design codes investigated, there is a lack of literature and design clauses that address design temperatures in road tunnels.

A heat transfer model and structural model of the Airport Trail Tunnel was used to simulate temperature distribution and structural response, respectively, under long term temperature conditions. The heat transfer model and the structural model were conducted using finite element software ABAQUS.

Sensor data from the Airport Trail Tunnel in Calgary was used to evaluate the surface temperature in the tunnel as well as the temperature in the slab/walls. There were also displacement sensors installed at select movement joints. The Airport Trail Tunnel was equipped with 37 temperature sensors at several locations along the tunnel that provide 3 readings at each location and 4 displacement sensors at two movement joint locations. Data from a select number of sensors were chosen for analysis based on their location and data quality. Data processing and analysis was conducted using MATLAB and Microsoft Excel software.

The analysis results and interpretations of the models and the sensor data from the Airport Trail Tunnel can in turn be used to establish recommendations for design temperature in road tunnels. Applying the results from this study may assist structural designers when considering thermal loads in tunnels.

The main objectives of this thesis are outlined as follows:

- Evaluate the temperature distribution and temperature effects in the Airport Trail Tunnel under long term ambient temperature conditions using heat transfer and structural numerical models
- Study the temperature distribution in Calgary's Airport Trail Tunnel using temperature sensor data collected from September 2014 to January 2016* and study the structural response of the Airport Trail Tunnel using available displacement
- Utilize the data from the tunnel and results from the model to evaluate current design practices regarding thermal load

*Data collection is ongoing from May 2014 and the selected time period for analysis was based on the thesis timeline and data quality.

1.3 Organization of the Thesis

Chapter 2 provides a literature review of current design codes that address design temperature and gradients in tunnel and bridge structures along with a review of the temperature distribution in mass concrete structures and relevant thermal monitoring case studies of tunnels. Lastly, heat transfer studies conducted for various concrete structures are discussed and reviewed.

Chapter 3 describes the methodology of the model and data analysis used in the thesis. This chapter also provides an introduction to the Airport Trail Tunnel project along with structural design and tunnel instrumentation details.

Chapter 4 discusses the heat transfer models and structural models of the tunnel. Modelling was done using Abaqus software. The purpose of these models was to determine the ambient temperature gradient distribution and stress distribution in the tunnel so the results could be compared to the sensor data.

Chapter 5 involves the analysis of the temperature and displacement sensor data for the Airport Trail Tunnel. A set of temperature measurements were also conducted in the

tunnel using an infrared camera. Sensor data was validated with the measurement data and model outputs. In this chapter, a comparison with the model results is also discussed.

Chapter 6 presents a summary and conclusions along with recommendations and future work.

Chapter 2: Literature Review

The literature review covers current design code provisions for temperature load in tunnels, temperature distribution in concrete subject to thermal loads, case studies that involve monitoring of the temperature field in tunnels, and studies that discuss general heat transfer in concrete structures such as frames, slabs, dam and bridge cross sections.

2.1 Current Design Code Provisions for Temperature Load

Currently, there are no direct structural design codes that consider design temperatures and temperature variations (i.e. gradients) in buried structures such as tunnels based on a comprehensive literature investigation however it is typical for designers to apply bridge design code provisions, which was the case for the Airport Trail Tunnel. Several bridge codes such as CSA S6-06, American Association of State Highway and Transportation Officials Load Resistance Factor Design (AASHTO LRFD) Bridge Design Specifications 2012, and Eurocode 1991-1-5 provide design temperature provisions that can be used as an ancillary reference for tunnel structures.

In CSA S6-06 Clause 3.9.4, for type C superstructures (concrete system with concrete deck) the design temperature range shall be 10°C above the maximum mean daily temperature to 5°C below the minimum mean daily temperature. There will be reduction/increase to the maximum and minimum temperature respectively depending on the depth of the superstructure. The reduction in maximum effective temperature increases linearly from 0°C to 7°C corresponding to section depths of 0.4 m to 2 m. A constant reduction of 7°C is applied when the section depth is equal to or greater than 2 m. The increase in minimum effective temperature increases linearly from 0°C to 10°C corresponding to section depths of 0.4 m to 2 m and a constant increase of 10°C is applied when the section depth is equal to or greater than 2 m.

CSA S6 defines thermal gradient effects as temperature differentials through the cross section of a member. This gradient effect induces certain stresses in the member which must be considered for design. For thermal gradient effects, the code states that a positive

temperature differential should be considered for summer conditions and a positive and negative temperature differential should be considered for winter conditions. The magnitude of the temperature differential is dependent on the depth of the superstructure according to Section 3.9.4.5. The gradients are determined considering solar radiation data as well as maximum/minimum daily temperature data. For depths up to 0.4 m, a ±8°C temperature differential shall be considered in the winter and a +15°C temperature differential shall be considered in the summer. For depths between 0.4 m and 1 m, the temperature differential for consideration decreases linearly. Note that a positive differential implies that the surface is warmer. Also note that in type C structures, temperature variations are nonlinearly distributed through its depth. For design purposes, the gradient can be considered linear as a conservative approach. In this thesis, when the term thermal gradient is used, it refers to the temperature differentials through a cross section as opposed to the temperature change per unit length.

The effective temperature range for the Airport Trail Tunnel was determined to be -38°C to 34°C and for gradients a ±5°C temperature differential shall be considered in the winter and a +10°C temperature differential shall be considered in the summer since the depth of the concrete slabs/walls in the tunnel are 1.25 m and 1 m, respectively.

The code also states that the effective construction temperature is 15°C with the absence of site-specific data (Clause 3.9.4.2). Furthermore, for type C, cast-in-place (CIP) structures it is acceptable to assume that the concrete cool by 25°C from its initial set to the effective construction temperature.

Note that there were no revisions to the temperature load clauses from the CSA S6-06 to the recent CSA S6-14 version of the code. The code provisions are based on studies conducted by Bosshart (1970), Radolli and Green (1975), Emerson (1976), Ostapenko (1976), and Emanuel and Hulsey (1978).

According to AASHTO LRFD, the design temperature range is -17.8°C to 26.7°C using Procedure A for Cold Climate and Concrete Structures and a non-linear positive and negative temperature gradient profile is suggested.

According to Eurocode 1991-1-5, the design temperature range is -30°C to 30°C. Note that the design temperature range has a correction for shade temperature and maximum and minimum daily mean temperatures from S6-06 were used to obtain the design temperature since Eurocode does not have climate data for Canada. Two approaches are given to determine the vertical temperature gradient. Approach 1 suggests a linear temperature gradient where a heating (positive) gradient of 15°C and cooling (negative) gradient of 8°C was determined. Approach 2 suggests a nonlinear temperature gradient for both heating and cooling.

The US Department of Transportation Federal Highway Administration (FHWA) Technical Manual for Design and Construction of Road Tunnels provide direct guidelines for temperature and joint design however the basis for the temperature load guidelines is AASHTO LRFD. Further design guidelines for cut and cover tunnels are as follows.

Expansion joints may not be required except close to the portals however contraction joints are recommended throughout the tunnel. Expansion joints are usually provided at the interface with ventilation buildings or portals or other rigid structures to allow for differential settlements and movements associated with temperature changes. Contraction joints are recommended to be placed at intervals of approximately 9 m. It is common for cut and cover tunnels to be constructed without any permanent expansion or contraction joints. It is known that significant changes in support stiffness or surcharge can cause differential settlement so relieving joints can be used to accommodate localized problems.

Note that joints are sources of high maintenance costs over the life of the tunnel since they are potential areas where leaks can occur. Thus, the number of joints should be minimized and special care should be taken in the detailing of joints to ensure water tightness. The type and frequency of joints required should be a function of the structural system required and should be evaluated in the overall decision based on the type selected according to Section 5.4.5 FHWA-NHI-10-034.

According to AASHTO LRFD specifications, loads to be considered in the design of cut and cover tunnel structures are divided into permanent loads and transient loads.

Permanent loads include dead load, horizontal earth pressure load, earth surcharge load, and vertical pressure from the dead load of the earth fill. Transient loads include creep, vehicular collision force, earthquake, vehicle dynamic load allowance, vehicular live load, shrinkage, water load, temperature gradient, and uniform temperature.

In regards to thermal load, cut and cover structural elements are typically constructed of thick concrete which may result in large thermal lag through the slab. Combined with being surrounded by an insulating soil backfill that maintains a relatively constant temperature, the temperature gradient across the thickness of the members can be significant (Section 5.5.1 FHWA-NHI-10-034). Thus, the thermal load should be examined on a case by case basis depending on the local climate and seasonal variations in average temperatures. In AASHTO LRFD, Paragraph 4.6.6 provides guidance on calculating this load as briefly described above. Note that the paragraph C3.12.3 allows the use of engineering judgement to determine if this load needs be considered in the design of the structure.

The uniform temperature load is primarily used to size expansion joints in the structure for movement in the longitudinal direction. If movement is permitted at the expansion joints, no additional loading is required to be applied to the structure. The effects of the friction force resulting from thermal movement is typically neglected in the design since the structure is rigid in the primary direction of thermal movement. Additional force effects caused by expansion and contraction at connections is typically not considered in the case of a cast-in-place concrete box structure due to the insulating qualities of the surrounding ground and the large thermal lag of the concrete. (Section 5.5.1 FHWA-NHI-10-034)

2.2 Temperature Distribution in Mass Concrete

Mass Concrete is defined as any volume of concrete with dimensions large enough to require that measures be taken to cope with the generation of heat from hydration of cement and attendant volume change to minimize cracking (American Concrete Institute 207.1R-96). The minimum dimension (thickness) of a member to be defined as mass concrete is approximately 3 feet (0.914 m).

Temperature distributions in a mass concrete structure differ from distributions in a bridge structure as described in bridge codes due to the type of section. Since tunnel sections have the potential to be thick, mass concrete behavior must be considered. For instance, in the Airport Trail Tunnel, the wall thickness is 1 m and the slab thickness is 1.25 m thus the structure meets the minimum requirements of a mass concrete structure.

Although the early rise in temperature during hydration is a concern for mass concrete (thermal effects), the main focus for this thesis is temperature variations in mass concrete after the initial heat of hydration period. It can be noted that for the Airport Trail Tunnel, several measures were implemented to reduce the rise in temperature caused by heat of hydration, which included adding ice to the concrete mix as well as injecting liquid nitrogen on site (Azarnejad et al., 2013). The temperature sensors did not measure the increases in temperature caused by the heat of hydration due to the time the sensors started to collect data as well as issues with the initial quality of the data.

In mass concrete structures that are deep, only the upper and lower surfaces of the superstructure are affected by rapid changes in climatic conditions. The central portion of deep concrete structures are mainly influenced by long-term variations in mean daily temperatures but not by diurnal (daily) heating cycles. This permits reductions to the effective temperature range with increasing depth. Also, due to the low thermal conductivity of concrete, large gradients may form in deep concrete superstructures. In shallow sections less than 0.3 m deep, the critical temperature gradients considered for design are nearly linear while in deeper sections gradients are non-linear. These nonlinear temperature differentials arise during transient condition where the boundary conditions i.e. ambient temperature is changing over time. Note that ‘rapid’ and ‘long-term’ changes and ‘large’ gradients are not well defined. (CSA S6)

2.3 Thermal Monitoring Case Studies in Tunnels

Lai (2012) studied the temperature distribution of tunnels in cold regions through temperature measurements of the Qing Shashan highway tunnel. In the study, the Qing Shashan tunnel is described as an extra-long tunnel however no exact length is given. Hygrometers were placed 50 m outside the tunnel as well as inside the tunnel 500 m from

the portal and at the middle. It could be observed that longitudinal variations in temperatures were dependent on the month. The range of temperature difference between the entrance/exit and middle of the tunnel was between 1°C to 11°C. Some factors that affect the temperature in the Qing Shashan tunnel include solar radiation exposure at the portals, tunnel wind speed, ventilation system, tunnel geometry (length and cross sectional area), and changes in tunnel altitude at the portals, soil cover, freeze thaw cycles, and tunnel traffic.

Junfeng et al. (2014) studied the temperature field distribution in the Houanshan tunnel. The purpose of this study was to analyze the temperature distribution of surrounding rock, the longitudinal temperature distribution, and the insulation effect of the liner. The Houanshan tunnel is 6551 m in length with headroom of 92 m^2 and a double lining. The annual average temperature at the tunnel location is 5.9°C, the maximum temperature is 37.7°C and the minimum temperature is -42.5°C. In order to monitor the longitudinal temperature distribution, 18 hanging temperature hygrometers were set in the wall at the exit portal and at distances of 25 m, 50 m, 100 m, 200 m, 500 m, 1000 m, 2000 m, and 3000 m from the entrance portal.

A few key results of the study are as follows: (1) the temperature distribution in the tunnel with time changed synchronously with the outside temperature, (2) the influence of temperature to the surrounding rock weakens in the radial direction but was dependent on the boundary conditions i.e. soil type and soil cover, (3) the temperature distribution was gradually uniform from the tunnel portal to a certain distance, and (4) the temperature field displays a parabolic distribution through time in the longitudinal direction, which is most likely dependent on factors such as tunnel length.

It could be observed that the temperature pattern was periodic. The most significant changes in temperature occur at 50 m from the portals. At distances greater than 50 m, the temperatures were nearly constant. In winter, it was evident that the portal was colder than the inside of the tunnel by up to 8 °C in January and in the summer, the portal was warmer than the inside of the tunnel by up to 12°C in July. Note that there was no information on additional factors such as car exhaust, ventilation fans, etc. that may affect

the temperature in the tunnel. Furthermore, since insulation was provided in the tunnel liner, the temperature gradient results through the cross section were influenced. It was observed in the study that the insulation board used had a maximum temperature difference of 9.21 °C thus providing a good insulation effect.

Li et al. (2015) studied the tunnel lining surface temperature of the Hongfu tunnel. In this study, an automatic recorder was invented to adapt to low temperature environments and used to record the surface temperature at the lining every hour for approximately two years. The data obtained was used to determine patterns in annual temperature changes and air flow inside the tunnel. Hongfu tunnel is a two portal, two-way road tunnel that is 2250 m long and 10.75 m wide per portal.

It could be observed that the effect of daily temperature cycles was pronounced at the entrance compared to 1500 m into the tunnel as expected. Temperatures at different sections up to 350 m into the tunnel changed in the same rhythm. The temperature at 50 m and 100 m into the tunnel were near identical and the fluctuations in temperature tend to decrease at points further into the tunnel. The lining surface temperatures were compared a year later in December 2012 where the temperature was much colder than December 2011. It was observed that the temperatures at 50 m and 300 m into the tunnel were now near identical. The temperature difference at the 1000 m point compared to the 50 m point was highest at lower temperatures but was near zero at temperatures around -5 °C.

Overall, in each study the temperature distribution in the tunnel was dependent on several factors mentioned above. The combined effect and magnitude of these factors in each particular case also affect temperature distribution.

2.4 Heat Transfer Studies for Concrete Structures

Theoretical principles, modelling techniques, analysis results, and conclusions from the following studies were considered in this thesis. Several studies have investigated the temperature gradient effects in various bridge type structures that are applicable to this

thesis in principle. Studies that involved temperature distribution and structural response in concrete slab and frame systems and dam structures are also discussed.

Larsson and Svensson (2013) investigated thermal effects in a portal frame concrete bridge using real climate data and finite element analysis (FEA) modelling. Results were then compared to design temperature gradients in the Eurocode. A study was also done to determine the thermal response when concrete cracks form. It was determined that temperature effects are complicated loads thus it is unclear how to model these effects correctly and how they affect the structure during different events. It is also difficult to predict the size of the load in a cracked section. The resulting load effects are highly dependent on the thermal properties used such as the expansion coefficient as well as the boundary conditions in the model. In order to obtain a better representation of the temperature distribution and stresses in the real structure, simulating temperature using a full 3D model and modelling concrete with crack behavior instead of as an isotropic material should be considered.

Ding and Wang (2013) studied temperature differences in flat steel box girders of a cable-stayed bridge. Statistical analysis was used to characterize temperature differences. A probability distribution function (PDF) using the sum of two Weibull distributions was considered and extreme value analysis (EVA) technique was also applied to estimate extreme temperature differences. It was determined that these statistical methods considered fit the measurement data well.

Tong et al. (2001) investigated temperature changes under the combined influence of solar radiation, daily air temperature variations, and wind speed for steel bridges. A series of sensitivity analyses were conducted to show the response of the temperature distribution to the variation in parameters such as film coefficients, absorptivity, and emissivity. It was determined that the top surface film coefficient and absorptivity have the most significant effect on temperature distribution.

Roberts-Wollman (2002) investigated temperature measurement data through a segmental concrete box girder bridge and compared the output with various editions of the AASHTO design codes to determine if provisions regarding temperature load were

conservative or non-conservative. It was determined that a typical positive gradient curve and negative gradient for the structure considered can be represented with a fifth-order parabola, which is the main applicable conclusion of this paper.

Elbadry and Ghali (1983) incorporated a parametric study to find the effects of various parameters on self-equilibrating (Eigen) and continuity stresses on concrete bridge structures. The parameters included geometry, location (latitude and longitude), orientation, material, thermal properties, and climatology conditions. It was mentioned that many bridge designers recognize that the temperature variations can produce high stresses however little guidance is given in bridge design codes on how these stresses can be accurately calculated (Elbadry and Ghali, 1983). Temperature distribution through the member cross section must be evaluated in order to calculate the stresses, reactions at the supports, and member deformations. However, the temperature distribution is difficult to determine since temperature varies with time and longitudinally from section to section. A finite element analysis method was used to determine the time-dependent temperature variation within the cross section of a concrete bridge of arbitrary geometry and orientation for a given geographic location and environmental conditions. The analysis was conducted in 2D because it was assumed that temperature was constant in the bridge over a long length if the cross-sectional properties were constant. Thus, the analysis was essentially a 2D transient heat flow problem through the bridge cross-section. To accurately model the boundary conditions of the problem, the amount of solar radiation and surface convection and irradiation from or to the atmosphere was considered, where solar radiation is dependent on the angle of the sun and convection is dependent on air and surface temperatures. Two applicable conclusions are as follows: (1) the temperature distribution through a cross section is non-planar in nature and will cause longitudinal stresses and (2) variable conditions were considered and it was determined that critical temperature conditions occur when the daily ambient temperature range is large and wind speed is minimum.

Priestley (1978) studied the design of pre stressed and reinforced concrete bridges for temperature gradients under ambient thermal loading. The paper discusses methods for

predicting design temperature gradients from local meteorological conditions and a general analytical method for predicting the vertical distribution of thermally induced stress was developed. For normal reinforced concrete bridges, it is expected that substantial cracking will have occurred under dead load plus live load, prior to thermal loading. Thus, when an isotropic homogeneous medium is considered this approach has limitations when assessing design significance. It was also determined that ambient thermal fluctuations can induce stress levels of substantial magnitude in continuous concrete bridge superstructures. Due to the deformation nature of the loading, thermal effects are generally insignificant when assessing the ultimate load characteristics of a concrete bridge and need only be considered during serviceability checks.

Léger et al. (1993) studied seasonal temperature and stress distributions in concrete gravity dams. It was determined that seasonal thermal stresses contribute significantly to the long-term degradation of strength and stiffness of concrete dams located in northern regions. The study consisted of two parts which were modelling and behavior. A novel methodology was created to identify the critical temperature states and to compute the related stresses for dam structures which is applicable to this thesis. The modelling portion of the study involved an extensive parametric analysis was conducted to determine the relative influence on the thermal stress-strain response due to (i) geometrical, thermal, and mechanical properties of the dam, (ii) reservoir, foundation, and air temperature distributions, and (iii) heat supply from solar radiation (Léger et al., 1993).

The following studies have been dedicated to the general behavior of other reinforced concrete subject to thermal loads, such as frames and slabs. The studies that follow also mention details regarding temperature sensor placement in mass concrete members and modelling techniques in ABAQUS.

Vecchio et al. (1993) mentioned that reinforced concrete structures are exposed to thermal loads as a result of the design function of the structure, ambient conditions, heat of hydration, and/or exposure to fire. Thermal loads are known to give rise to stress levels, distortion, and damage as a result of nonlinear temperature and strain profiles and

restrained structural deformation which causes primary and secondary or continuity thermal stresses, respectively. In this study, eight large-scale reinforced concrete slab specimens were tested under combined thermal and mechanical load conditions. Temperature gradients of 40°C were applied which is considered low under service conditions. It was determined that when the specimens were restrained against free thermal deformation, significant internal forces developed causing increased stressing and cracking. It was also determined that thermal creep effects cause a significant decay in force. Furthermore, in order to consider the nonlinear behavior of the member accurate modelling of the load-deformation responses, stresses, and failure modes was required in the finite element model. The main factor which resulted in the accuracy was the inclusion of concrete post-cracking tensile stresses so that post-cracking restraint forces would not be underestimated

Vecchio and Sato (1990) studied three large-scale reinforced concrete frame structures that were tested and subject to a combination of thermal and mechanical loads. It was determined that thermal loads can cause significant stressing of a structure which can lead to concentrated damage in local regions. When evaluating the gradient in a member an effective thermal gradient should be used since this is primarily based on changes in near-surface temperatures, with not so much emphasis given to internal steady-state conditions because it takes a while for a linear gradient to develop. It is important to note that the restraint forces developed at a particular section or member are significantly influenced by conditions throughout the structure such as reinforcement details and coexisting mechanical loads. For example, more damage may be expected in weaker sections. Thus, a proper analysis must consider tension-stiffening effects and force redistributions (Vecchio and Sato, 1990).

Prasanna and Subhashini (2010) investigated the thermal strain variation from a rise in temperature in a mass concrete section to determine if the section was going to crack by comparing tensile strain capacity values. In the surface gradient analysis, it was determined that the strain in the concrete was dependent on the coefficient of thermal expansion, temperature difference through the member, and the internal restraint factor.

This study suggests that the temperature distribution can induce tension near the surface and compression within the interior of the concrete and the tensile and compressive stresses/strains induced by a temperature gradient must be balanced for sectional stability.

Priestley (1984) suggests that thermal stresses may be induced in concrete structures as a result of the actions of one or more of three basic categories of heat source: ambient thermal loading, heat of hydration, and function thermal load. Complete thermal analysis of concrete structures is extremely complex since stresses induced by temperature changes are influenced by creep and effective age of the concrete. These effects as well as the mechanical material properties are also dependent on temperature and time history which adds to the complexity. The paper discusses the location of temperature sensors in a slab to provide adequate definition of the temperature gradients. Since temperature changes rapidly over the first 250 mm of concrete adjacent to the surface, temperature sensors at 50 – 100 mm intervals of depth from the surface are recommended to define the gradient with reasonable accuracy and within the body of concrete, sensors can be more sparsely distributed (Priestley, 1984).

Saetta et al. (1995) states that thermal effects have frequently been related to the damage to concrete bridges and dams. Thus, it is important to predict stress levels due to time-variable and space-variable thermal loads which is the focus of this paper. The study suggests a simplified uncoupled problem where the thermal transient problem is first solved followed by the mechanical problem using the constitutive laws of the material. The transient heat transfer is a dynamic problem since it requires the integration along the time dimension and the stress-strain analysis is a static problem. This is a potential simplified method that can be utilized to solve the stress distribution in the member from the temperature distribution output.

Thurston et al. (1980) discussed the thermal analysis of thick concrete sections subjected to heat-of-hydration release and surface heat transfer. An analysis technique was developed that considered transient heat-flow analysis, thermal stress analysis, and the interactive effects of creep and shrinkage. It was mentioned that since a complete thermal analysis of concrete structures under hydration effects and ambient fluctuations is

extremely complex the heat transfer problem is typically simplified into a one or two dimensional problem that will suffice in most cases.

El-Metwally et al. (2015) studied reinforced concrete flab slab systems with lengths much greater than code limits to examine the effect of temperature variation if expansion joints are neglected. ABAQUS software was used to model the slab. Material nonlinearities were considered in the model which includes the effect of cracks. It was determined that cracking contributes to the release of a significant portion of temperature restrain and this restrain could be eliminated due to the presence of cracks (El-Metwally et al., 2015). It was also determined that the response of the system was dependent on the temperature profile and the presence of gravity loads. Variables that affect the amount of thermally induced movement include the percentage of reinforcement which affects the amount of cracks, restrain at the foundation which affects movement at the foundation level, and geometry of the structure which may influence location of stress concentrations. In regards to modelling in ABAQUS, to increase the accuracy of the thermal response important factors to consider include proper mesh size, material behavior i.e. nonlinearity, combined load effects which will affect the stress in the member, and a realistic temperature profile through the cross section.

Chapter 3: Methodology and Airport Trail Tunnel Project Details

3.1 Methodology

In order to investigate the temperature field and thermal response of the Airport Trail Tunnel, numerical modelling was conducted using ABAQUS software. Temperature field refers to the temperature distribution through the tunnel's cross section as well as in the longitudinal tunnel direction. Thermal response refers to the stresses and displacements associated with the temperature field. The numerical model will mainly focus on the temperature distribution through a cross section of the tunnel such that the temperature gradient can be determined. Heat transfer theory was utilized in order to determine the heat flow through the cross section. An outline of the generalized methodology used in this thesis is illustrated in Figure 3.1. The methodology was adopted and modified from Léger et al. (1993).

In order to determine the temperature distribution, a detailed heat transfer model was conducted where a transient (time dependent) analysis was considered. Inputs into this model can include environmental conditions such as ambient temperature, foundation temperature, wind speed, and solar radiation in time history form (if data is available). In order to simulate realistic ambient temperature conditions for the site, Environment Canada data from the Calgary International Airport (CIA) station (CALGARY INTL A) was used. The location of the CALGARY INTL A station is 51°07'21.000" N, 114°00'48.000" W, and 1,099.10 m. Data was available dating back to 2006 and is presented in Figure 3.2. The data is periodic in nature as expected, however it is evident that some years' experience varying amounts of cold/hot day periods than others. The annual temperature ranges were investigated and are illustrated in Figure 3.3.

Long-term temperature data was considered in the model such that results could be analyzed and compared to the sensor data collected in the same time period. Another important input into the heat transfer model are the thermal material properties such as

density, thermal conductivity, specific heat, emissivity coefficient, absorptivity, and convection coefficient. In the thesis, a literature search was conducted to determine the range of each property and a parametric study was conducted to determine the effect of each property on the thermal response such that baseline properties could be determined for input into the heat transfer model. The main result from the model would be the temperature distributions through the cross section as a time history. In turn, the temperature distributions could be analyzed to study the temperature gradients and envelopes.

The second model was the structural model where a coupled temperature-displacement model analysis was considered. The mechanical loads, material properties, and boundary conditions were inputted along with the thermal properties from the previous model. The output of the structural model was a time history of the thermal stress distributions under temperature load only and combined loading. The results were used to evaluate the thermal load.

A comprehensive temperature monitoring system consisting of temperature and displacement sensors was installed in the Calgary Airport Trail Tunnel. Data analysis was conducted in order to determine the temperature distribution through the tunnel cross section and longitudinally through the tunnel. Displacement sensor data from select expansion joint locations were also available for analysis. Furthermore, sets of field temperature measurements were conducted to validate the sensor data.

As mentioned before, the main objective of this study is to compare findings from the modelling and the sensor data with provisions from CSA 06 regarding temperature loads. Applying bridge codes to tunnels may underestimate the temperature gradient through a cross section and conservatively estimate the ambient temperature of the tunnel mainly due to the fact the tunnels are predominantly unexposed to the ambient environment and may have thick cross sections.

Details of the numerical models are presented in Chapter 4 and Chapter 5; and, details regarding the sensor data analysis are presented in Chapter 6.

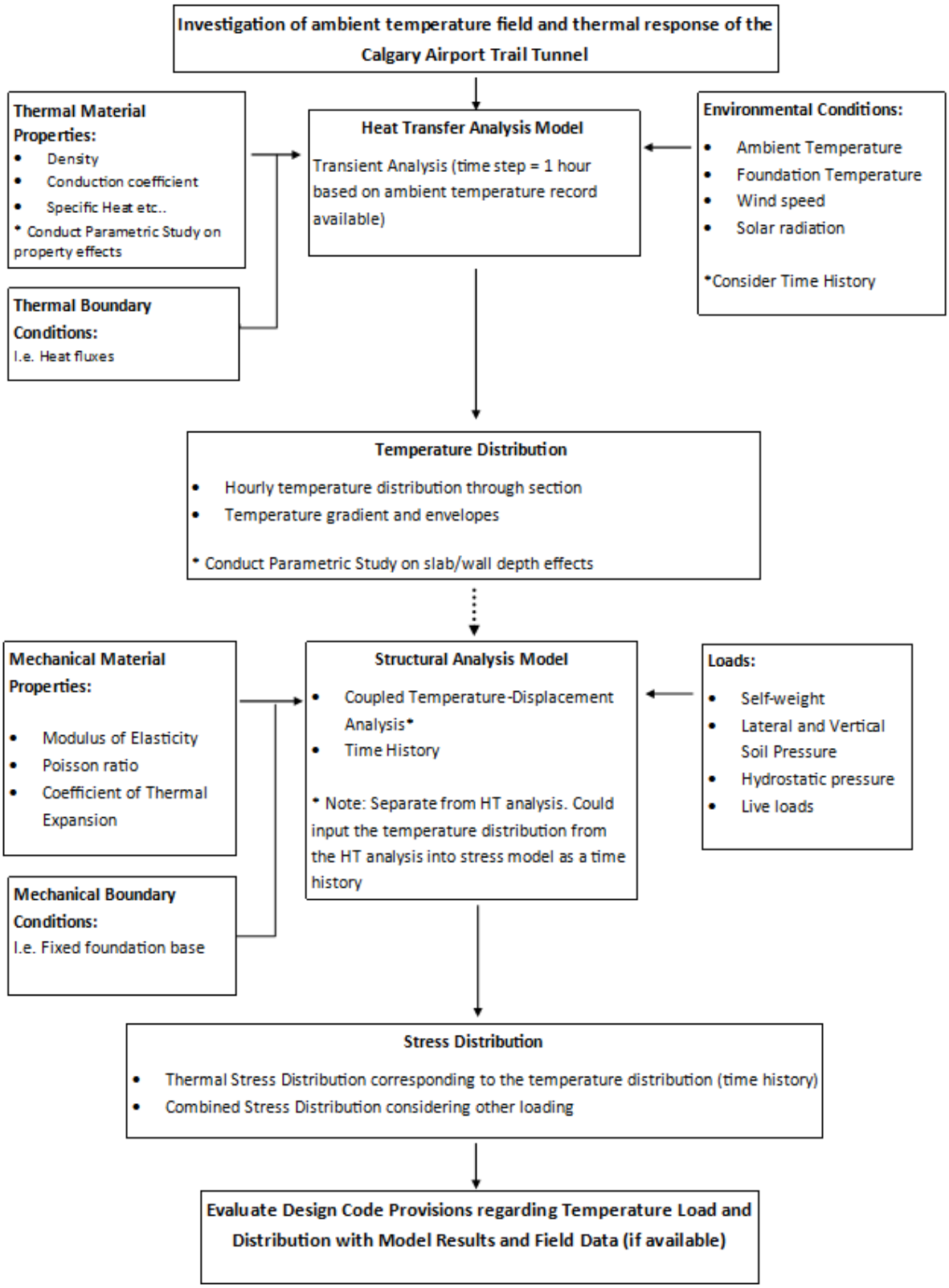

Figure 3.1. Methodology used to evaluate design code provisions

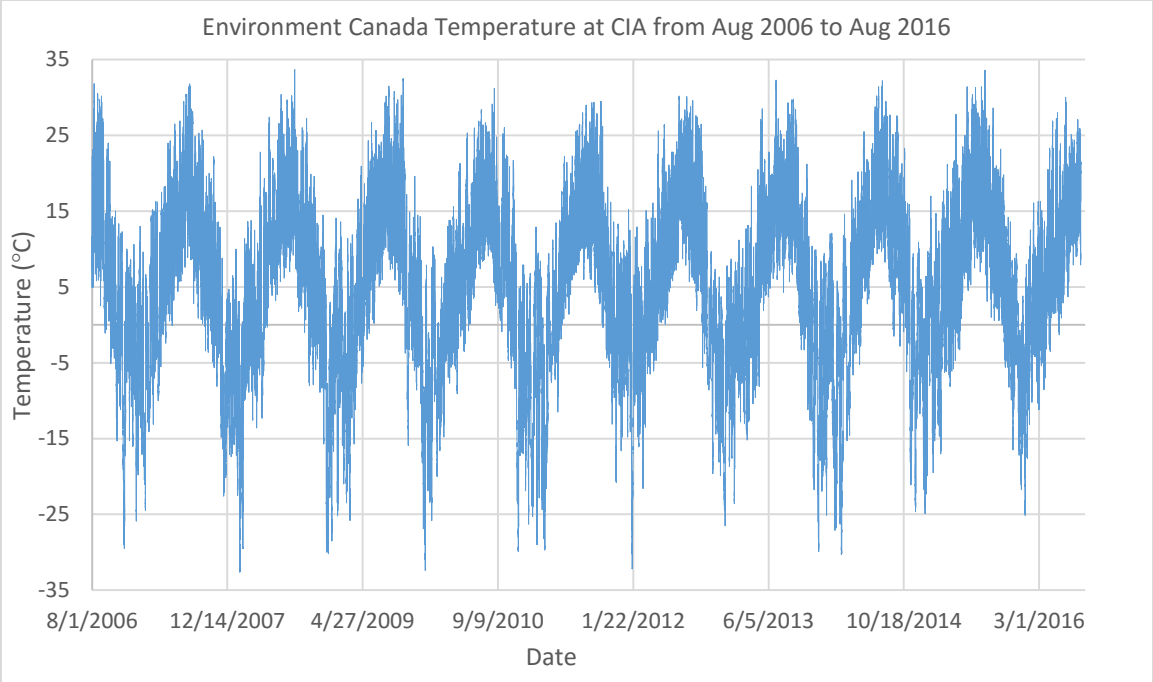

Figure 3.2. Environment Canada Temperature at CIA from Aug 2006 to August 2016

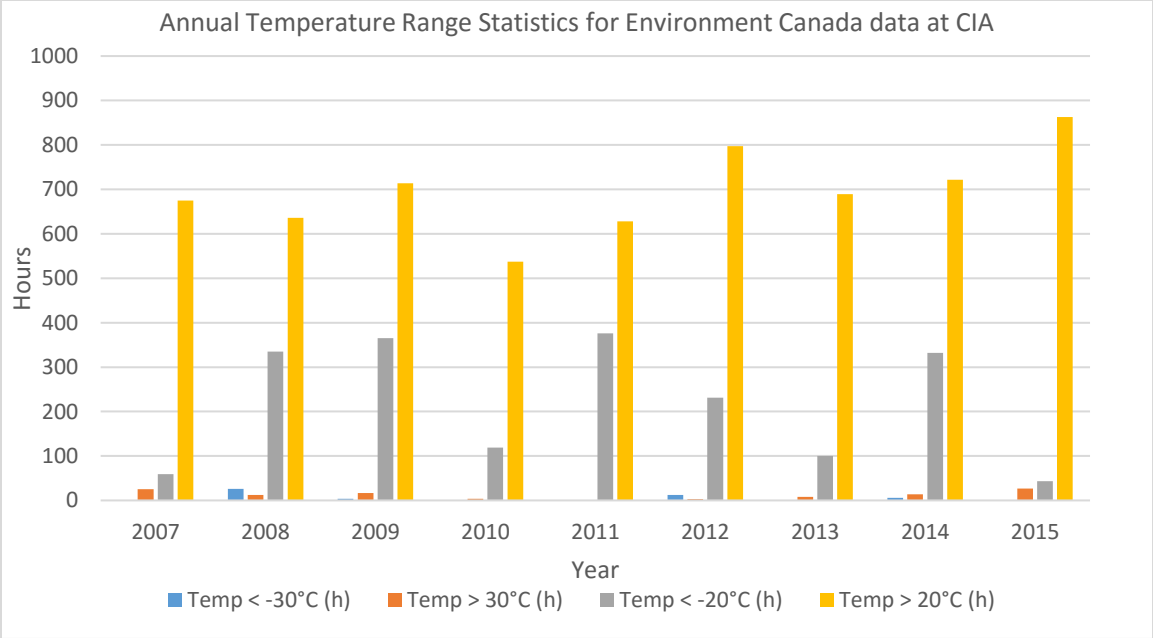

Figure 3.3. Annual Temperature Range Statistics for Environment Canada data at CIA

3.2 Introduction to Calgary Airport Trail Tunnel

The Airport Trail Tunnel is a cast-in-place concrete road tunnel located in Calgary, Alberta, Canada (see Figure 3.4). It extends Airport Trail road from Barlow Trail to 36 Street N.E. The Airport Trail Tunnel is the first vehicular tunnel and forms an integral part of the multimodal transportation network in the City's rapidly growing northeast quadrant (CH2M, 2015). The tunnel is comprised of a six-lane roadway which has been operable since May 2014. A portion of the tunnel also lies below a newly constructed airplane runway. During construction, a comprehensive temperature monitoring system consisting of temperature and displacement sensors was implemented.

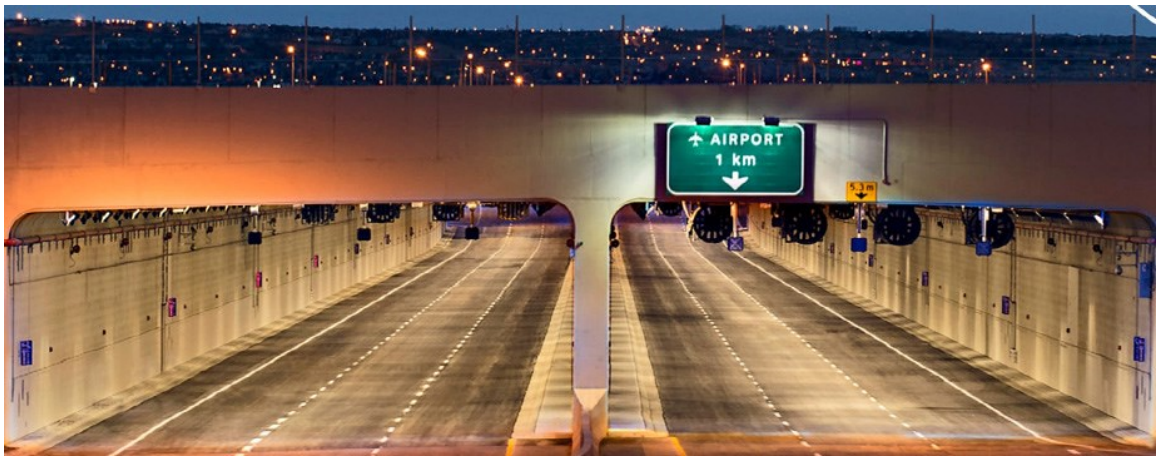

Figure 3.4 Calgary Airport Trail Tunnel looking East (Associate Engineering, 2016)

3.3 Tunnel Design Details

3.3.1 Tunnel Geometry

The road tunnel consists of two portals and is approximately 620 m in length. Each portal has a 16.28 m horizontal width and 7.00m vertical clearance. The exterior and interior walls of the tunnel are 1.00 m thick and the ceiling slab is 1.25 m thick. The exterior walls of the tunnel sit on a 4.30 m by 1.00 m strip footing and the middle wall sits on a 5.50 m by 1.50 m strip footing. See Figure 3.5 for the typical cross section of the tunnel.

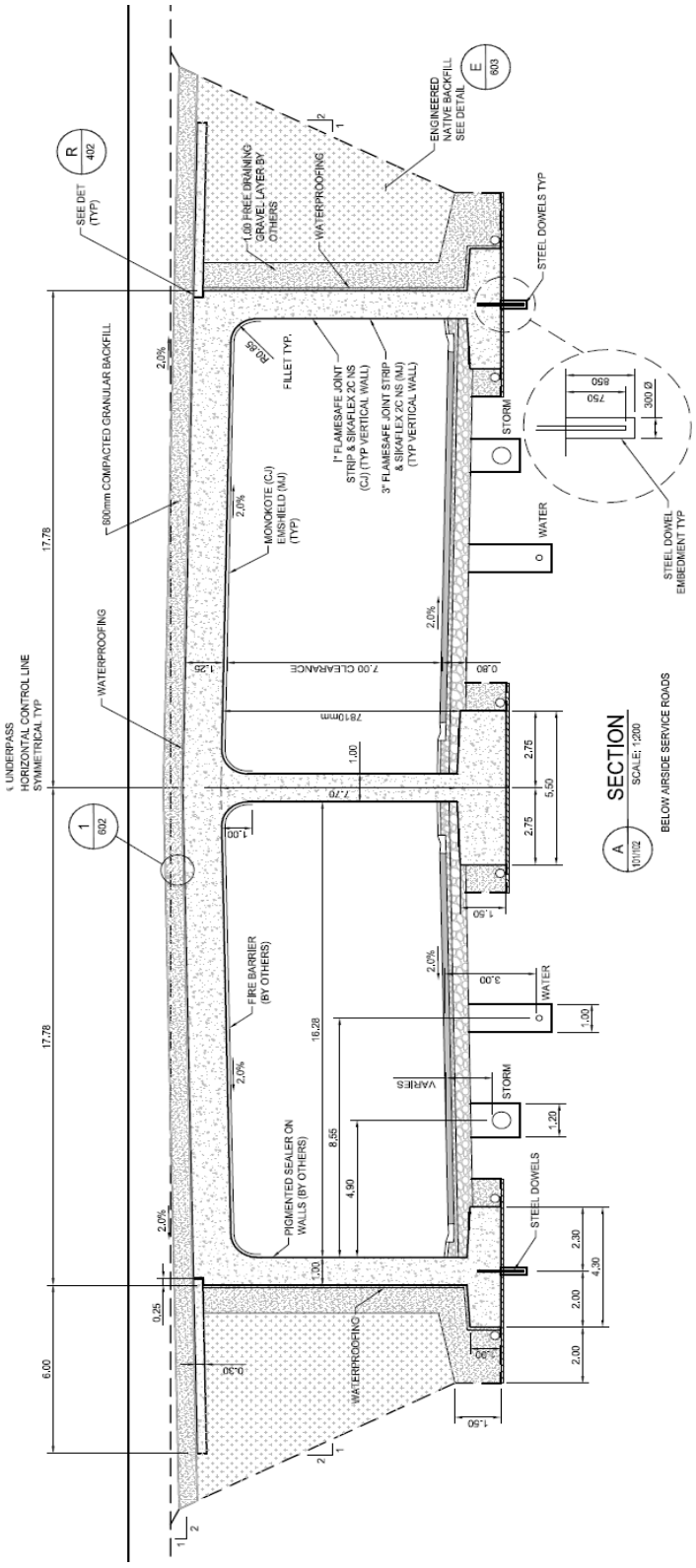

Figure 3.5. Typical cross section of the tunnel (City of Calgary construction drawings)

3.3.2 Construction Method and Details

The tunnel was constructed using cast-in-place concrete and was cast from the center outwards. The tunnel was cast in 48 sections of 12.5 m length with a 9.0 m West portal section and 11.0 m East portal section. The portal sections are incorporated into a retaining wall system at the West and East tunnel face. Movement joints exist between the portal section and retaining wall. The portal wall thickness is approximately 1.0 m. Since movement joints exist between the portal section and wall, the retain wall was assumed to allow sufficient movement such that there would be no additional restrain on the tunnel due to the retaining wall.

For each section, either a Lead or Infill form was used to cast the concrete. Lead sections were cast first followed by Infill sections in-between Lead sections. The construction joint detail between sections consists of longitudinal bars that would extend out of the Lead section and connect to the Infill section. The movement joints consisted of two steel sleeves connected to glass fiber reinforced polymer (GFRP) bars. Movement joints are located at intervals of 37.5 or 50 m otherwise a construction joint is present between sections. Typical construction joint and movement joint details are shown in Figure 3.6. Based on the construction drawing details, the construction joints are assumed to be continuous to allow for complete load transfer and the movement joints are assumed to be partially continuous to allow for partial load transfer and movement.

The tunnel was designed to be free-draining thus a gravel layer was placed adjacent to the exterior tunnel walls and ceiling slab followed by engineered native backfill material.

To protect the concrete structure, waterproofing material was placed on the tunnel exterior. For the interior face of the walls, Class 1 finish with Sika Guard 550 elastomeric coating was applied. For the interior face of the roof slab and top meter of the interior wall, a fire barrier system was installed.

The concrete strength at 28 days, f_c', for the roof slab and walls in portals and first section in from the portals was 45 MPa high performance concrete (HPC) and for the roof slabs and wall in other locations 35 MPA Type B concrete was used. The

compressive stress of concrete is noted here since it affects the tensile capacity of the concrete.

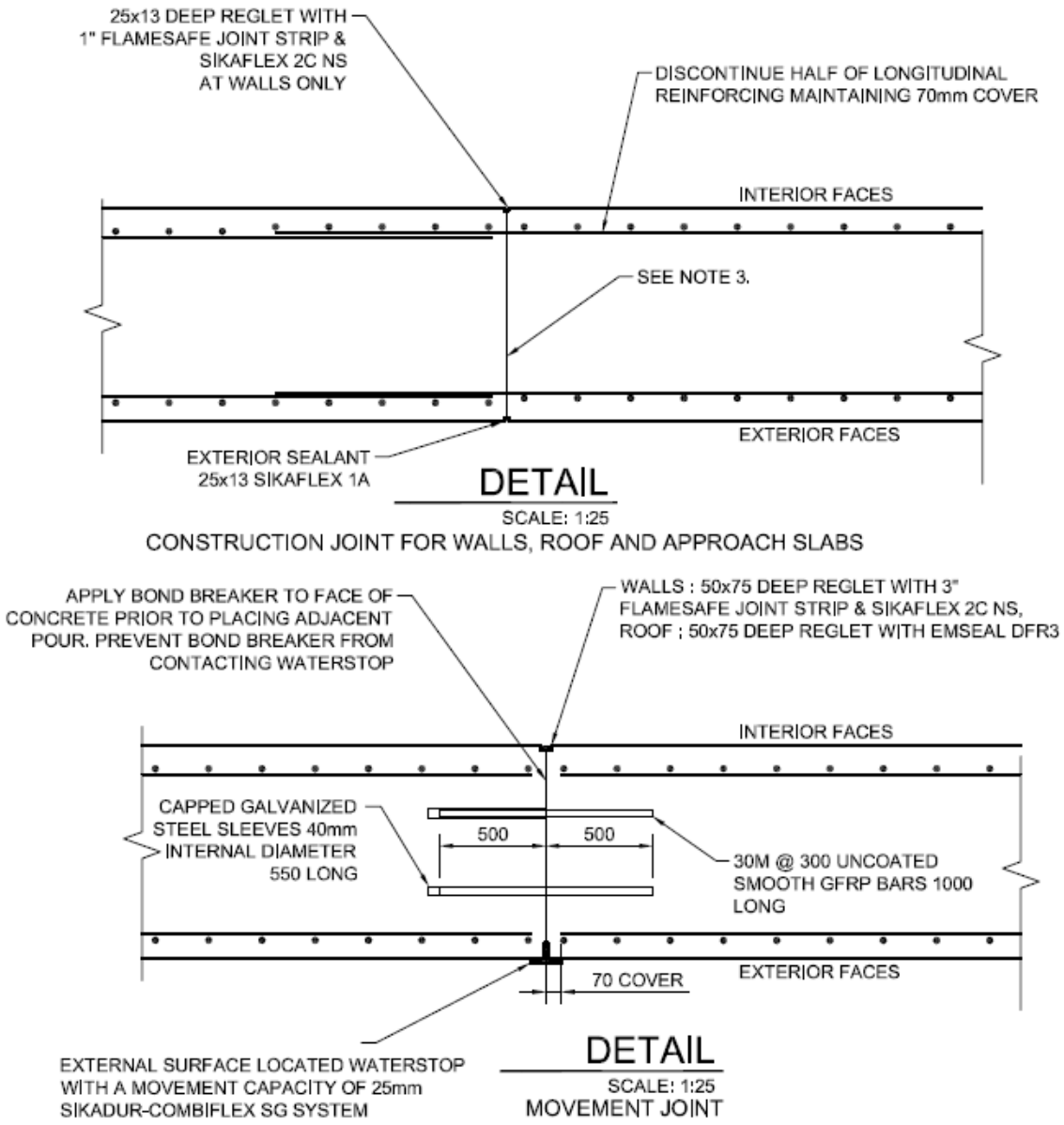

Figure 3.6. Typical construction joint and movement joint details (City of Calgary construction drawings)

3.4 Tunnel Instrumentation

Temperature sensors were installed at 37 locations along the tunnel (see Figure 3.7). At each location, there are 3 readings: an internal surface temperature sensor and two temperature probes that extended to the mid-slab/mid-wall and to the exterior rebar. In Figure 3.7, "L" and "I" refer to the Lead and Infill section, respectively. Furthermore, Section A, B, and C refer to the location of roads, taxiways, and the airplane runway above the tunnel, respectively. The sensor that extends to the exterior rebar is referred to as the dirt sensor in the raw data for the exterior walls/slabs and interior wall (see Figure 3.8 and Figure 3.9).

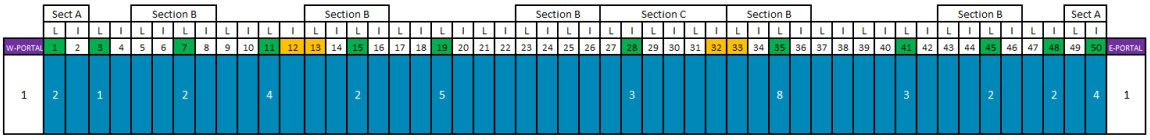

Figure 3.7. Location of temperature sensors along the tunnel (adopted from CH2M)

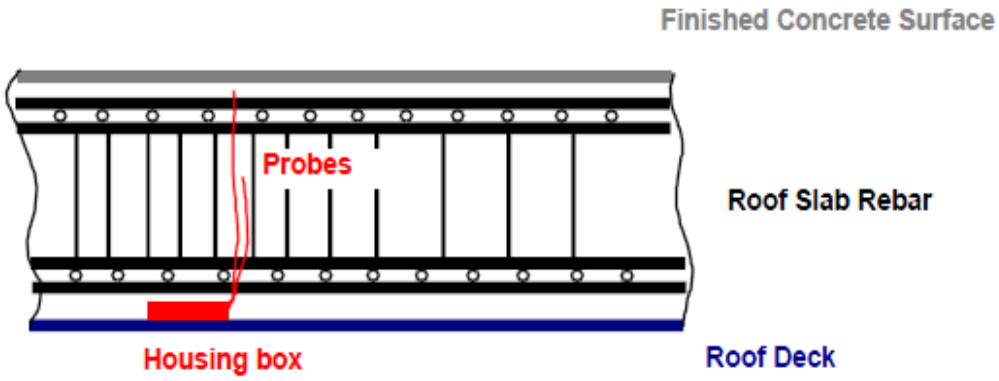

Figure 3.8. Typical temperature sensor installation for ceiling slab (adopted from CH2M)

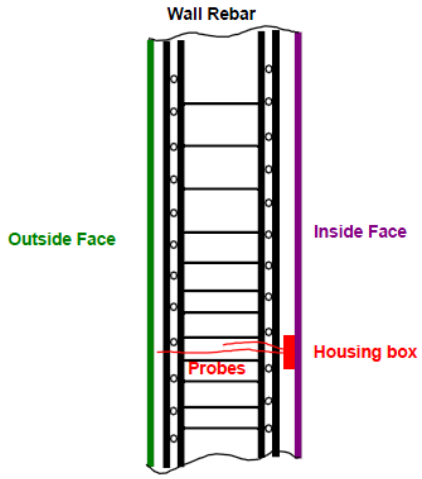

Figure 3.9. Typical temperature sensor installation for wall (adopted from CH2M)

Displacement sensors were installed at the two movement joint locations which are between Sections 12-13 and Sections 32-33 (see Figure 3.7). At each location there is one triaxial displacement sensor and one uniaxial displacement sensor which measures displacement in the longitudinal direction. Note that each displacement sensor also has an internal temperature sensor.

Sensor Type

Resensys wireless SenSpot™ Humidity/Temperature sensors and SenSpot™ Displacement Meter sensors were installed in the tunnel. The sensors used in the tunnel are similar to the ones shown in Figure 3.10 and Figure 3.11 below. Both sensors contain a TI CC2530 microcontroller which has an internal temperature sensor with a resolution of 0.5°C an ambient operating temperature of -40 °C to 125°C. The temperature probes have a resolution of 1°C and a working temperature of -40 °C to 65°C. The displacement sensors have a resolution of 0.1 mm.

The temperature probes utilize the Microchip TC1047 which is a linear voltage output temperature sensor whose output voltage is directly proportional to the measured temperature (Microchip). The displacement sensors utilize the Honeywell HMC1501 magnetic displacement sensor. The sensor controls a single saturated-mode Wheatstone bridge sense element that creates an output voltage with respect to the direction of the magnetic flux passing over the sensor surface (Honeywell).

Figure 3.10. SenSpot™ Humidity/Temperature sensor

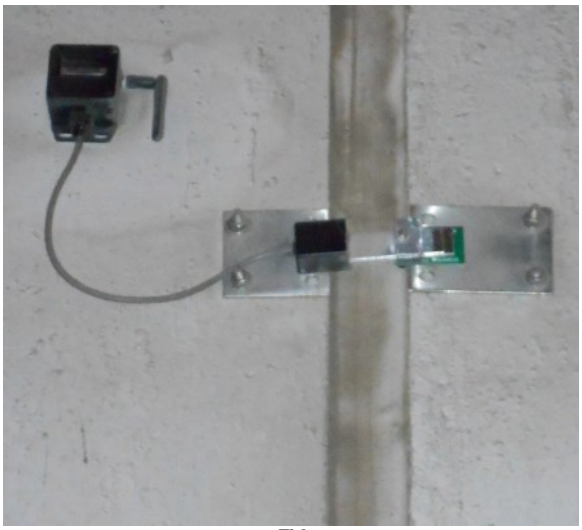

Figure 3.11. SenSpot™ Displacement Meter sensor

Data Collector

Resensys SeniMax™ is an ultra-low power and high performance data collector with a remote communication gateway (see Figure 3.12). Two SeniMax™ were installed in the tunnel to collect the sensor data. In the north tunnel, the SeniMax™ is located at the West Portal's north wall and in the south tunnel it is located at the East Portal's middle wall. Repeaters were installed approximately mid-way in each tunnel to strength the wireless signal from the sensors to each SeniMax™.

Figure 3.12. Resensys SeniMax™ Communication gateway

Chapter 4: Numerical Modelling of Tunnel

4.1 Heat Transfer Model of Tunnel

4.1.1 Introduction to the Heat Transfer Model

The heat transfer analysis model was conducted using Abaqus finite element software which is a powerful finite element analysis software used for various engineering problems. In addition, WUFI Pro was used to validate the Abaqus model, which can be found in the Appendix A.

4.1.2 Objectives of the Heat Transfer Model

The objective of the heat transfer analysis was to determine the temperature distribution through the cross section. The analysis was conducted in 2D, assuming a critical cross section, such as the portals, where ambient environment temperature is expected to be similar to the surface temperatures at this location. The results from the gradient output were then compared with design code provisions and sensor data.

4.1.3 Heat Transfer Theory

Factors that affect thermal environment of the tunnel include solar radiation (at the portals), heating and cooling effects of surrounding air due to forced convection i.e. wind and ventilation system, radiation from other sources such as lighting and traffic. These factors concurrently influence the structural response i.e. displacements and stresses in the structure.

Heat flow is governed by the Fourier heat transfer in Equation 1, where ρ is density in kg/m^3, c is specific heat in J/kg K, k is thermal conductivity in W/m K, T is temperature in Kelvin, and t is time in seconds (Hyeong, 2007).

$$\rho c \frac{\partial T}{\partial t} = k(\nabla \cdot \nabla T) \quad [1]$$

The transient heat conduction equation for an isotropic material in the x-y plane can be expanded as follows in Equation 2 with the inclusion of the internal heat generated within the member, Q, due to processes such as hear of hydration in W/m^3 (Léger et. al., 1993).

$$\rho c \frac{\partial T}{\partial t} = k(\frac{\partial^2 T}{\partial x^2} + \frac{\partial^2 T}{\partial y^2}) + Q \quad [2]$$

The boundary conditions for the heat transfer problem depend on the heat flux imposed on the system described in Equation 3. Typically heat flux sources including solar radiation, long wave radiation from the surrounding environment and emitted from the structure, and the heating and cooling effects due to convection. Heat fluxes are in units of W/m^2.

$$q = -k\frac{\partial T}{\partial n} = q_{solar} + q_{sur} - q_{emit} - q_{wind} \quad [3]$$

Solar radiation is dependent on the absorptivity of the surface and the amount of solar radiation that reaches the surface (see Equation 4). The amount of solar radiation that reaches the surface of the structure is dependent on several factors. These include the condition of the atmosphere, angle of incidence of the sun rays and the location of the structure (latitude and longitude). Studies that investigate these effects in detail include Elbadry and Ghali (1983), Léger et al. (1993), Hyeong (2007), and Svensson and Larsson (2013).

$$q_{solar} = \propto_{solar} I_{solar} \quad [4]$$

Long wave radiation is typically combined into one expression through the Stefan-Boltzmann law that describes the energy emitted by the surface and the energy that is emitted by the surrounding onto the surface and then absorbed by the surface (see Equation 5). Note that within the ambient temperature range difference between air and concrete surface heat loss by radiation is not expected to be significant and is typically disregarded (Léger et. al., 1993).

$$-q_{emit} + q_{sur} = -\varepsilon\sigma(T^4 - {T_{sky}}^4) \quad [5]$$

Convective heat flux is dependent on the convection coefficient and the difference in ambient temperature and surface temperature which could either by a cooling or heating effect (see Equation 6). It is important to note the convection coefficient is dependent on many factors such as surface roughness and flow pattern of the natural environment which is constantly changing (Hyeong, 2007). Consequently, experimental calibrations are generally required to describe the convection coefficient such as form present in Equation 7. In Equation 7, the coefficient is dependent on free convection (buoyancy driven) and forced convection (i.e. wind). The larger the convection coefficient, the more the surface temperature will follow the air temperature exactly.

$$-q_{wind} = -h(T - T_{air}) \quad [6]$$

$$h = h_0 + h_1 v_{wind} \quad [7]$$

4.1.4 Model Inputs

4.1.4.1 Geometry

Geometry of the tunnel model is based on Airport Trail Tunnel (see Figure 3.5). The top slab is 1.25 m thick and the walls are 1 m thick. The footing foundation was neglected in the model. Corner fillets at the wall-slab joints were removed from model for ease of meshing. The mesh scheme was kept as regular as possible and the cross section was 4 elements wide initially to provide sufficient representation of temperature distribution through a cross section. A 4-node linear heat transfer quadrilateral brick (DC2D4) was considered in the 2D model.

4.1.4.2 Material

The main thermal material properties that influence heat transfer are density, heat capacity, and thermal conductivity. Additional factors that influence the boundary conditions of the problem include the emissivity coefficient and the absorptivity coefficient. A range of values for each parameter for concrete were examined based on literature is presented in Table 4.1.

Table 4.1. Thermal material properties for concrete from various sources in literature

Parameters	Notation	Zhou et al.	Léger et. al.	Larsson and Svensson	Elbadry and Ghali	Engineering Toolbox
Density	ρ (kg/m^3)	2400	2400	2400	2400	2240-2400
Heat capacity	c (J/kg K)	925	870-1080 (912)	900	960	880
Thermal conductivity	k (W/m K)	2.71	1.87-3.68 (2.62)	2.5	1.5	0.1-1.8
Emissivity coefficient	ε_v	0.88	0.65-0.90 (0.88)	0.9	0.88	0.85
Absorptivity coefficient	α	0.65	0.50-0.65 (0.50)	0.5	0.5	0.60

* Léger et al. (1993) used the values in parenthesis as their baseline values

Note that due to the ambient temperature range the structure is subject to, the material properties are not expected to vary too much with temperature. Based on literature, material properties were chosen for the baseline model.

Table 4.2. Baseline parameters used in Abaqus model

Parameters	Notation	Concrete
Density	ρ (kg/m^3)	2400
Heat capacity	c (J/kg K)	900
Thermal conductivity	k (W/m K)	1.5

*Note that contribution from solar radiation, long wave radiation, and convection were considered separately.

4.1.4.3 Boundary Conditions

Boundary conditions influence the heat transfer problem. These include convection (wind), solar radiation, and longwave radiation. A convective heat transfer coefficient of concrete of 5 to 35 W/ m^2K (Lee. et al., 2009) will be considered which is range determined based on several studies. The study mentions that convective heat transfer changes with factors such as the wind velocity, curing condition, and thermal conductivity. The coefficient influences the temperature distribution, which naturally produces tensile stresses thus it is a crucial material property of concrete with respect to the prediction of thermal cracking. The emissivity coefficient is dependent on the surface material since all black bodies emit longwave radiation. For concrete the emissivity coefficient ranges from 0.65 to 0.95. The tunnel ceiling has fireproofing material covering the concrete and the walls have an elastomeric coating however these were not considered in the emissivity range. For the solar absorptivity coefficient of concrete, typical values range from 0.5 to 0.65.

Convection was inputted using the surface film condition interaction in Abaqus. In the definition of the interaction the film coefficient, representing the convection coefficient, was applied as a constant amplitude through the analysis and the sink temperature applied represents the air temperature.

Long wave radiation was inputted using the surface radiation interaction in Abaqus. The definition requires the emissivity of the concrete surface and ambient temperature as input. Note that the absolute zero temperature (-273.15°C) and Stefan-Boltzmann constant (5.67 x 10^{-8} W/m^2) must be specified in model attributes for long wave radiation to be considered.

Solar radiation is typically considered as a periodical heat flux load or by adjusting the ambient temperature the structure is subject to in the heat transfer model. However, since the portals are only exposed to solar radiation, which is a small portion of the tunnel, and rigorous calculations considering incident angle of sun rays etc.…are required to accurately determine the solar heat flux, its contribution was not considered in the analysis.

The tunnel is overlain by backfill material. The fill material varies in thickness from 0.5 to 3.5 m. The soil adjacent to the structure consists of free draining material. Soil temperature is a function of several factors such as air temperature, depth, and soil surface condition. Based on soil

temperature data collected over a 10 year period in Alberta, at 12-15 m depths, temperatures remained at 5°C ± 0.5°C. At 2 m, the temperature fluctuated between a minimum temperature of 1.5°C and maximum temperature of 10°C. In the same time period, the mean minimum temperature was -18°C and the mean maximum temperature was 16°C (Toogood 1976). A constant soil temperature of 7.5°C was considered for the soil boundary condition. Several studies, such as Nofziger (2003), suggest an equation that relates soil temperature as a function of depth and time. However, considering the depth of cover and lack of site specific soil data, assuming a constant soil temperature is reasonable for modelling purposes.

To simulate realistic surface temperature conditions, an hourly temperature record from available Environment Canada data was applied to the tunnel surface. The assumption is that Environment Canada temperatures are equivalent to the temperature that tunnel surface experiences at the portal locations.

The heat transfer analysis requires the initial temperature of the system to be specified. An initial temperature of 15°C was considered for the structure as a predefined field. The initial temperature was based on the temperature of concrete during construction given in CSA S6-06. In the analysis step definition, a transient was selected which considers temperature distribution over time. The increment size was chosen to be 1 hour which corresponds to the increment size of the temperature record applied to the interior tunnel surface.

4.2 Parametric Study of Thermal Material Properties and Boundary Conditions

A parametric study was conducted to determine the effect of each thermal material property on temperature distribution. The baseline thermal material properties for concrete used in the numerical model along with the high and low values for each property (see Table 4.3). Note for concrete, a density of 2400 kg/m^3 was considered as the baseline value since it is the most common.

Table 4.3. Thermal properties of concrete considered in parametric study

Parameters	Notation	Baseline	Low	High
Density	ρ (kg/m^3)	2400	2240	2400
Heat capacity	c (J/kg K)	900	870	1080
Thermal conductivity	k (W/m K)	1.5	1	3.68

A section of the model used in the analysis and boundary conditions are represented in Figure 4.1. It consists of a 1 m dirt layer overlying a 1.25 m concrete layer. The concrete layer was modelled with a finer mesh since the main source of heat flux was the interior concrete surface and the distribution of temperature through the dirt layer was not the main focus of this study. For the soil layer, a density of 2000 kg/m3, heat capacity of 1140 J/kg K, and thermal conductivity of 0.75 W/m K were assumed based on average values for the soil material (Engineering Toolbox). At the exterior boundary of the soil layer in the model, a constant temperature of 7.5°C was applied to represent the average soil temperature previously described. The 1 m thick layer of soil was mainly incorporated in the model to accurately capture the structure-dirt boundary temperature.

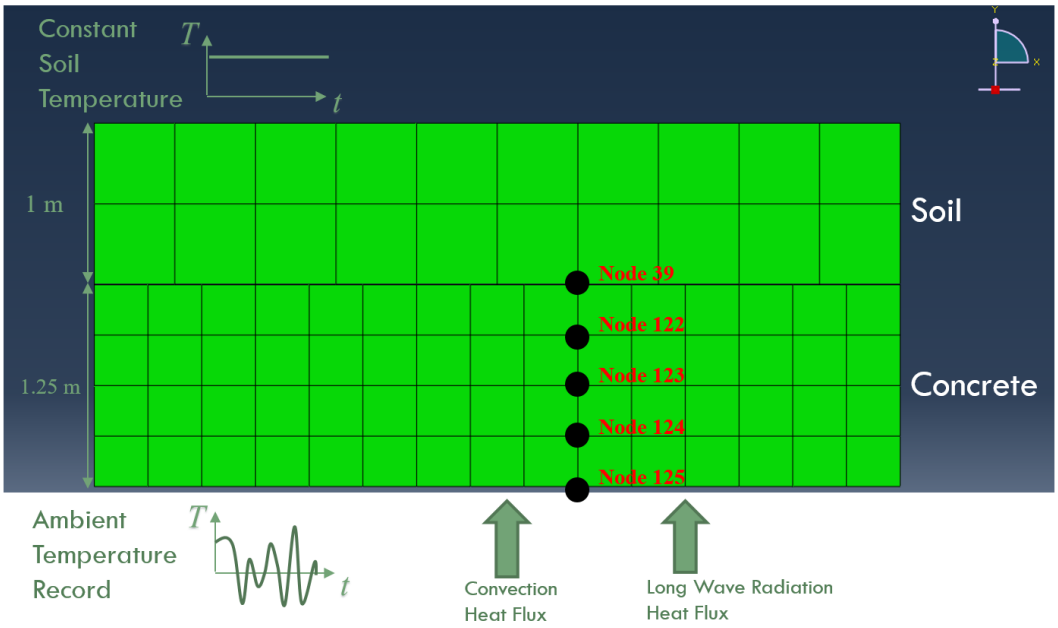

Figure 4.1. Section of concrete and soil model in Abaqus

Furthermore, for the ambient temperature of the tunnel, a temperature record was applied to the model from Environment Canada Calgary International Airport station. Figure 4.2 illustrates the temperature record from September 1, 2014 to January 1, 2015. The time period is a total of 2929 hours or 122 days. In this time period temperature has a mean value of 2.9°C, maximum value of 27.6°C, and minimum value of -24.6°C.

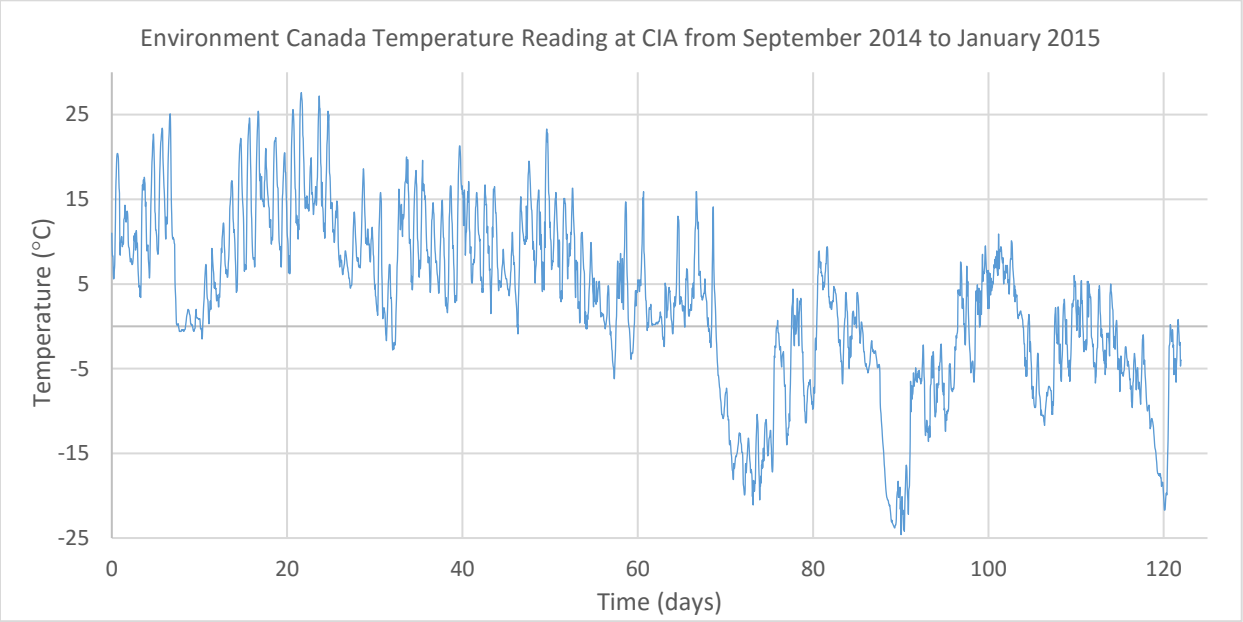

Figure 4.2. Environment Canada Temperature Reading at CIA from September 2014 to January 2015

In the model, the temperature of the top slab cross section was examined at intervals of approximately 312 mm intervals. Node 125, Node 124, Node 123, Node 122, and Node 39 represent nodes from the surface to dirt (respectively) where the temperature output was extracted from the model as illustrated in Figure 4.1. The nodal temperature output using the baseline properties is illustrated in Figure 4.3. The results from the material property study were plotted in Figure 4.4 to Figure 4.8.

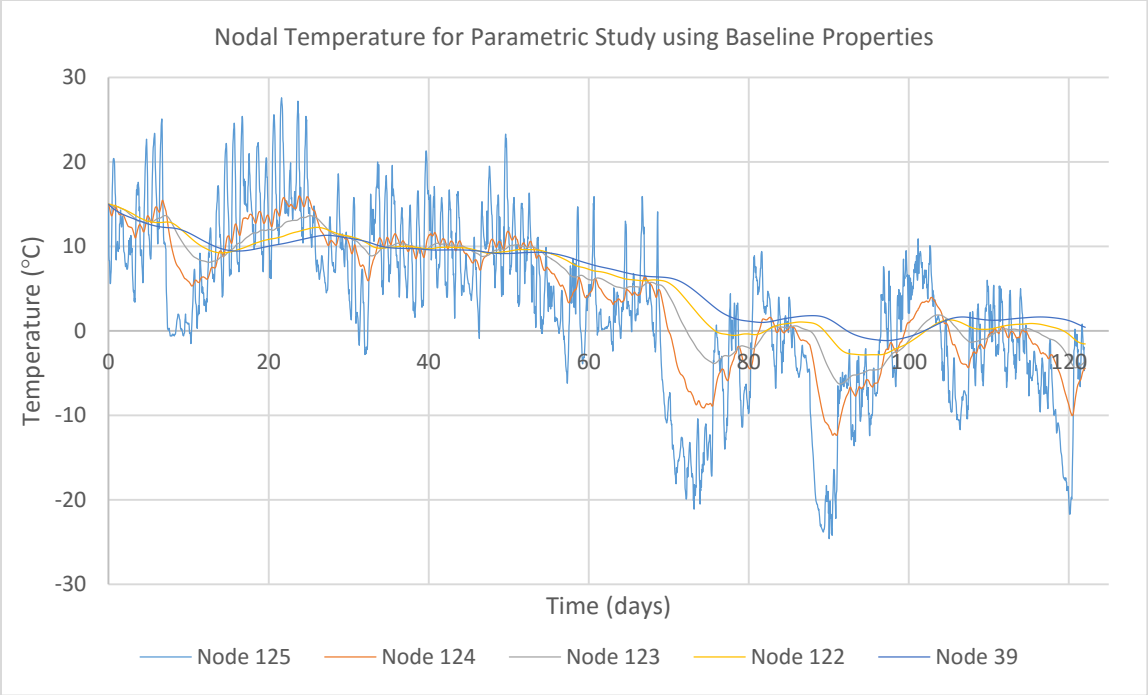

Figure 4.3. Nodal Temperature Output for Parametric Study using Baseline Properties

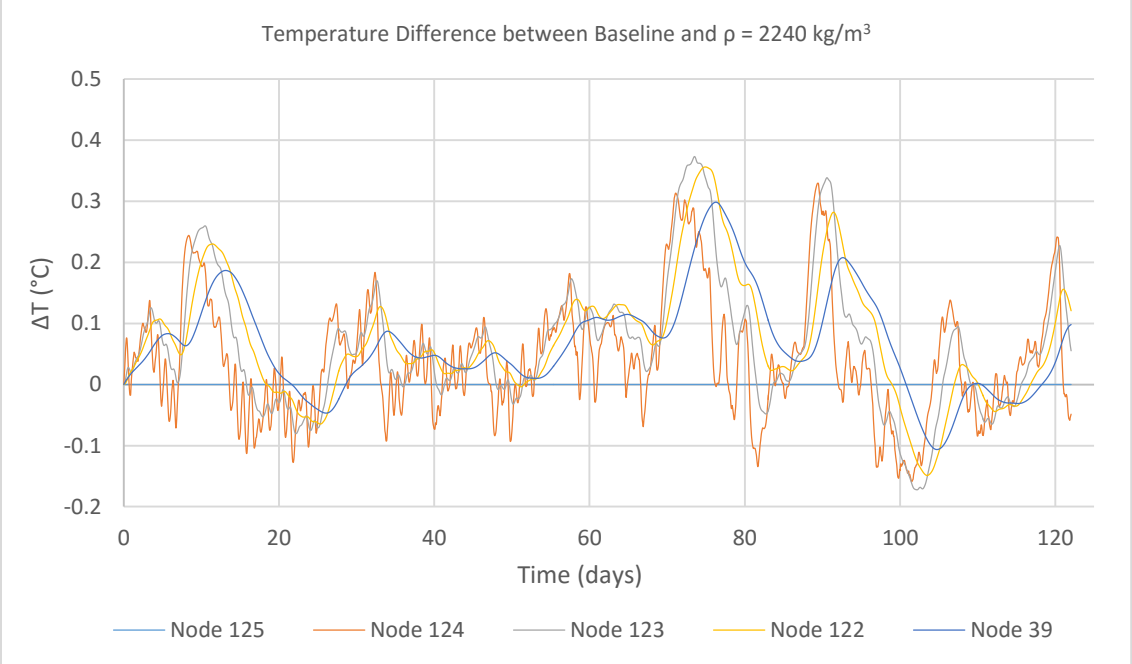

Figure 4.4. Temperature Difference between Baseline and ρ = 2240 kg/m^3

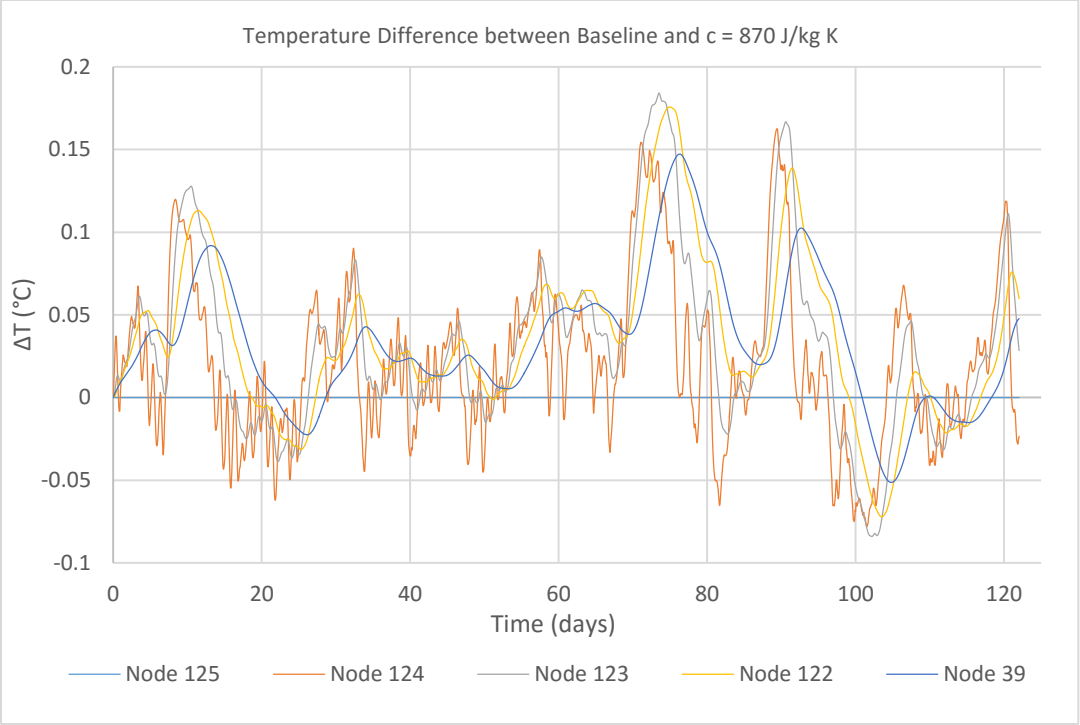

Figure 4.5. Temperature Difference between Baseline and c = 870 J/kg K

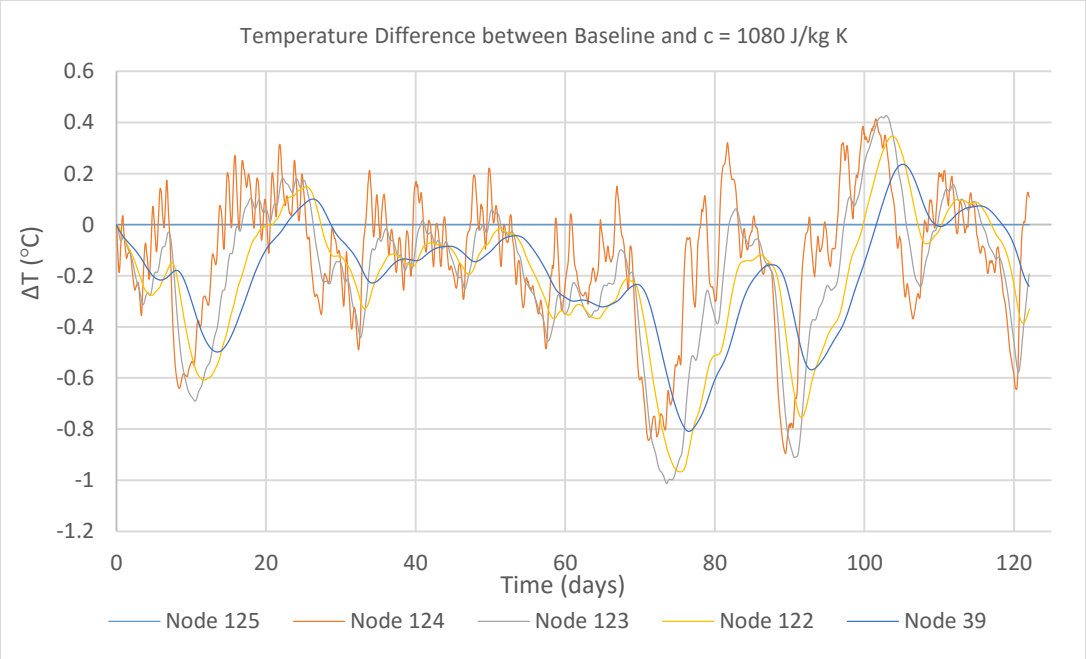

Figure 4.6. Temperature Difference between Baseline and c = 1080 J/kg K

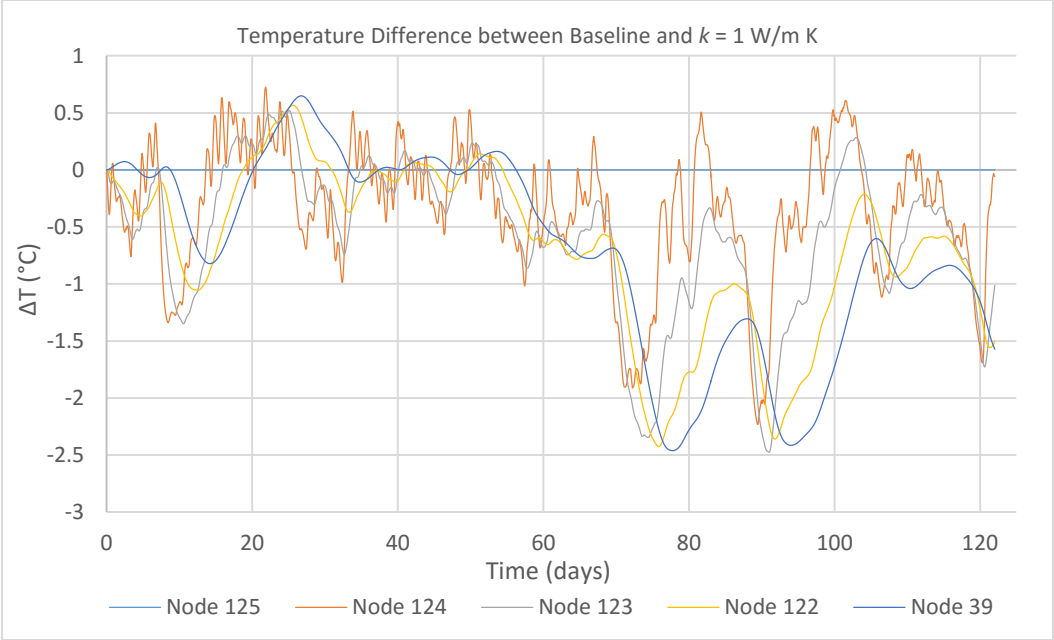

Figure 4.7. Temperature Difference between Baseline and k = 1 W/m K

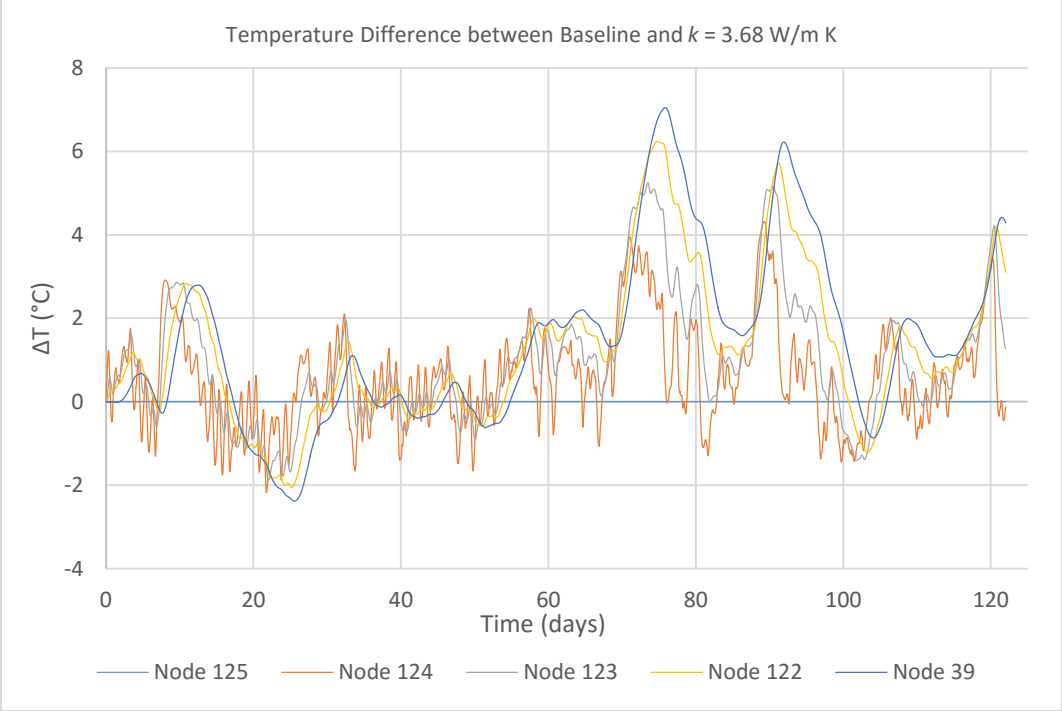

Figure 4.8. Temperature Difference between Baseline and k = 3.68 W/m K

It is evident that the effect of density and specific heat was negligible, however the effect thermal conductivity was significant with temperature differences of up to 7 °C when compared to the baseline case, which occurred at the concrete soil boundary (node 39) when k = 3.68 W/m K.

To further examine the effect of thermal conductivity, the temperature output for interior nodes (124, 123, and 122) and concrete soil boundary node (39) were extracted. The comparison results are plotted in Figure 4.9 to Figure 4.12. There is an evident thermal lag and reduction in temperature fluctuations as the thermal conductivity decreases.

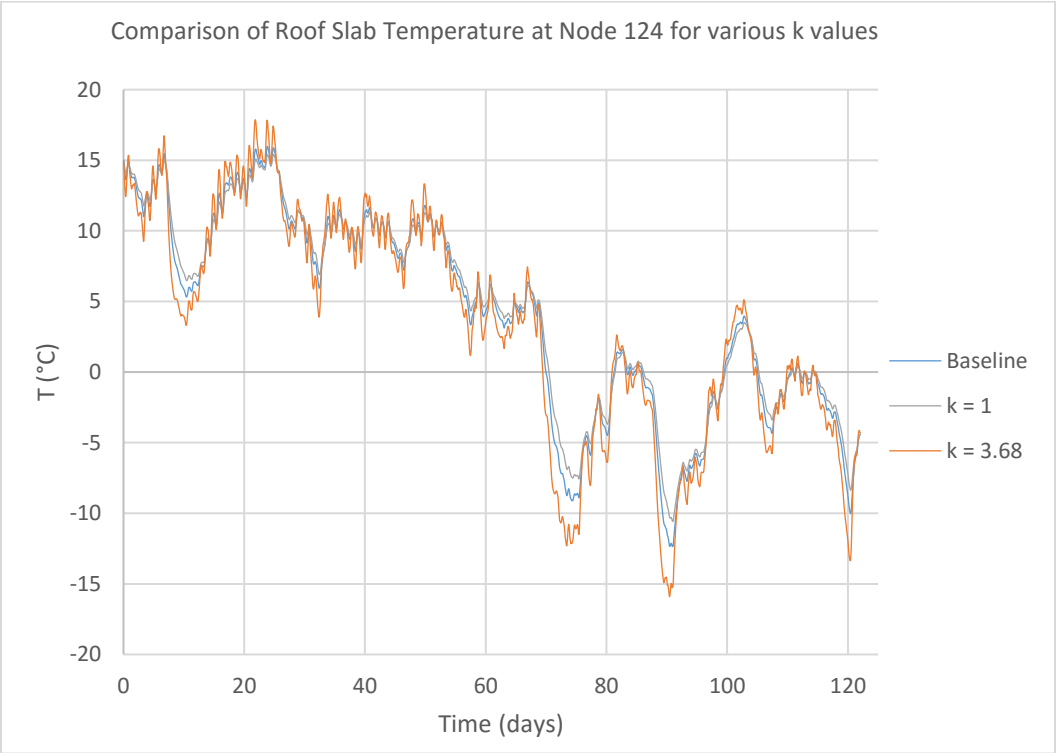

Figure 4.9. Comparison of Roof Slab Temperature at Node 124 for various k values

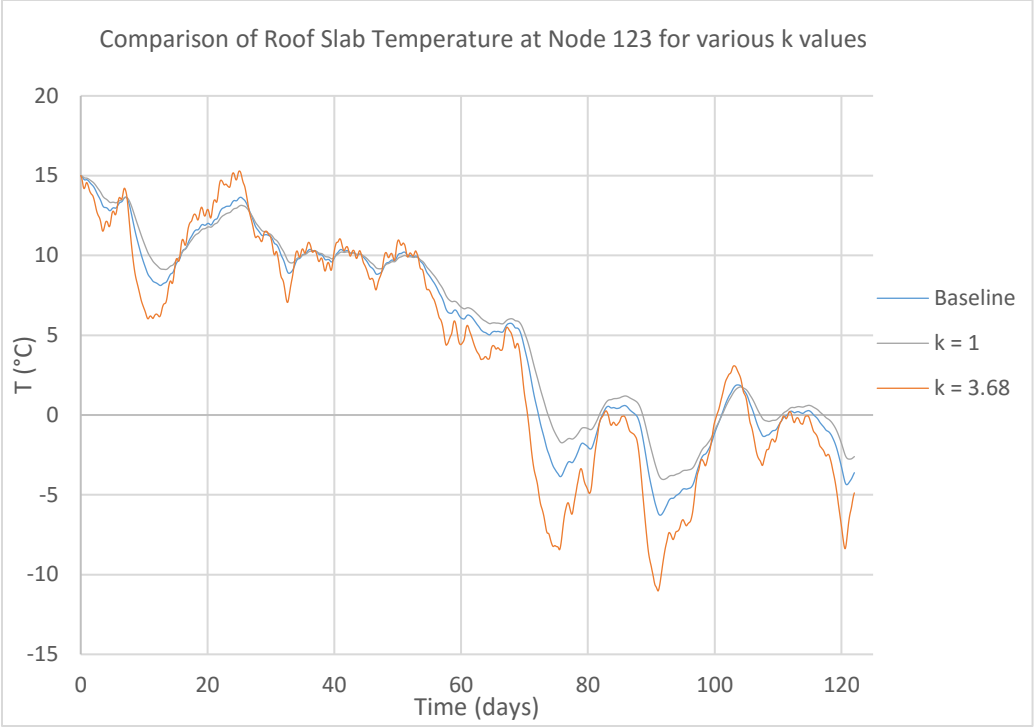

Figure 4.10. Comparison of Roof Slab Temperature at Node 123 for various *k* values

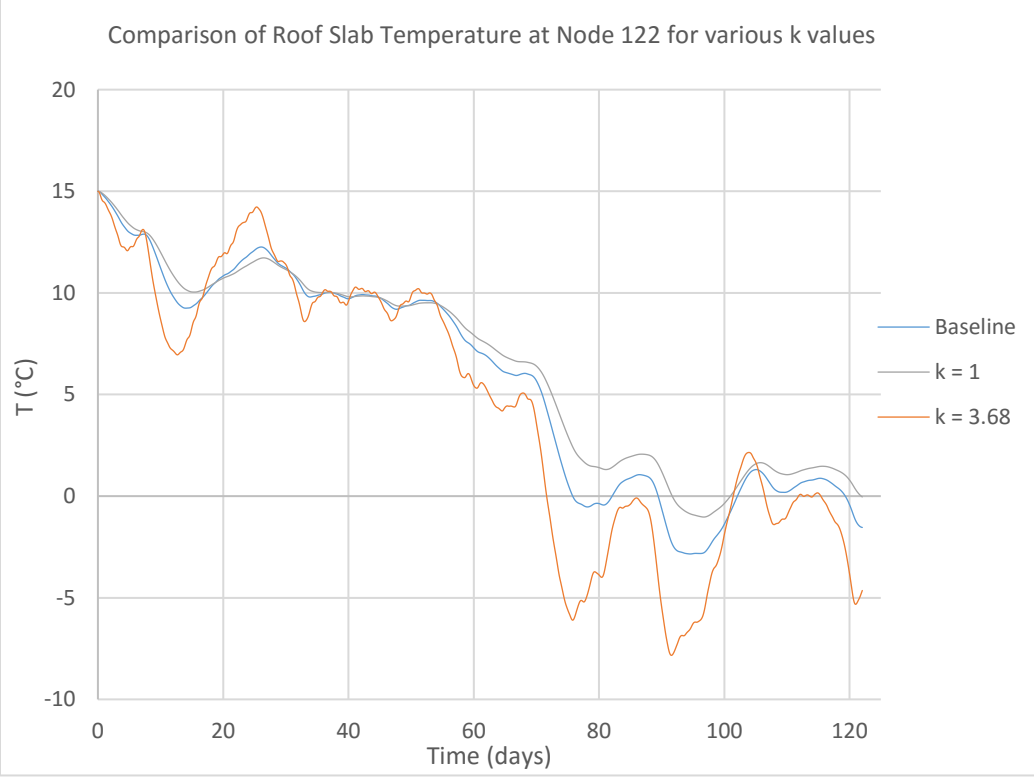

Figure 4.11. Comparison of Roof Slab Temperature at Node 122 for various *k* values

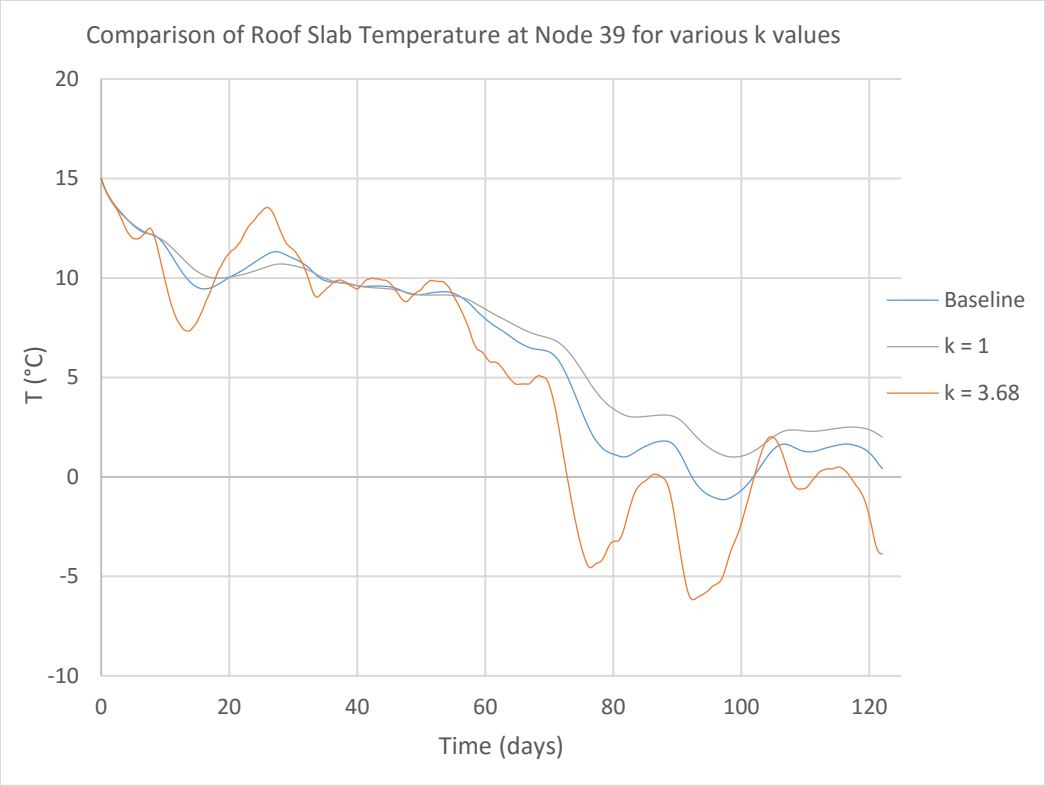

Figure 4.12. Comparison of Roof Slab Temperature at Node 39 for various *k* values

For boundary conditions, a parametric study was conducted considering a convective coefficient range of 5 to 35 W/ m^2K and long wave emissivity coefficient range of 0.65 to 0.95 for concrete. The results from the convective coefficient are plotted in Figure 4.13 to Figure 4.17. The higher the convection coefficient the more close the temperature is to the baseline case which represents ambient temperature. It can be observed that differences in nodal temperature are most prevalent at the surface node.

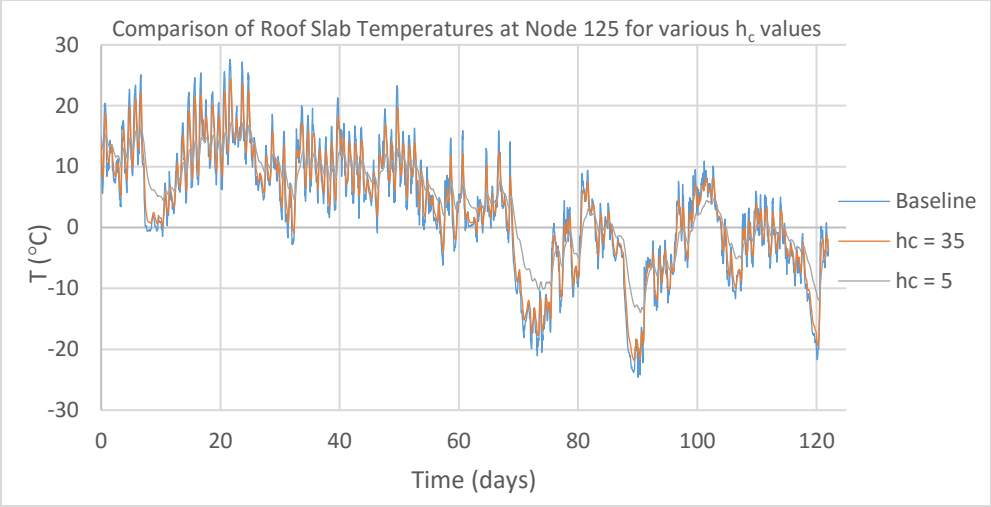

Figure 4.13. Comparison of Roof Slab Temperature at Node 125 for various h_c values

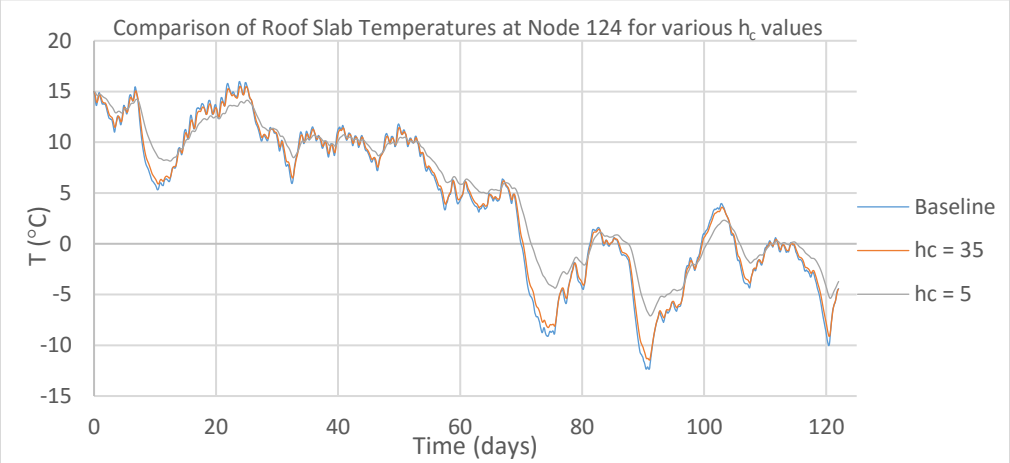

Figure 4.14. Comparison of Roof Slab Temperature at Node 124 for various h_c values

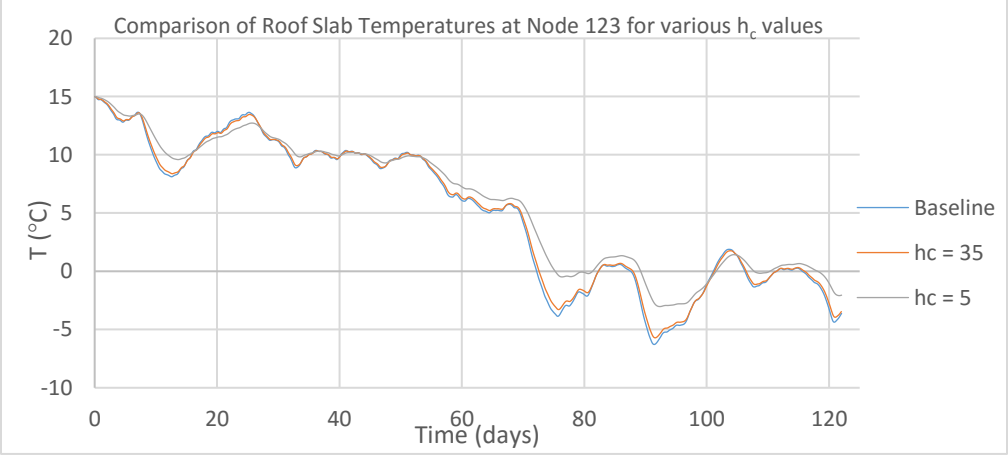

Figure 4.15. Comparison of Roof Slab Temperature at Node 123 for various h_c values

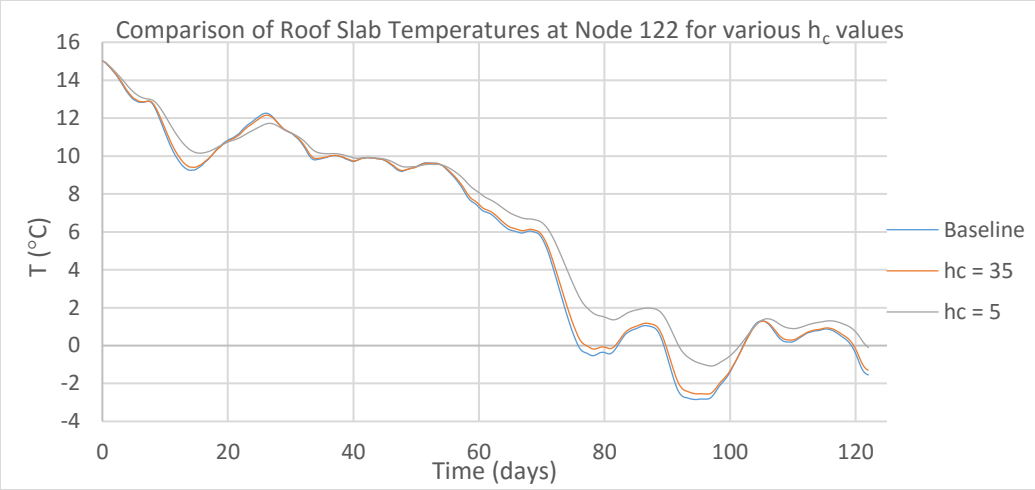

Figure 4.16. Comparison of Roof Slab Temperature at Node 122 for various h_c values

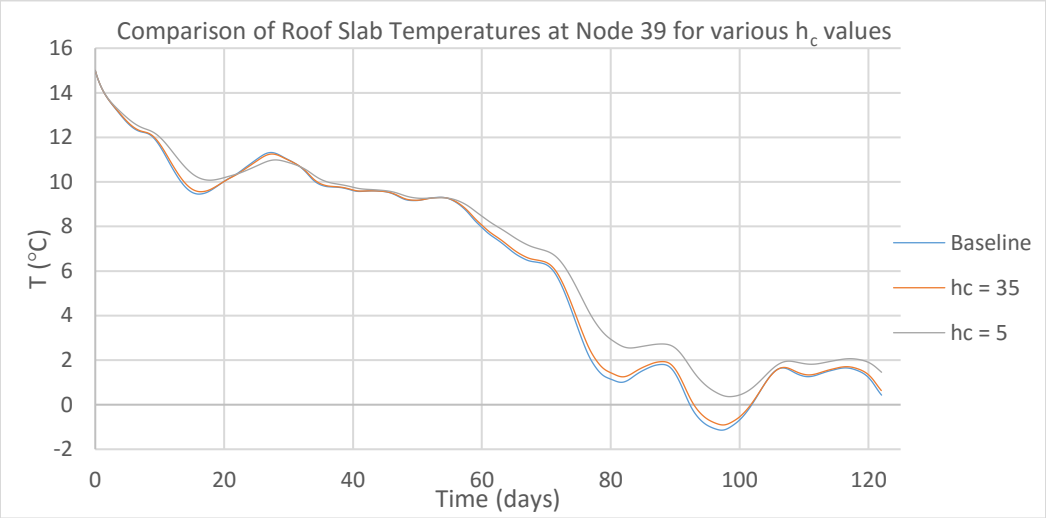

Figure 4.17. Comparison of Roof Slab Temperature at Node 39 for various h_c values

Likewise, the results from the emissivity coefficient study are plotted in Figure 4.18 to Figure 4.22. When emissivity is introduced into the model there is a significant decrease in fluctuation of the surface temperature (Node 125). Another observation is that the temperature difference between an emissivity coefficient of 0.65 and 0.95 was insignificant as the maximum temperature difference was less than 1°C at each node investigated

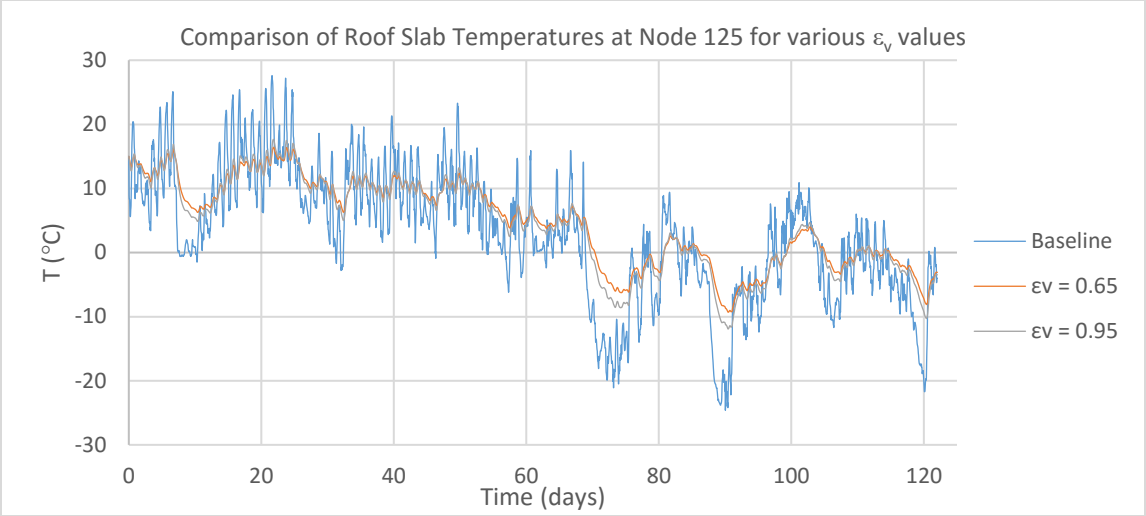

Figure 4.18. Comparison of Roof Slab Temperatures at Node 125 for various ε_v values

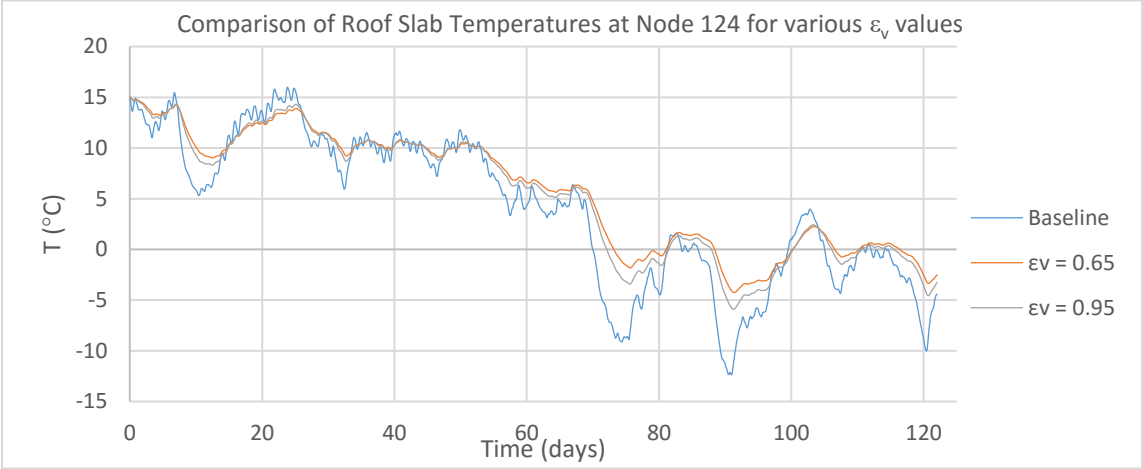

Figure 4.19. Comparison of Roof Slab Temperatures at Node 124 for various ε_v values

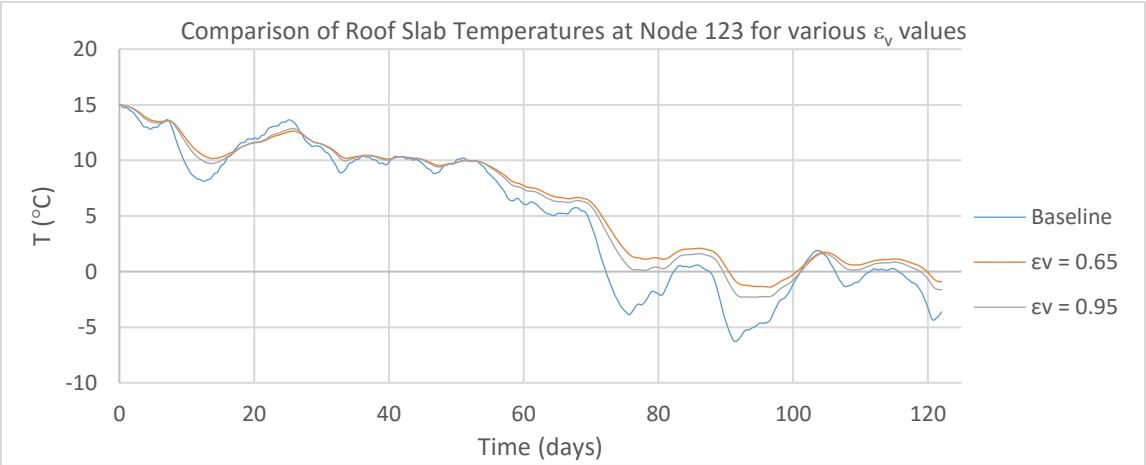

Figure 4.20. Comparison of Roof Slab Temperatures at Node 123 for various ε_v values

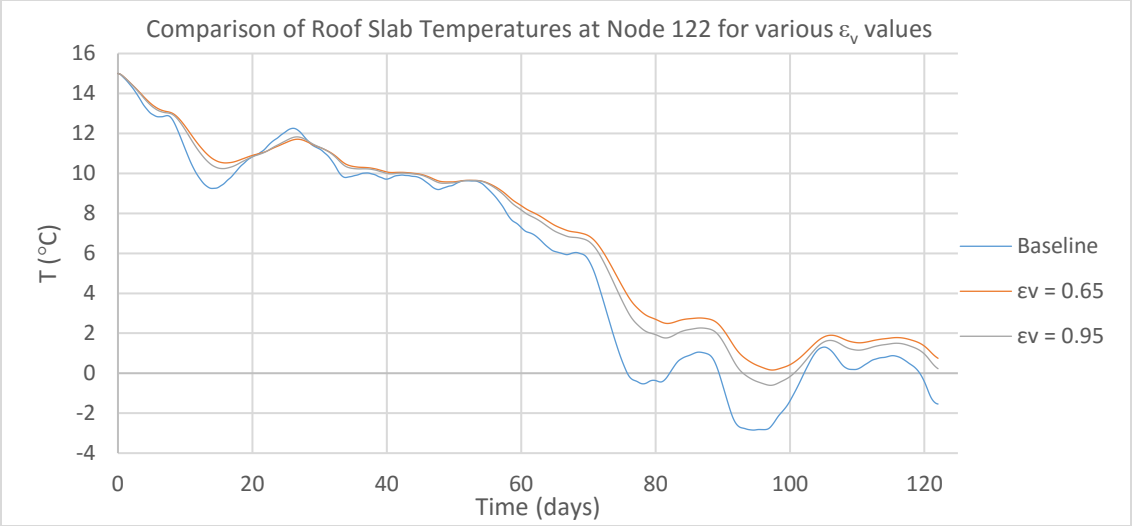

Figure 4.21. Comparison of Roof Slab Temperatures at Node 122 for various ε_v values

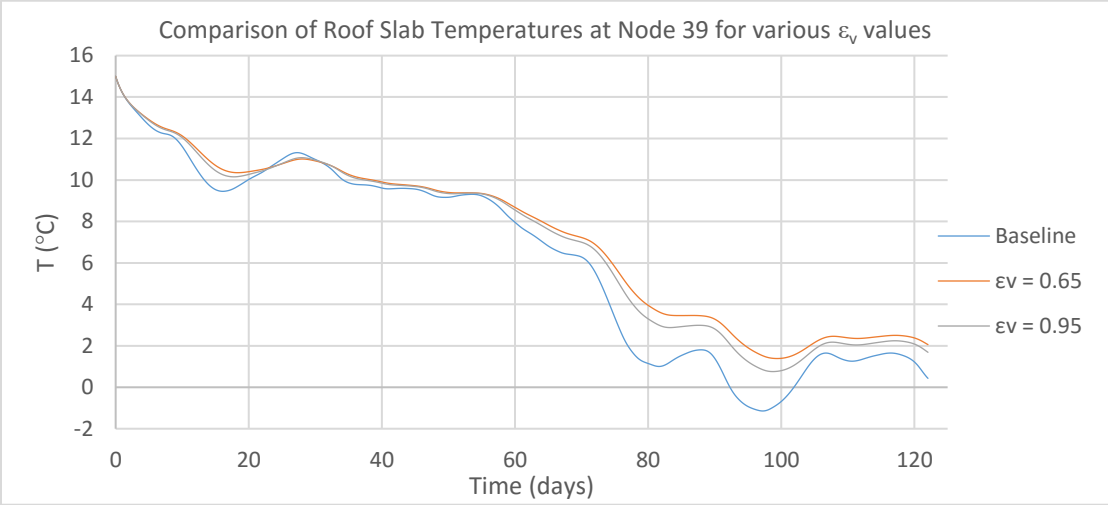

Figure 4.22. Comparison of Roof Slab Temperatures at Node 39 for various ε_v values

4.3 Gradient Analysis

A temperature gradient analysis was conducted for the roof slab using the baseline material properties and an applied ambient temperature record. The soil-concrete model section described in the previous section was considered for the gradient analysis. A convection coefficient of 20 W/m^2K and an emissivity coefficient of 0.8 were considered in the model. These represent the mean values in their respective ranges as previously discussed. These coefficients were assumed to be constant in the analysis because time history data was not available. The objective of the

analysis was to evaluate temperature distribution in the cross section and compare results to values specified for temperature gradient effects in the CSA code. For the gradient analysis, a 3-year temperature record at the CIA from May 2013 to May 2016 was considered (see Figure 4.23). The reason for the longer time period is to be more representative of the gradient envelope and to simulate that time period in which tunnel sensor data was collected. In Figure 4.23 daily and seasonal fluctuations, which may affect the gradient, vary each year although the temperature record is generally sinusoidal and regular. The nodal temperature output for a slab depth of 1.25 m is illustrated in Figure 4.24.

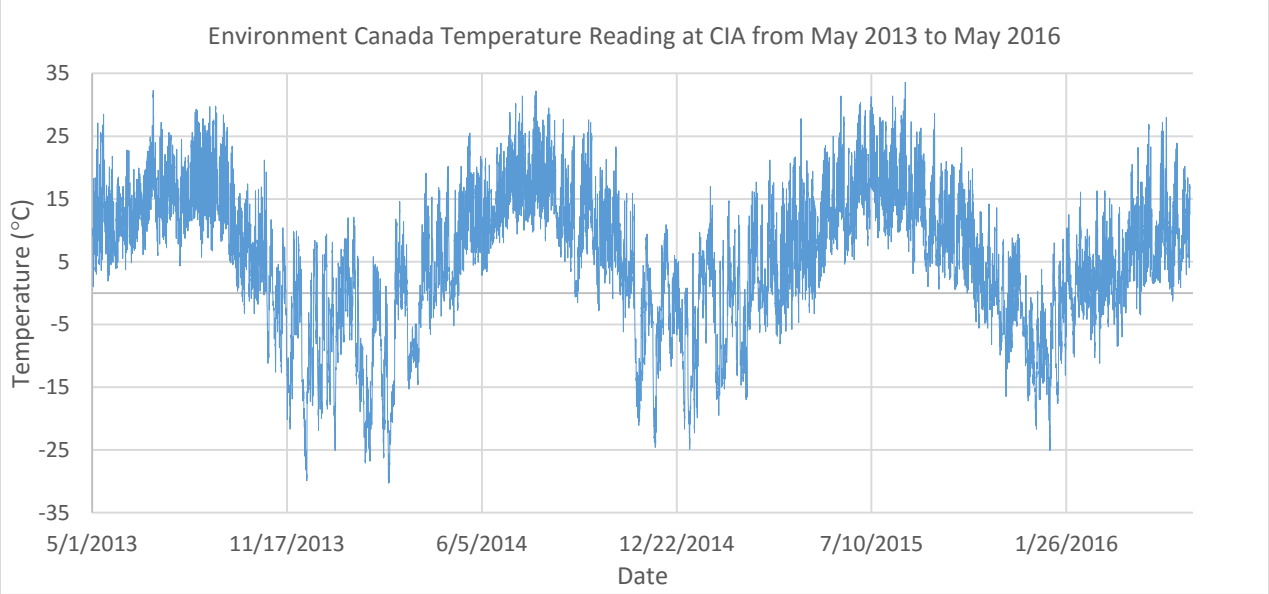

Figure 4.23. Environment Canada Temperature Reading at CIA from May 2013 to May 2016

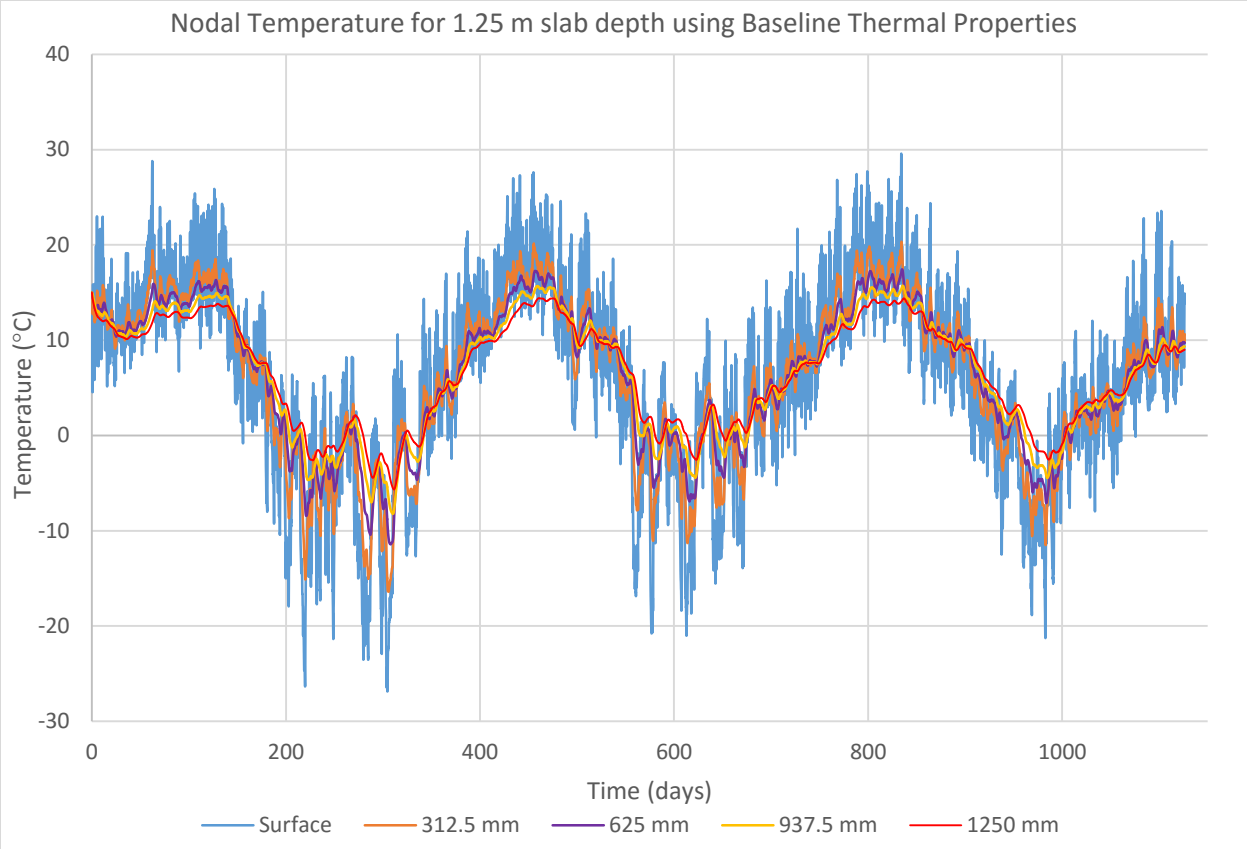

Figure 4.24. Nodal Temperature for 1.25 m slab depth using baseline thermal properties and CIA temperature record from May 2013 to May 2016

Another component of the gradient analysis was to determine the effect of changing the concrete depth and thermal boundary conditions constant. The depth considered varied from 0.25 m to 2 m in increments of 0.25 m. Figure 4.25 to Figure 4.32 illustrates individual hourly temperature distributions through the slab depth that form the temperature profile envelopes.

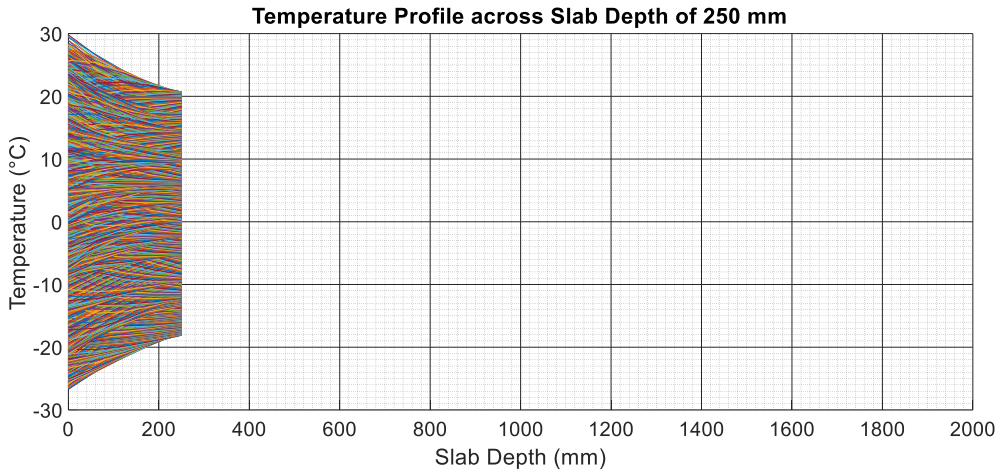

Figure 4.25. Temperature Profile Envelope across Slab Depth of 250 mm

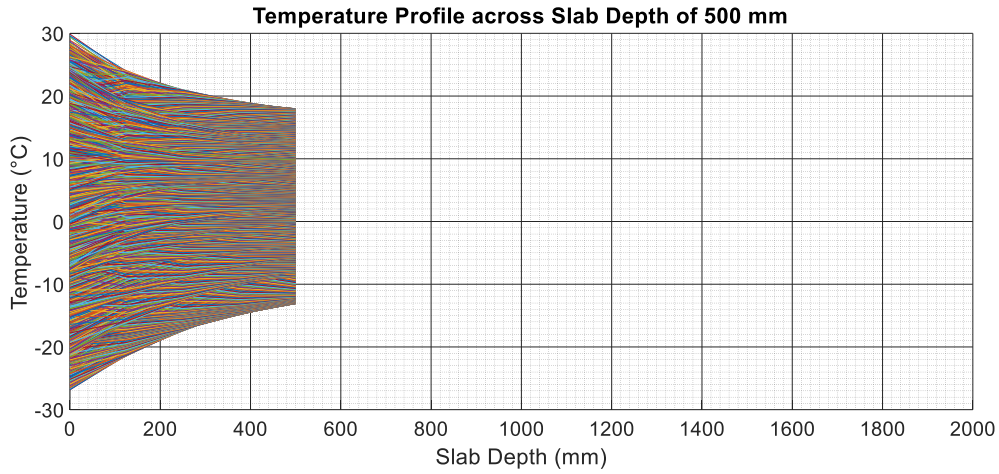

Figure 4.26. Temperature Profile Envelope across Slab Depth of 500 mm

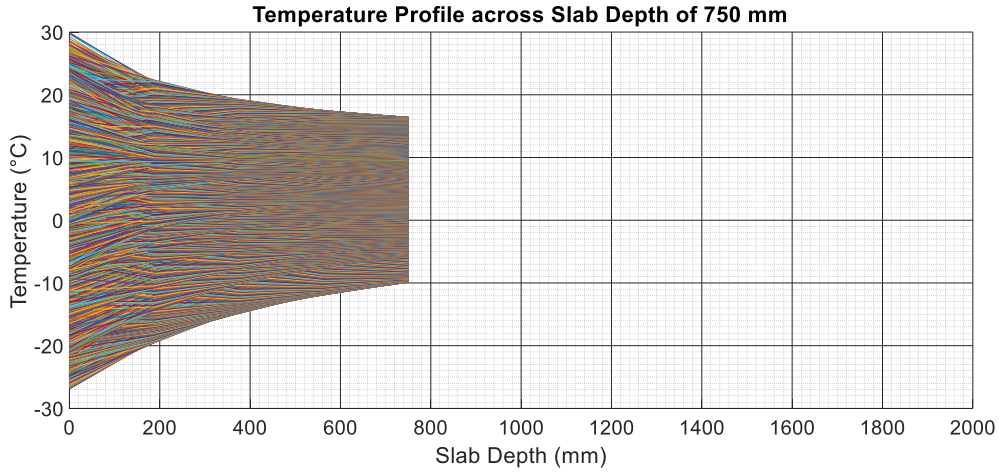

Figure 4.27. Temperature Profile Envelope across Slab Depth of 750 mm

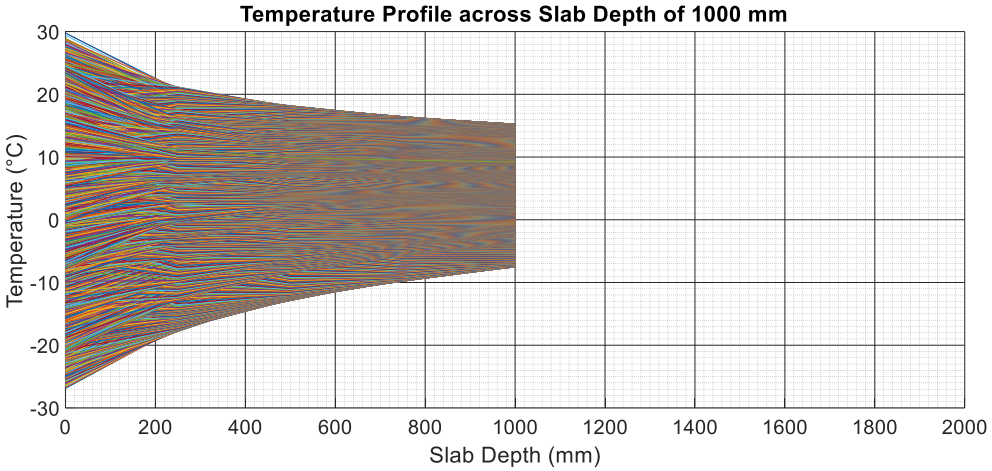

Figure 4.28. Temperature Profile Envelope across Slab Depth of 1000 mm

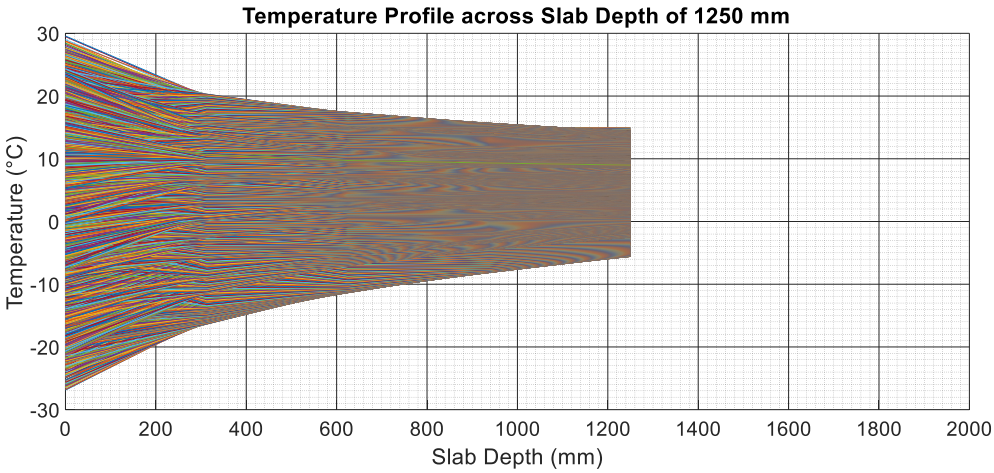

Figure 4.29. Temperature Profile Envelope across Slab Depth of 1250 mm

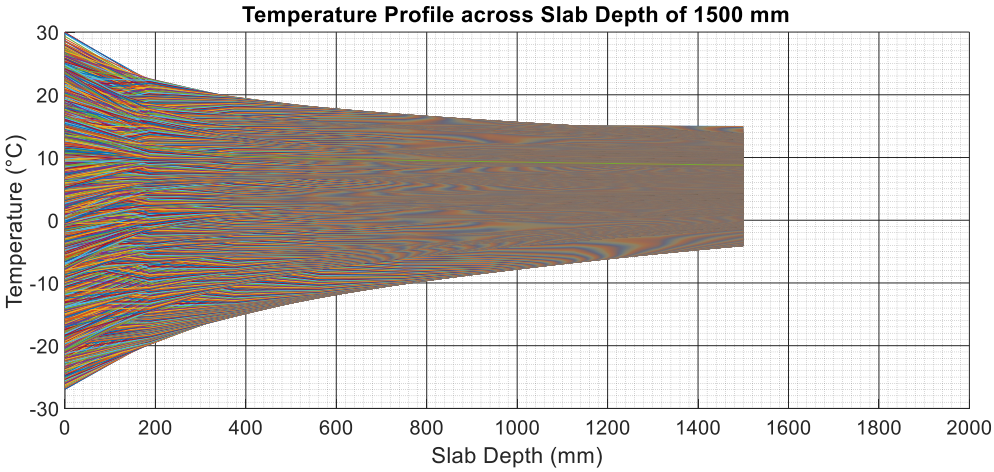

Figure 4.30. Temperature Profile Envelope across Slab Depth of 1500 mm

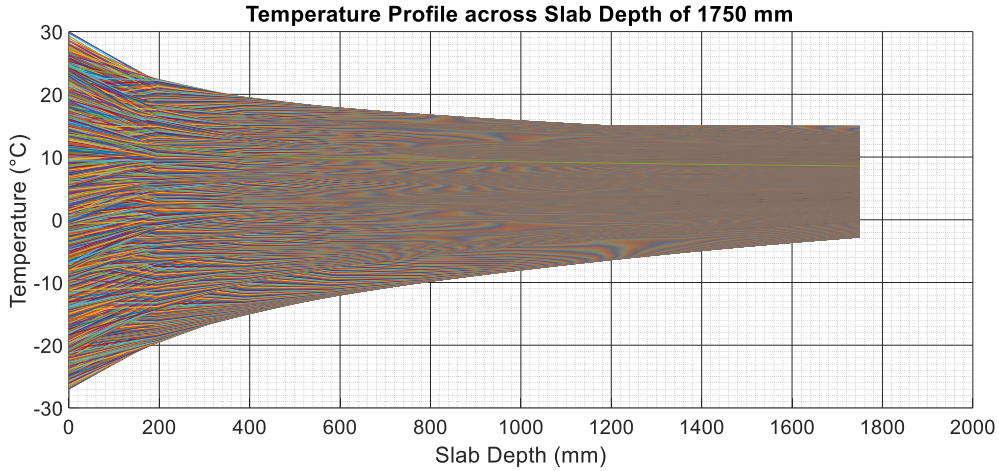

Figure 4.31. Temperature Profile Envelope across Slab Depth of 1750 mm

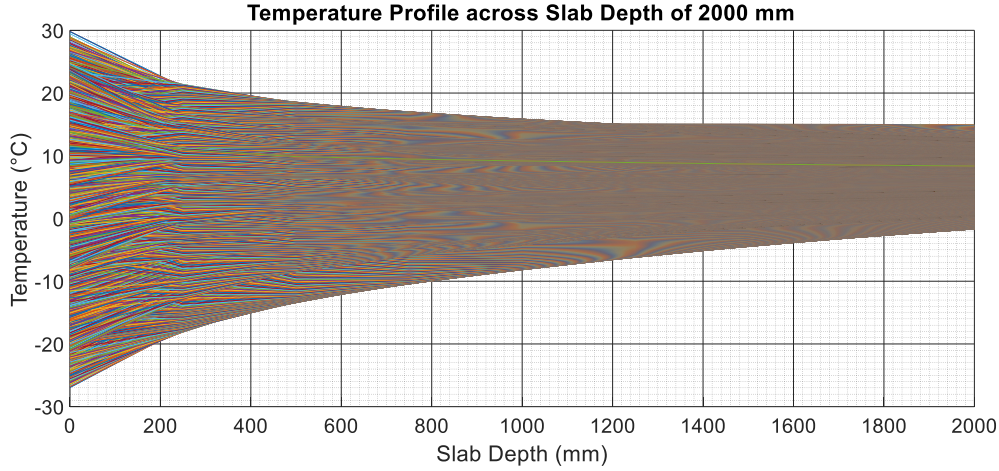

Figure 4.32. Temperature Profile Envelope across Slab Depth of 2000 mm

From the temperature profile envelope it is evident that the highest fluctuations in temperature occurs at approximately 250-300 mm from the surface. This result agrees with the theoretical temperature distribution for mass concrete members described in several codes such as ACI 207.1R-96. It can be observed that the temperature differential is nonlinear and most significant near the surface. Also, regardless of depth, the profile becomes increasingly linear at approximately 250 mm to 300 mm from the surface. Figure 4.33 to Figure 4.40 display statistical analysis of the surface to dirt, surface to mid slab, and mid slab to dirt gradient, using histogram plots and normal distribution curves for each slab depth for comparison purposes.

Overall, the data fits the normal distribution relatively well, which is represented by the red curves on the histogram plots, except the fact that there is a slight skew to the negative gradient which is most noticeable in the surface to dirt gradient and surface to mid slab gradient plot. A likely reason for the skew is that the soil temperature was set to a constant value of 7.5°C. The skew is also dependent on the slab depth as it becomes less apparent as the depth increases. See Table 4.4 for mean and standard deviation values for each gradient.

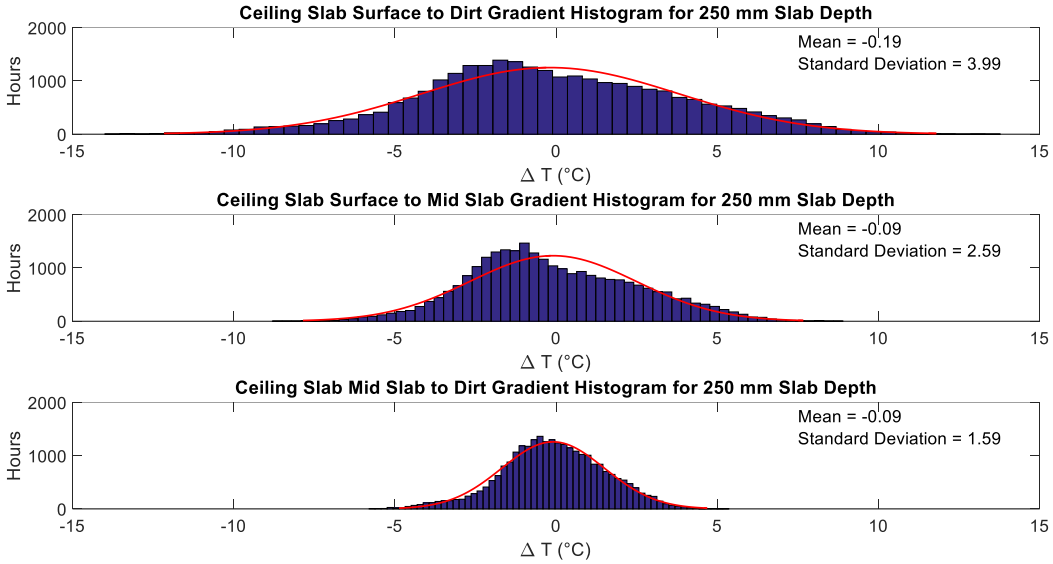

Figure 4.33. Gradient Histogram and Normal Distribution plot for Slab Depth of 250 mm

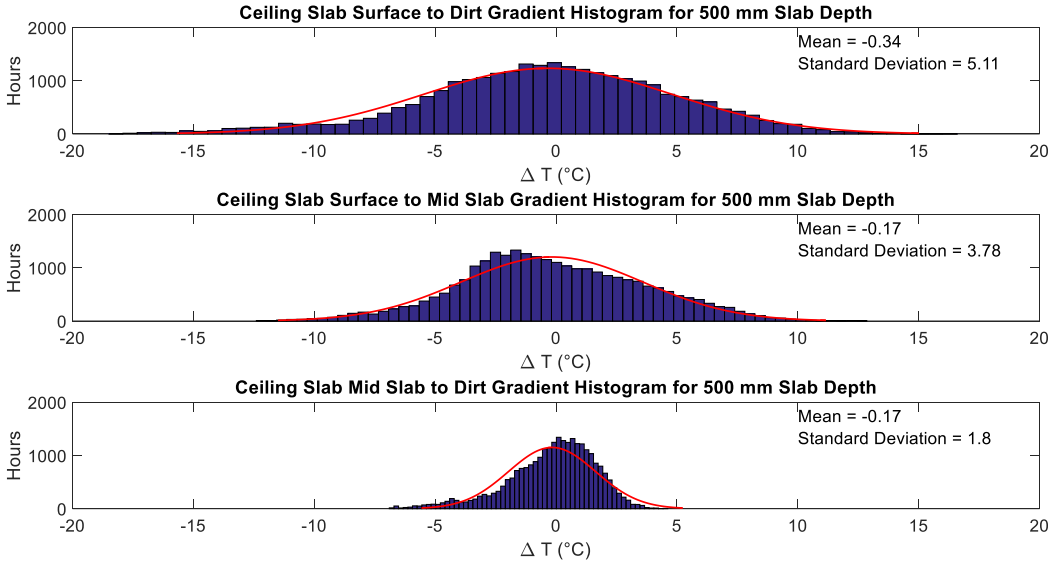

Figure 4.34. Gradient Histogram and Normal Distribution plot for Slab Depth of 500 mm

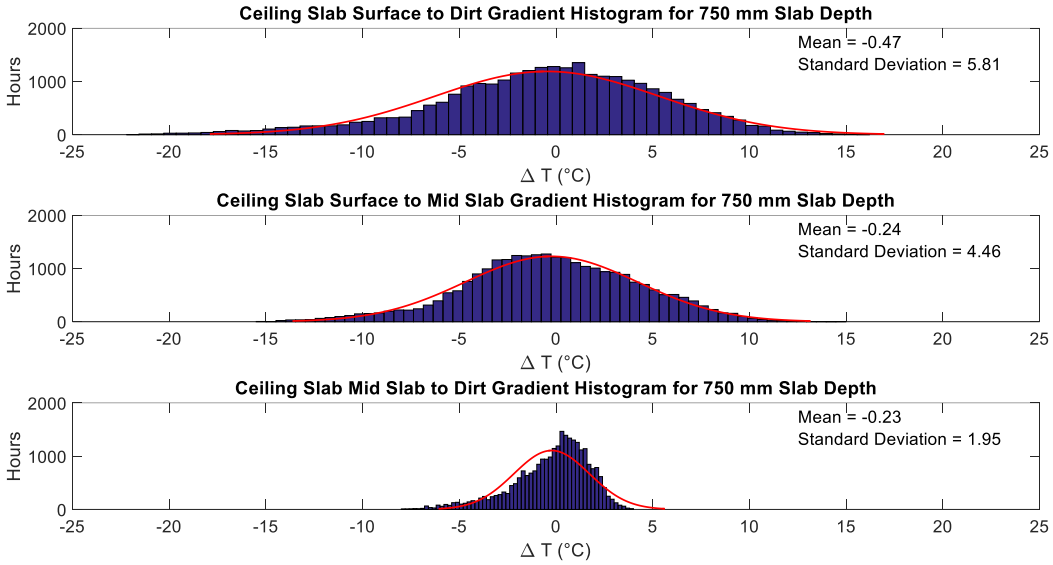

Figure 4.35. Gradient Histogram and Normal Distribution plot for Slab Depth of 750 mm

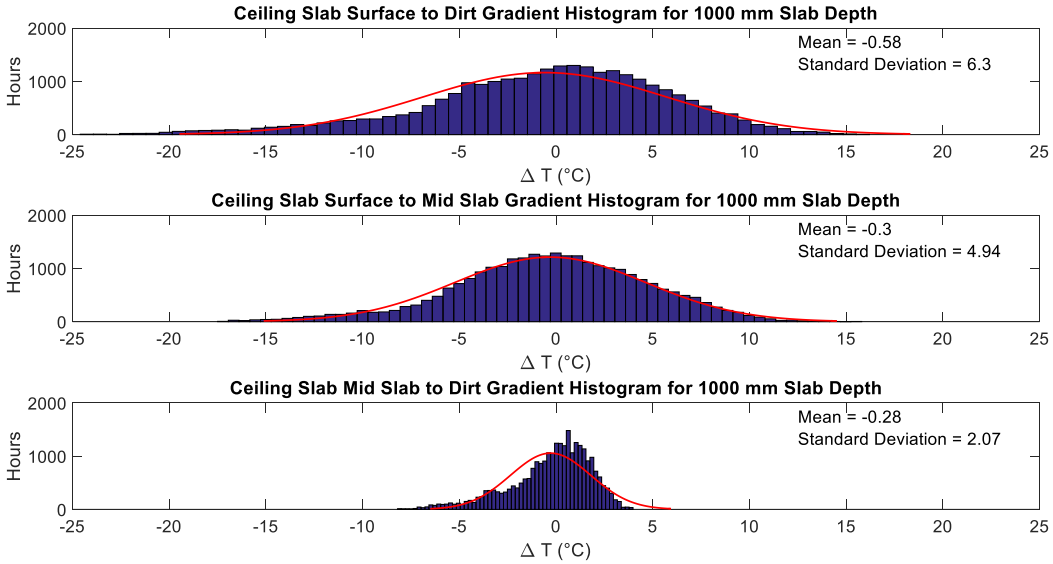

Figure 4.36. Gradient Histogram and Normal Distribution plot for Slab Depth of 1000 mm

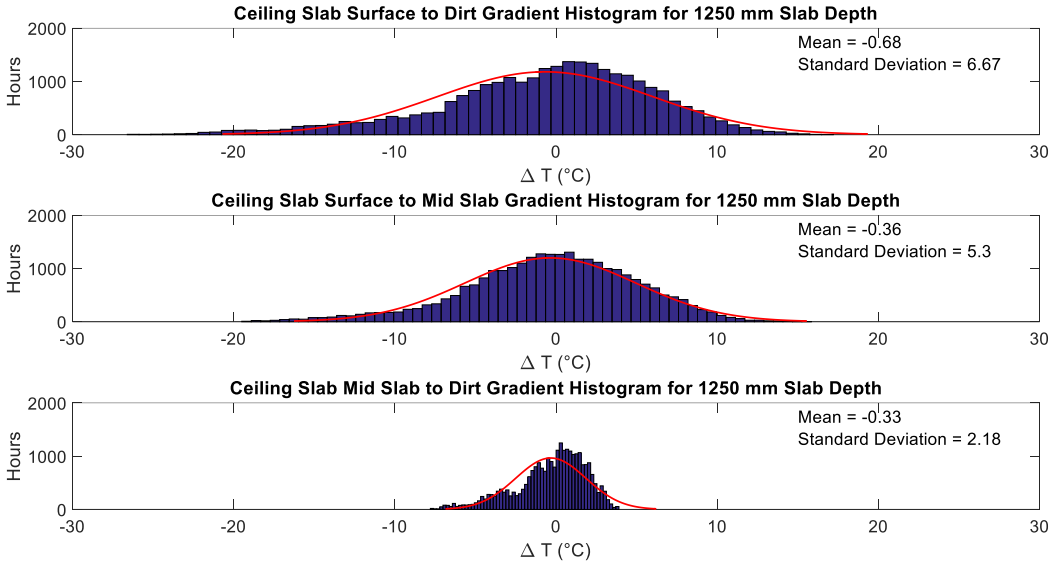

Figure 4.37. Gradient Histogram and Normal Distribution plot for Slab Depth of 1250 mm

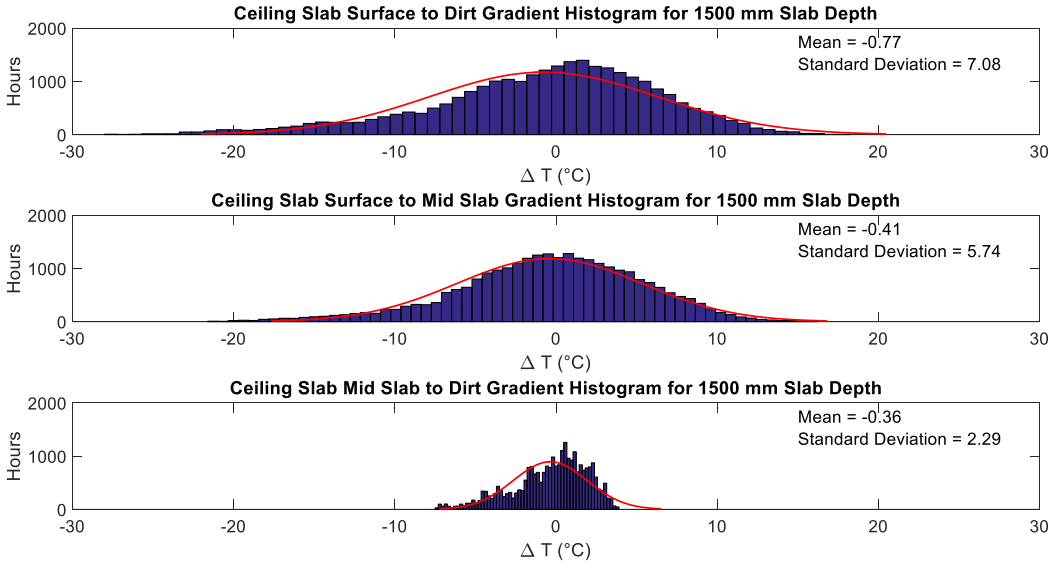

Figure 4.38. Gradient Histogram and Normal Distribution plot for Slab Depth of 1500 mm

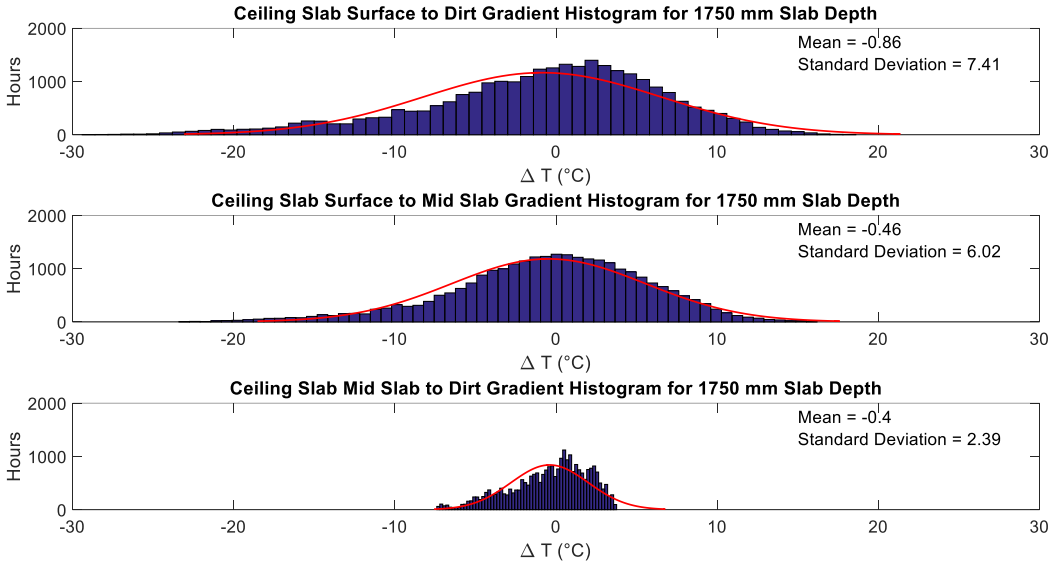

Figure 4.39. Gradient Histogram and Normal Distribution plot for Slab Depth of 1750 mm

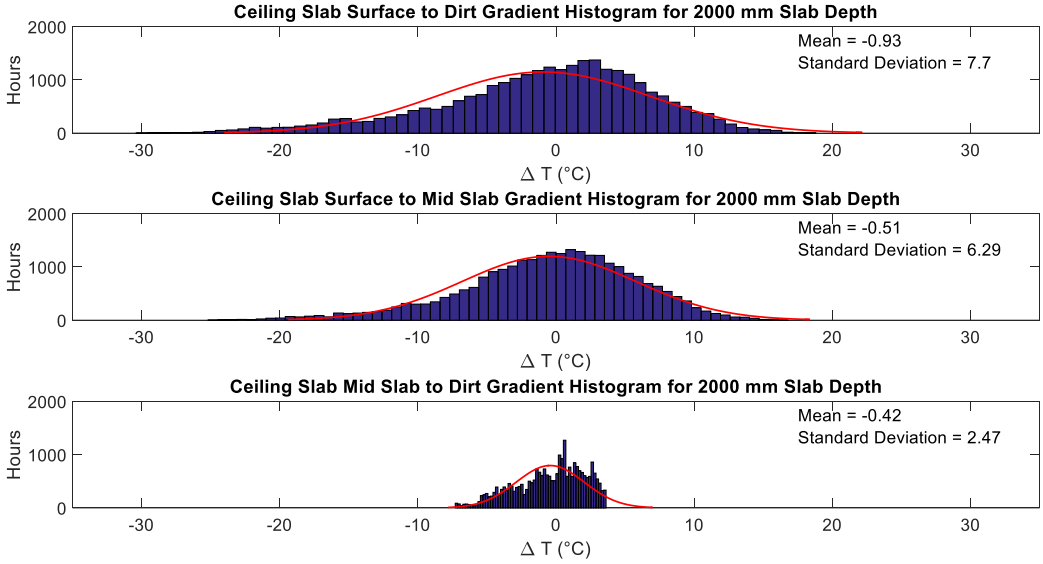

Figure 4.40. Gradient Histogram and Normal Distribution plot for Slab Depth of 2000 mm

Table 4.4. Temperature Gradients using Normal Distribution Statistics for various Slab Depths

Gradient	Slab Depth (mm)	Mean, μ (°C)	Standard Deviation, σ (°C)	μ + 1 σ (°C)	μ - 1 σ (°C)	μ + 2 σ (°C)	μ - 2 σ (°C)	μ + 3 σ (°C)	μ - 3 σ (°C)
Surface to Dirt	250	-0.19	3.99	3.8	-4.18	7.79	-8.17	11.78	-12.16
	500	-0.34	5.11	4.77	-5.45	9.88	-10.56	14.99	-15.67
	750	-0.47	5.81	5.34	-6.28	11.15	-12.09	16.96	-17.9
	1000	-0.58	6.3	5.72	-6.88	12.02	-13.18	18.32	-19.48
	1250	-0.68	6.67	5.99	-7.35	12.66	-14.02	19.33	-20.69
	1500	-0.77	7.08	6.31	-7.85	13.39	-14.93	20.47	-22.01
	1750	-0.86	7.41	6.55	-8.27	13.96	-15.68	21.37	-23.09
	2000	-0.93	7.7	6.77	-8.63	14.47	-16.33	22.17	-24.03
Surface to Mid Slab	250	-0.09	2.59	2.5	-2.68	5.09	-5.27	7.68	-7.86
	500	-0.17	3.78	3.61	-3.95	7.39	-7.73	11.17	-11.51
	750	-0.24	4.46	4.22	-4.7	8.68	-9.16	13.14	-13.62
	1000	-0.3	4.94	4.64	-5.24	9.58	-10.18	14.52	-15.12
	1250	-0.36	5.3	4.94	-5.66	10.24	-10.96	15.54	-16.26
	1500	-0.41	5.74	5.33	-6.15	11.07	-11.89	16.81	-17.63
	1750	-0.46	6.02	5.56	-6.48	11.58	-12.5	17.6	-18.52
	2000	-0.51	6.29	5.78	-6.8	12.07	-13.09	18.36	-19.38
Mid Slab to Dirt	250	-0.09	1.59	1.5	-1.68	3.09	-3.27	4.68	-4.86
	500	-0.17	1.8	1.63	-1.97	3.43	-3.77	5.23	-5.57
	750	-0.23	1.95	1.72	-2.18	3.67	-4.13	5.62	-6.08
	1000	-0.28	2.07	1.79	-2.35	3.86	-4.42	5.93	-6.49
	1250	-0.33	2.18	1.85	-2.51	4.03	-4.69	6.21	-6.87
	1500	-0.36	2.29	1.93	-2.65	4.22	-4.94	6.51	-7.23
	1750	-0.4	2.39	1.99	-2.79	4.38	-5.18	6.77	-7.57
	2000	-0.42	2.47	2.05	-2.89	4.52	-5.36	6.99	-7.83

From Table 4.4, the mean value for the gradient is near 0 °C, which again signifies the temperature differential between respective locations. This trend is consistent for the surface to dirt gradient, surface to mid slab gradient, and mid slab to dirt gradient. For all gradients investigated, the mean values become increasing lower but not significantly as the slab depth increased. There is also a noticeable increase in the standard deviation with an increase in the slab depth. When comparing gradients, the surface to dirt gradient standard deviation is the most significant. There is a slight decrease in standard deviation when comparing the surface to dirt gradient values with the surface to mid slab gradient values. The mid slab to dirt gradient standard deviation is significantly lower than the surface to dirt gradient and surface to mid slab gradient, as expected.

In regards to the temperature load provisions in CSA S6, recall that the effective temperature range for the Airport Trail Tunnel was determined to be -38°C to 34°C and for gradients a ±5°C temperature differential shall be considered in the winter and a +10°C temperature differential shall be considered in the summer for concrete slabs/walls with a depth greater or equal to 1 m,

as stated previously. The tunnel cross section temperature is within the design temperature limits of -38°C to 34°C, which is evident from the temperature envelopes in Figure 4.25 to Figure 4.32, based on the time period investigated in the model simulation. However, the gradients exceed code limits when gradient values exceed one standard deviation from the mean when considering the surface to dirt gradient for instance. These high gradients may influence the serviceability condition of the tunnel thus a structural analysis is required to further evaluate the effect of these gradients from a stress perspective. Details and results from the structural model are as follows in section 4.4.

4.4 Structural Model of Tunnel

4.4.1 Introduction

The models incorporate a transient, linear, coupled heat transfer-displacement analysis in Abaqus. This procedure is typically used to simultaneously solve for the stress/displacement and the temperature fields (Abaqus Manual Section 6.5.1). The couple analysis is used when the thermal and mechanical solutions affect each other (Abaqus Manual Section 6.5.1) thus is appropriate for the model.

4.4.2 Objectives

The objective of the structural models is to evaluate the effect of the temperature fields on the structural response i.e. stresses and displacements. The model consisted of a 2D plane cross section of the tunnel. The purpose of this model was to determine the effect of temperature gradient through the section depth on in-plane bending stresses and in-plane deflections of the walls and ceiling slab.

4.4.3 Model Inputs

Geometry

For the 2D model, the geometry is based on the Airport Trail Tunnel (see Figure 4.41). Details regarding the geometry of the model were outlined in section 4.1.4.1. A 4-node plane strain thermally coupled quadrilateral, bilinear displacement and temperature element (CPE4T) was considered for the coupled temperature-displacement 2D model.

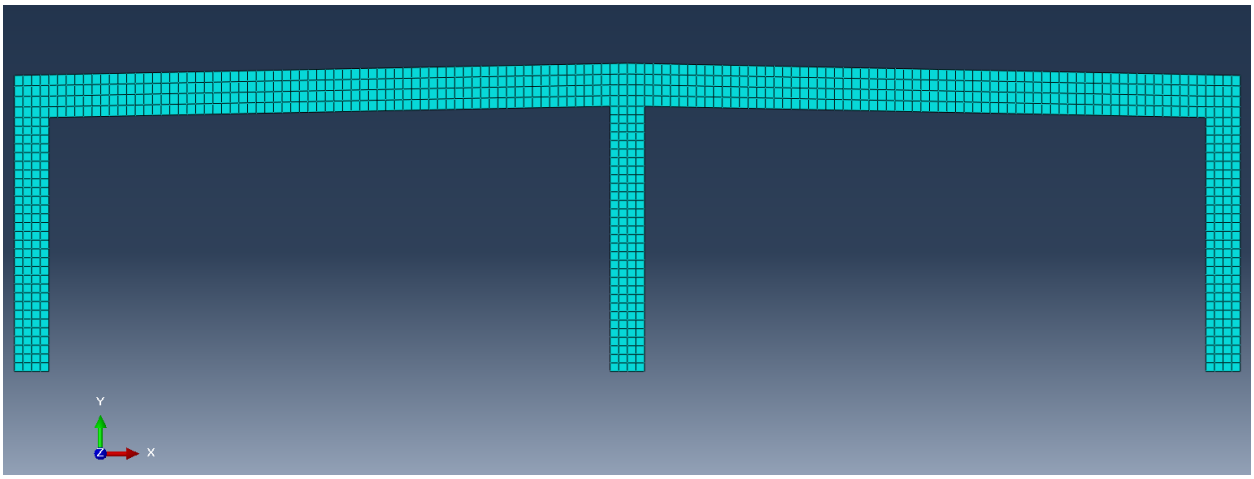

Figure 4.41. Assembly of 2D Tunnel Couple Model in Abaqus with Mesh

Material

For concrete, the baseline parameters discussed in section 4.1.4.2 were also considered in the coupled analysis. These include a density of 2400 kg/m^3, heat capacity of 900 J/kg K, and thermal conductivity of 1.5 W/m K. In addition, concrete was assumed to be a linear elastic material due to the expected magnitude of the loads and the size of the section and to simplify the analysis. The concrete mechanical properties in the model are as follows and summarized in Table 4.5: (1) coefficient of thermal expansion (α) of 10x10^{-6}/°C, (2) modulus of elasticity (*E*) of 30 000 MPa, and (3) Poisson ratio (ν) of 0.1.

Table 4.5. Mechanical properties of concrete considered in coupled analysis

Parameters	Notation	Baseline
Coefficient of Thermal Expansion	α (/°C)	10x10^{-6}
Modulus of Elasticity	*E* (MPa)	30 000
Poisson ratio	ν (unit-less)	0.1

Boundary Conditions

Similar thermal boundary conditions considered in section 4.1.4.3 were applied to the coupled model. These include a surface temperature record from Environment Canada, a convection surface condition, and long-wave radiation surface condition. The known structure-dirt interface temperature from the heat transfer analysis model was implemented as a boundary condition to reduce computational time.

For mechanical boundary conditions, the spread footing foundation was not modelled. Instead a fixed (all degrees of freedom restrained) boundary condition was assigned to the base of the walls.

Loading

The other significant load contributions considered, in addition to the temperature load, include dead load due to soil pressure above the tunnel, lateral soil pressure, and self-weight. Live loads due to airplane runway activity are expected but were not considered in the analysis due to the impact nature of the load. To determine the soil pressure, the soil density was assumed to be 20 kN/m^3. The vertical soil pressure was determined to be 60 kPa based on an average soil depth of 3 m above the tunnel. Additional vertical surcharge load was not considered. The lateral soil pressure was determined to be 160 kPa based on an 8 m wall height. The lateral pressure was applied as a constant load considering the potential for any overburden pressure. Note that hydrostatic pressure was not considered to be significant since the tunnel was designed to be free draining. It should also be noted that these loads are based on reasonable assumptions and expected to be reasonable accurate but they were not verified.

4.5 Results and Discussion of Structural Model

The coupled analysis was used to output the time history of the displacements and in-plane stress of the tunnel. The slab temperature, slab temperature gradient, in-plane stress, and vertical displacement at mid span for the roof slab is illustrated in Figure 4.42 to Figure 4.45. Note that baseline thermal properties were considered as well as the Environment Canada temperature record from May 2013 to May 2016 for CIA.

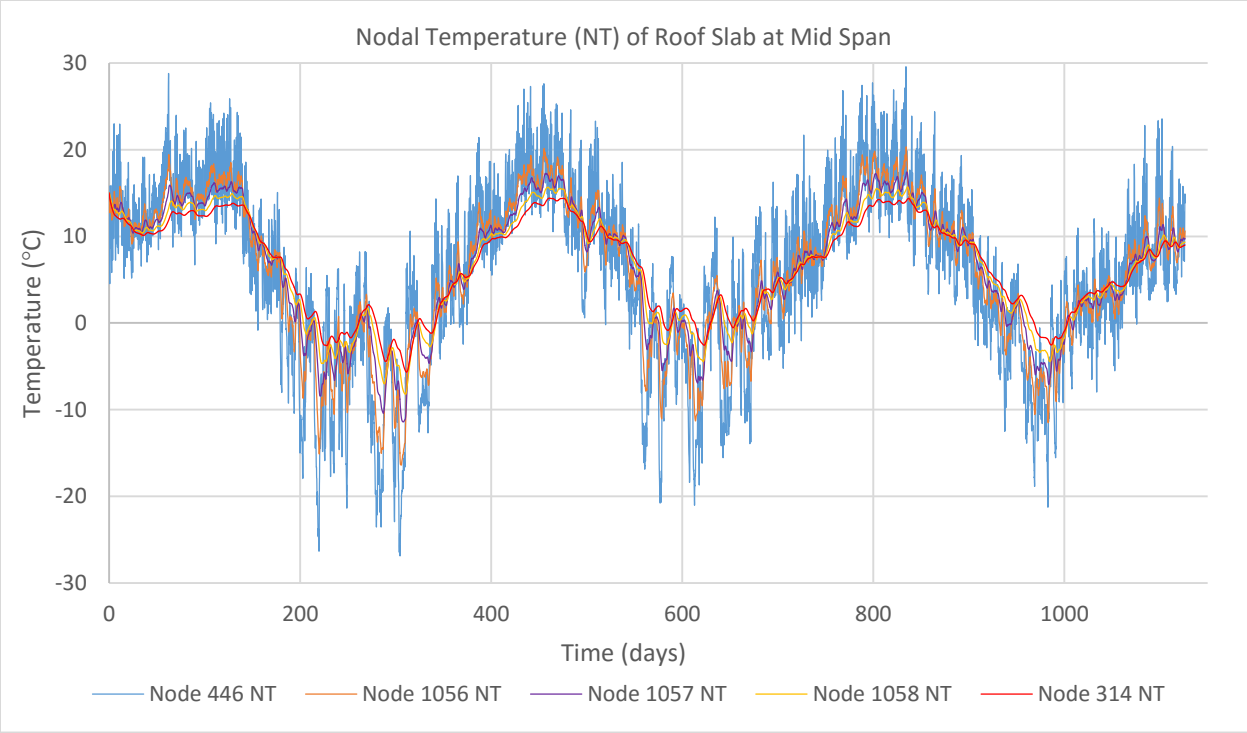

Figure 4.42. Nodal Temperature of Roof Slab at Mid Span

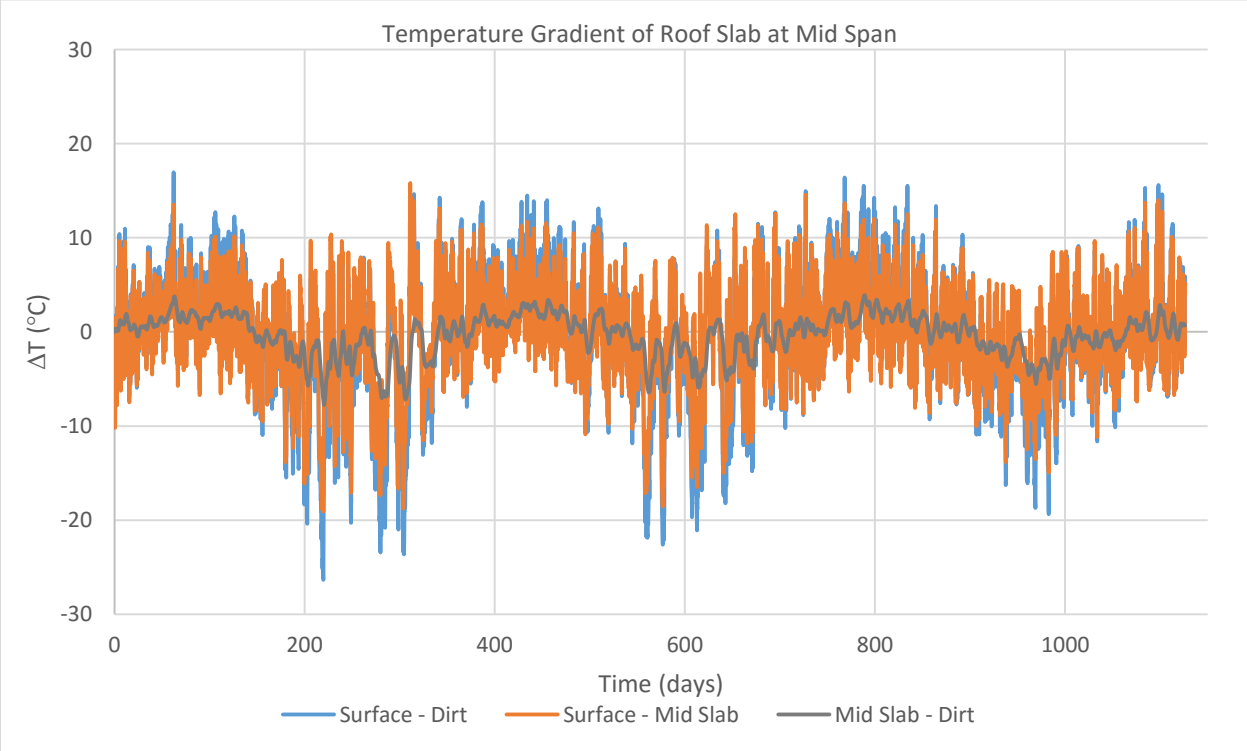

Figure 4.43. Temperature Gradient of Roof Slab at Mid Span

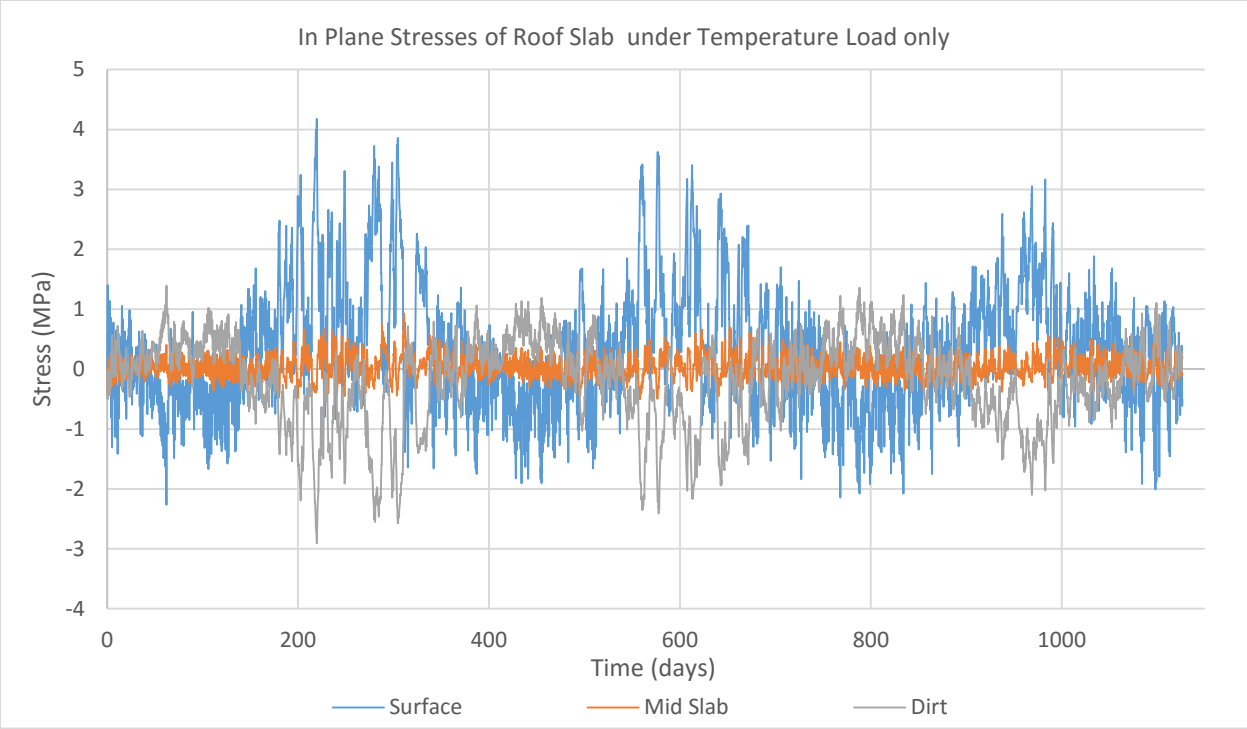

Figure 4.44. In Plane Stresses of Roof Slab at Mid Span under Temperature Load only

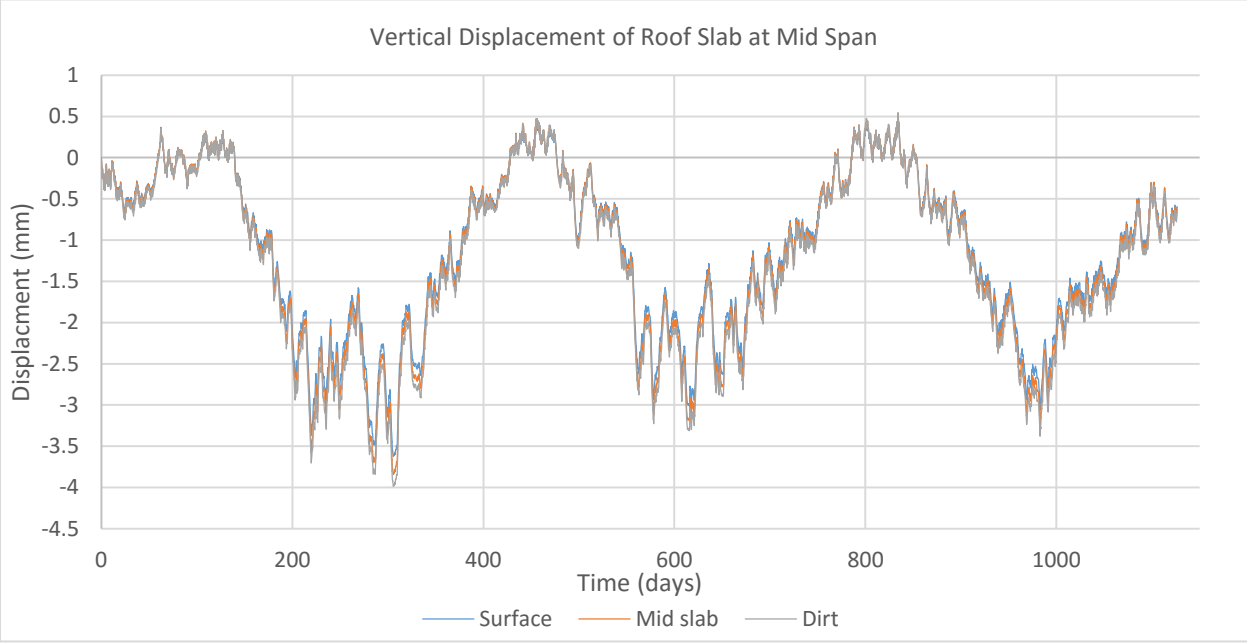

Figure 4.45. Vertical Displacement of Roof Slab at Mid Span

Note that the in plane stress and displacement time history plots, Figure 4.44 and Figure 4.45 respectively, do not consider the contribution of dead loads so that temperature load effects could be evaluated alone initially.

Nodal temperature and temperature gradient trends result have been discussed previously in section 4.3. To reiterate, the nodal temperature time history is sinusoidal in nature. Note that the coldest temperatures within the 3 year time period occurred in 2013 (first year). These temperatures correspond to the highest temperature gradients as evident in Figure 4.43. Also note that the surface to dirt and surface to mid slab gradients are relatively similar as it was determined that the majority of the temperature differences were near the slab surface exposed to ambient temperatures. The mid slab to dirt is not as significant.

For the structural response, in plane stresses and displacements were investigated. In plane stresses refers to the principle bending stresses in a member. Node 446 represents a surface node at mid span, Node 1057 is a mid-slab node at mid span, and Node 314 is the exterior most node at mid span. From Figure 4.44, the in plane stress response is synchronous with the temperature response. Under temperature load alone, there are stress reversals in the slab i.e. transition from tensile stress to compressive stress and vice versa. Also, the stress at mid span (Node 1057) fluctuates around zero stress since it is near the neutral axis of the section.

From Figure 4.45, the vertical displacements are also synchronous with the temperature and stress response. The displacement is consistent through the section since there is a negligible difference between top and bottom nodes. Note that the maximum displacement did not correspond to the maximum gradient in the time history most likely due to the temperature/stress condition from the previous step.

Since the tensile capacity of concrete is low, tensile stresses in the concrete are of concern as they may cause the member to crack. Cracks in reinforced concrete may lead to serviceability issues such as corrosion if water penetrates the member. For concrete with a compressive strength, f_c', of 35 MPa to 45 MPa the tensile capacity is approximately 3.55 MPa to 4.02 MPa considering the modulus of rupture of concrete (CSA A23.3 2004 Clause 8.6.4). From Figure 4.44, in some instances the tensile stresses in the slab exceeds the tensile capacity of concrete. Recall that the model assumed linear elastic, isotropic material which was determined to be acceptable for this application based on previous studies and current design codes and practices.

The effect of considering linear elastic behavior is such that tensile stresses will be overestimated once cracking occurs. In a cracked section, partial restrain in the member is released which causes a reduction in stress. Note that since thermal stresses are dependent on the extent of thermal restraint, the initial condition of the member will affect these stresses. For instance, cracking due to heat of hydration, shrinkage, and creep effects. Internal temperature stresses can be induced during the construction process where creep and shrinkage effects are present thus these effects are difficult to predict either experimentally or numerically (Léger et. al, 1993). The magnitude of the thermal stresses are also dependent on the temperature field distribution, the mechanical properties of the concrete, and the member restraints (Léger et al., 1993).

Creep is deformation (increased strain) under sustained/constant stress which is a common phenomenon in concrete. Thus, since self-equilibrating stress and indeterminate forces caused by temperature change are proportional to the modulus of elasticity, E, the thermal effects have the tendency to be overestimated when the value of E used in the analysis is based on the relation of stress to instantaneous strain when creep is ignored. (Ghali et al., 2009). Again, as a result stresses will be overestimated.

When the soil pressure loads and self-weight, mentioned in section 4.4.3 are considered, the resulting tensile stress at mid slab of the roof slab was 3.65 MPa. This implies that the temperature load is significant since it can cause stresses in similar order of magnitude as the dead load. It also indicates that the combination of the dead load and temperature load exceeds the tensile capacity of the concrete. In regards to the temperature design gradients, the high gradients have the potential to produce high tensile stresses thus must be considered.

Figure 4.46 and Figure 4.47 illustrate the temperature distribution corresponding to the maximum surface to dirt temperature gradient along with the associated in-plane principal stress distribution resulting in the maximum tensile stress state, respectively. Note that tensile surface stress extend from the interior roof slab surface to the top portions of the interior surface of the exterior wall. Also note that since the interior wall is exposed to ambient temperature on both surfaces, the temperature gradient and corresponding stresses/displacements were expected to be negligible and thus not evaluated.

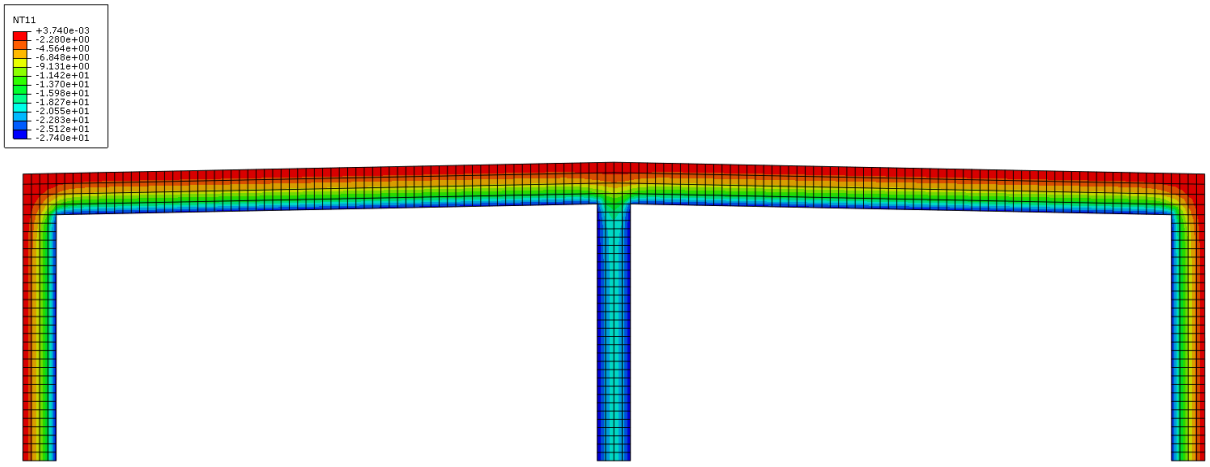

Figure 4.46. Nodal temperature distribution at hour 5272 corresponding to maximum surface to dirt temperature gradient

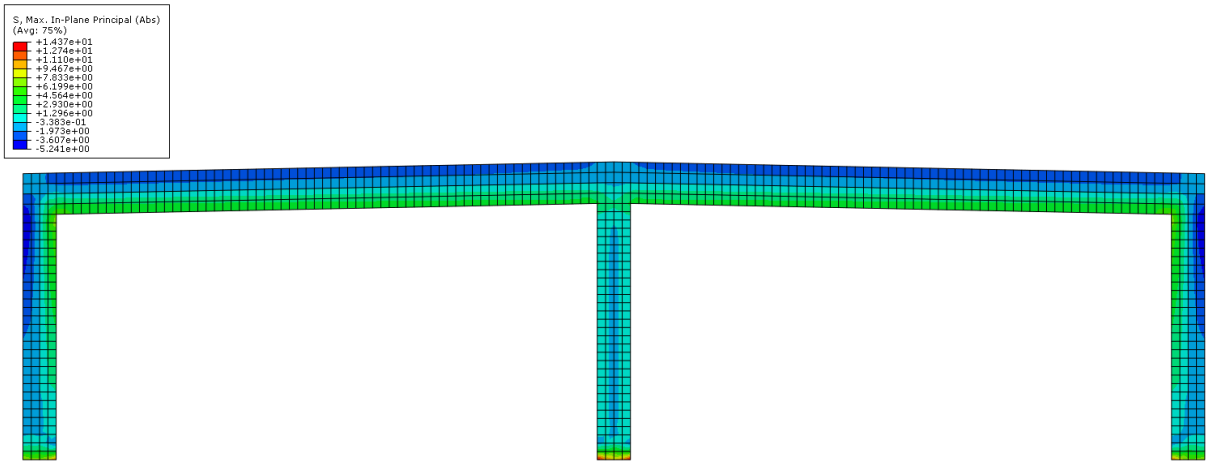

Figure 4.47. In-plane principal stress distribution at hour 5272 corresponding to maximum tensile stress

The critical temperature profiles for the roof slab correspond to the maximum and minimum surface to dirt temperature gradient as illustrated in Figure 4.48. The curves were interpolated using a bilinear scheme for simplicity. As mention previously, under transient conditions the fluctuations in ambient temperature at the surface results in the highest temperature fluctuations up to approximately 300 mm into the member. Thus, a bilinear curve were chosen to represent (1) the region between the surface and 300 mm into the slab and (2) 300 mm to 1250 mm (concrete-soil boundary). Recall that a positive gradient (temperature differential) occurs when the temperature of the surface is higher than the dirt. Likewise, a negative gradient occurs with the temperature of the surface is lower than the dirt. For the minimum and maximum curves, line 1 fits the curve well however line 2 slightly deviates from the curves. For the positive gradient, the temperature differential (ΔT) for line 1 and line 2 were 9.1°C and 7.9°C. For the negative gradient, the temperature differential (ΔT) for line 1 and line 2 were 11.7°C and 14.6°C.

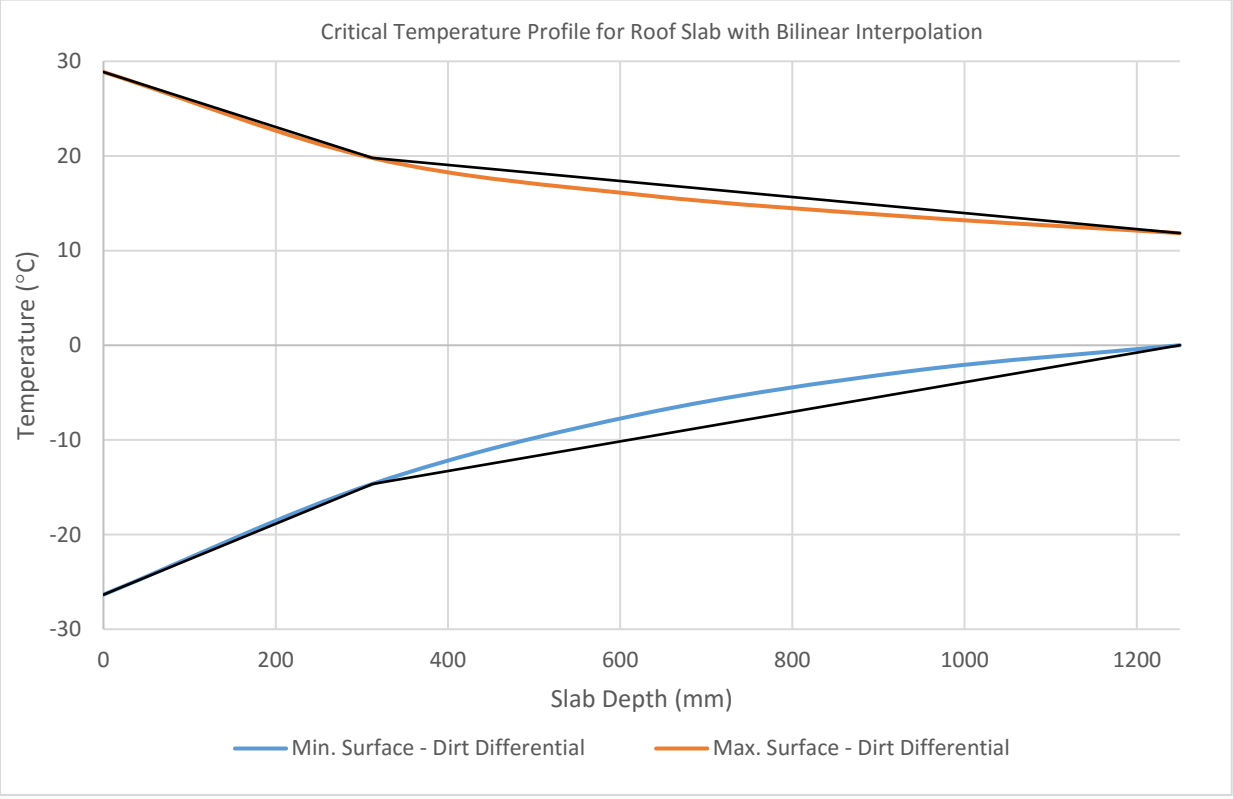

Figure 4.48. Critical Temperature Profile for Roof Slab with Bilinear Interpolation

Chapter 5: Airport Trail Tunnel Monitoring

5.1 Analysis of Tunnel Data

5.1.1 Objective

The objective of the field data analysis was to investigate the temperature field of the tunnel and temperature gradients in the walls and ceiling slab of tunnel and compare findings with existing design code provisions related to temperature loading. Results from the field data analysis could also be compared to the results from the finite element model results discussed in the previous chapter. In addition, the displacement at a movement joint was also considered to evaluate movement of the structure due to thermal loads and the location of movement joints in tunnels. Data was analyzed from September 2014 to January 2016.

5.1.2 Temperature Sensor Data

Various components of the tunnel such as the portals (East and West), ceilings (North and South), exterior walls (North and South), and interior wall were analyzed at 7 chosen sensor locations approximately 100 m apart listed below. The selected locations was also based on the condition of the sensors. The number of sensors at each Lead/Infill section varied. The specific sensor for each location can be found below in Table 5.1.

- Lead 01 (West Portal)
- Lead 11 (~138 m from West Portal)
- Lead 19 (~238 m from West Portal)
- Infill 28 (~350 m from West Portal)
- Lead 35 (~438 m from West Portal)
- Lead 45 (~563 m from West Portal)
- Infill 50 (East Portal)

Table 5.1. Temperature sensors used in data analysis

Location	Lead/Infill	Sensor ID
North Ceiling	Lead 11	Sensor ID: 07-16-12-01
	Lead 19	Sensor ID:08-09-13-13
	Infill 28	Sensor ID: 08-09-13-15
	Lead 35	Sensor ID: AA-AA-AD-1A
	Lead 45	Sensor ID: 08-09-13-06
	Infill 50	Sensor ID: 08-09-13-09
South Ceiling	Lead 11	Sensor ID: 08-09-13-05
	Lead 19	Sensor ID: 08-05-13-05
	Infill 28	Sensor ID: AA-AA-AD-24
	Lead 35	Sensor ID: AA-AA-AD-1E
	Lead 45	Sensor ID: 08-09-13-0F
	Infill 50	Sensor ID: AA-AA-AD-1D
North Wall	Lead 35	Sensor ID: 13-12-06-10
	Infill 50	Sensor ID: 08-09-13-08
Middle Wall	Lead 11	Sensor ID: 08-09-13-0E
	Lead 35	Sensor ID: 08-9-13-17
	Infill 50	Sensor ID: AA-AA-AD-21
South Wall	Lead 11	Sensor ID: 08-09-13-20
	Lead 35	Sensor ID: AA-AA-AD-20
West Portal	-	Sensor ID: 00-00-10-24
	Lead 01	Sensor ID: 13-12-06-12
	Lead 01	Sensor ID: 09-09-13-10
East Portal	-	Sensor ID: 00-00-10-28
	Infill 50	Sensor ID: 08-09-13-09
	Infill 50	Sensor ID: 08-09-13-08
	Infill 50	Sensor ID: AA-AA-AD-21
	Infill 50	Sensor ID: AA-AA-AD-1D

The approximate location of the temperature sensor housings are illustrated in Figure 5.1 to Figure 5.7 adopted from CH2M drawings. The figures provide a profile view of the tunnel cross section looking toward the east direction. Note that only the sensors selected for analysis are illustrated in the figures.

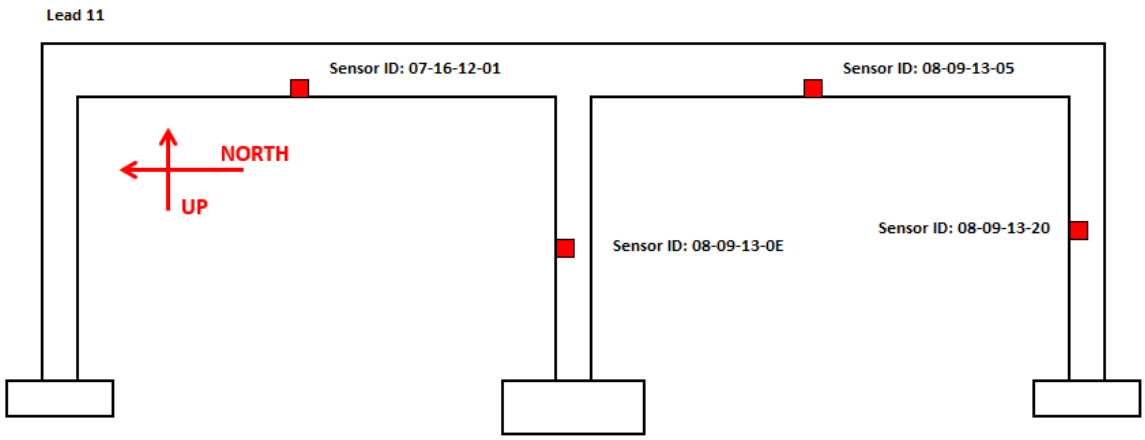

Figure 5.1. Profile view of the approximate temperature sensor housing locations at Lead 11 (adopted from CH2M drawings)

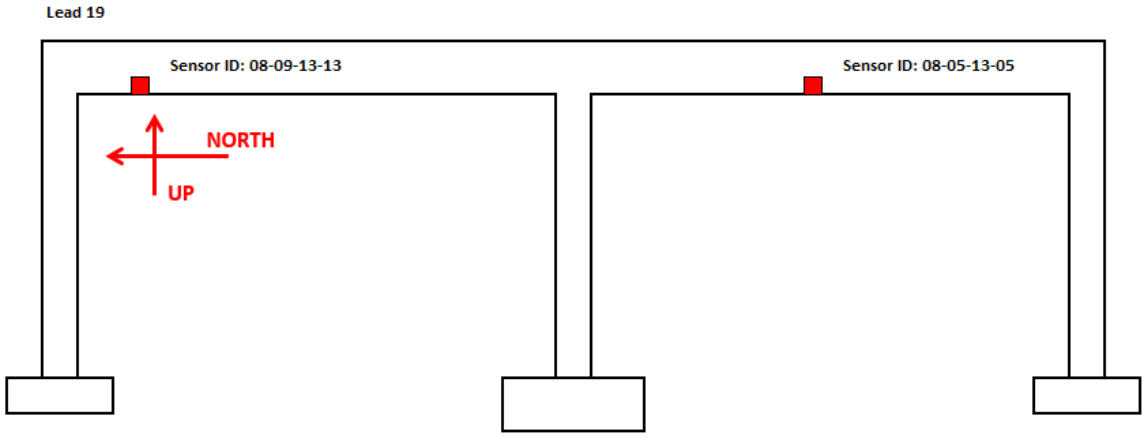

Figure 5.2. Profile view of the approximate temperature sensor housing locations at Lead 19 (adopted from CH2M drawings)

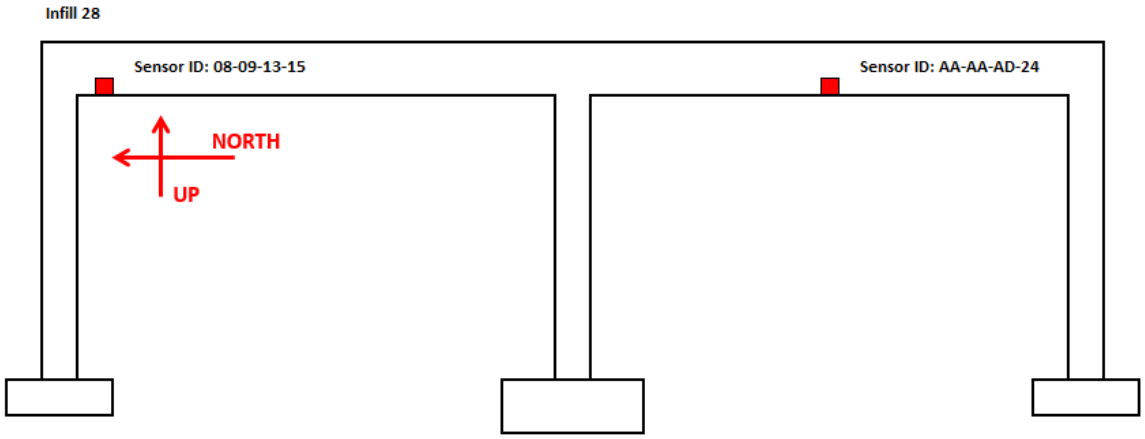

Figure 5.3. Profile view of the approximate temperature sensor housing locations at Infill 28 (adopted from CH2M drawings)

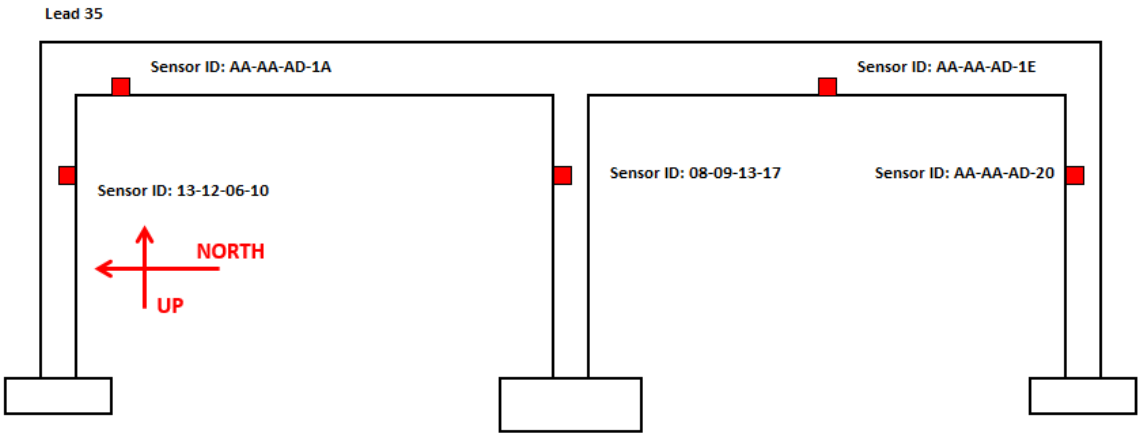

Figure 5.4. Profile view of the approximate temperature sensor housing locations at Lead 35 (adopted from CH2M drawings)

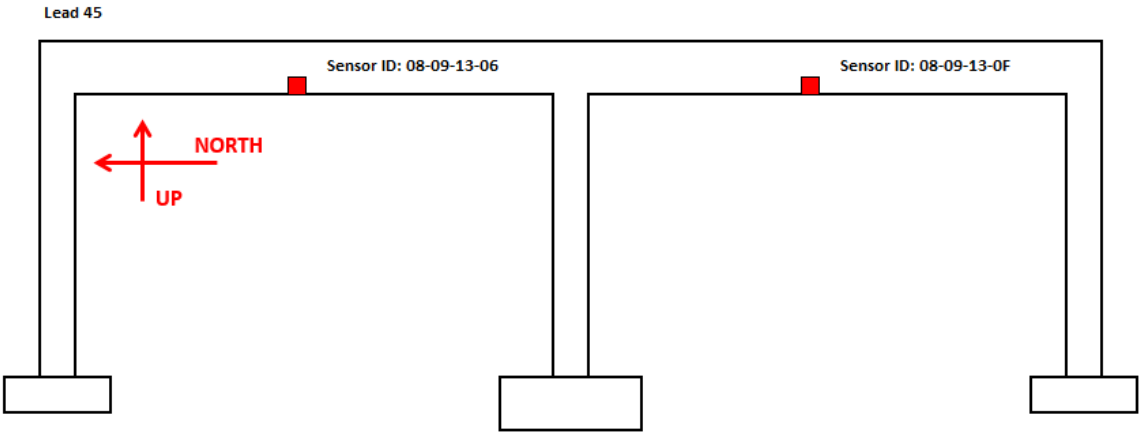

Figure 5.5. Profile view of the approximate temperature sensor housing locations at Lead 45 (adopted from CH2M drawings)

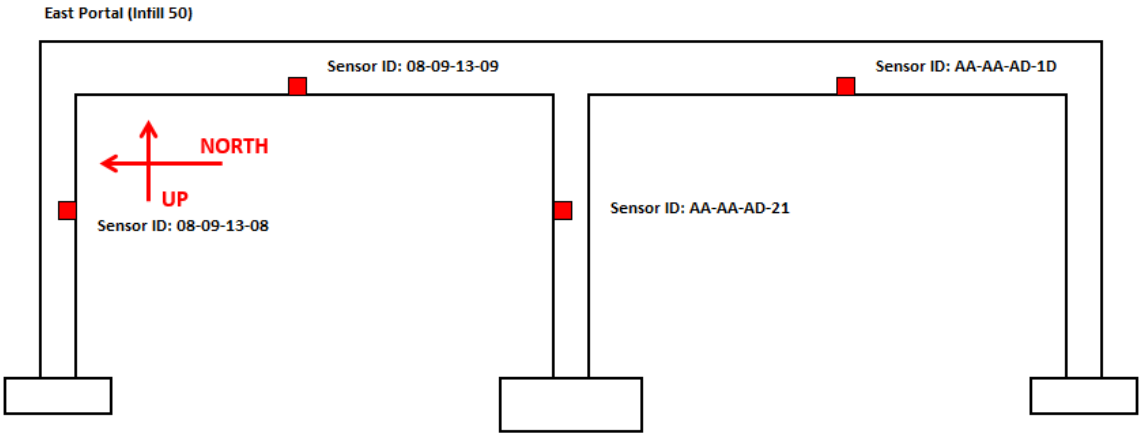

Figure 5.6. Profile view of the approximate temperature sensor housing locations at East Portal (Infill 50) (adopted from CH2M drawings)

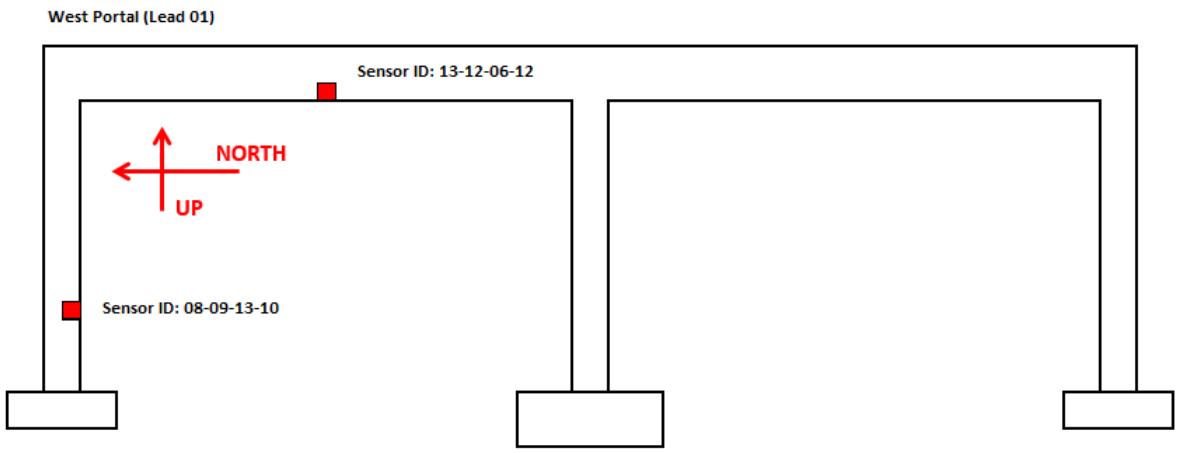

Figure 5.7. Profile view of the approximate temperature sensor housing location at West Portal (Lead 01) (adopted from CH2M drawings)

5.1.2.1 Tunnel Portal Temperatures

The temperature at the East Portal was compared to Environment Canada data (see Figure 5.8). At the West Portal, the Gateway SeniMax 10-24 surface temperature sensor was damaged/malfunctioning as well as the Lead 01 sensor. Likewise, at the East Portal the Gateway SeniMax 10-28 was determined to be damaged. These sensors were neglected from the analysis.

Since the Portals are located at the tunnel opening, it is expected that the surface temperatures at the Portals would be similar to Environment Canada data (ambient temperature), however, there are discrepancies as can be observed in Figure 5.9 and Figure 5.10, which are discussed in more detail below.

Figure 5.9 illustrates a typical winter temperature time period from November to December 2014. It can be observed that the difference between sensor data and Environment Canada data is highest at peak negative temperatures. It can also be observed that the sensor readings are relatively consistent however discrepancies between sensors occur at peak negative temperatures.

Figure 5.10 illustrates a typical summer temperature time period from June 2015 to July 2015. It can be observed that there are discrepancies at minimum peak temperatures between sensor data however they are not as pronounced as ones seen in Figure 5.9. Unlike Figure 5.9, small

discrepancies at the maximum peak temperatures can be observed. There is no lag time between sensor and Environment Canada data, which is expected at the portal location.

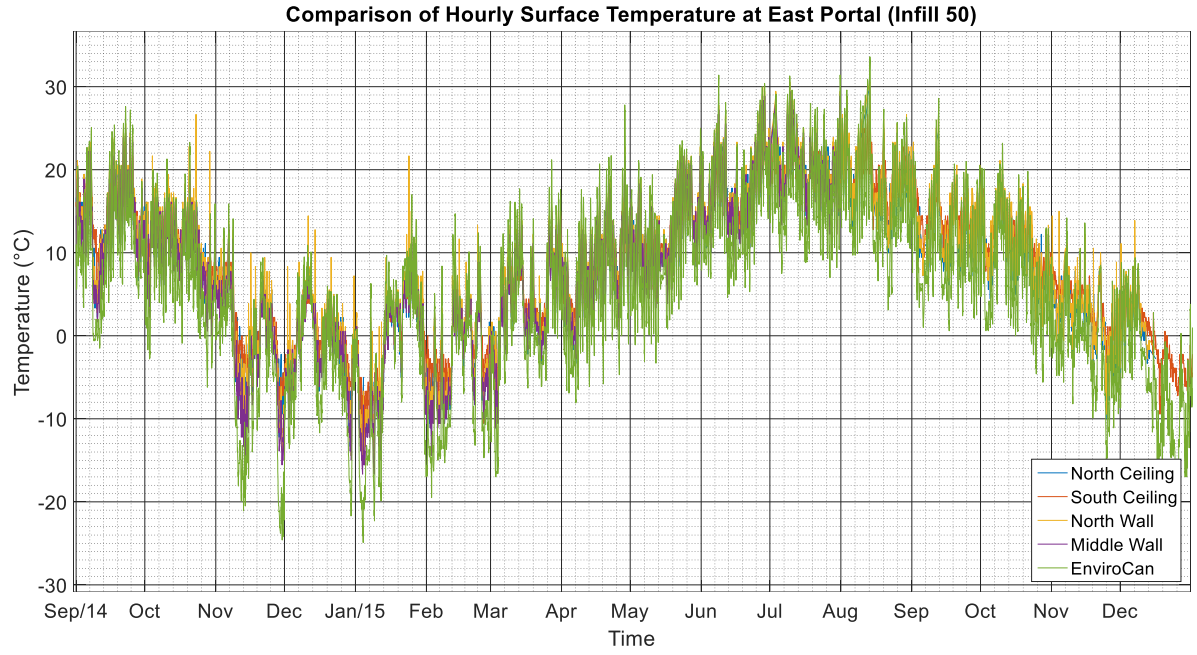

Figure 5.8. Comparison of Hourly Surface Temperature at East Portal (Infill 50)

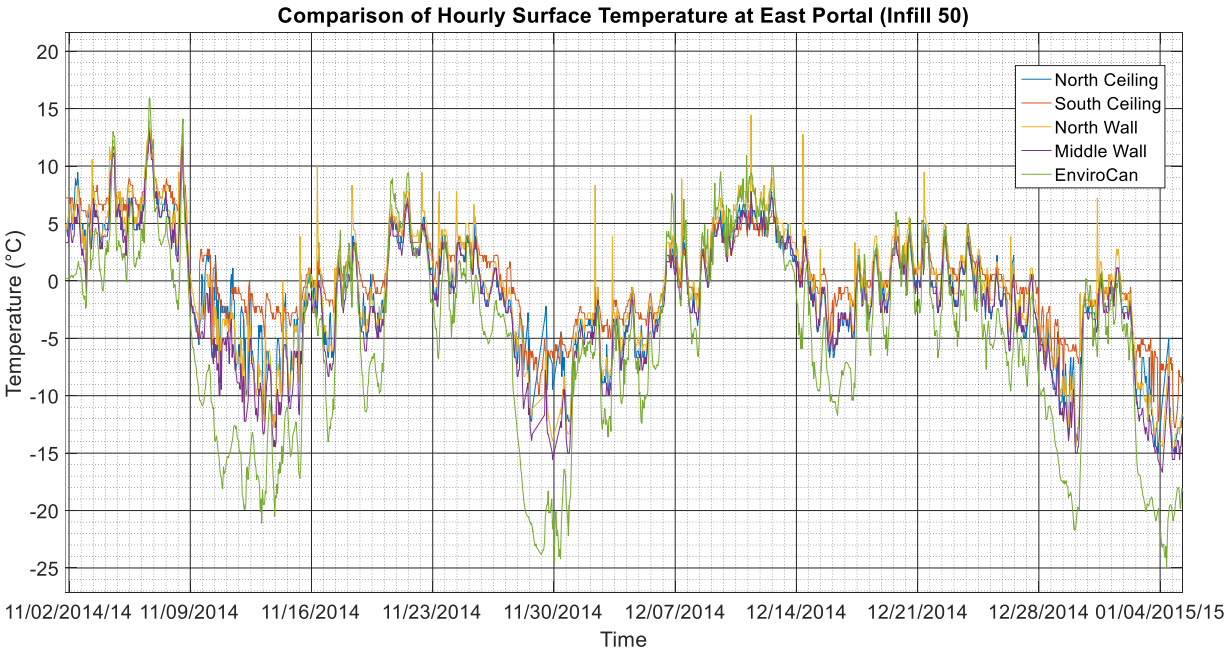

Figure 5.9. Comparison of Hourly Surface Temperature at East Portal from November 2014 to December 2014

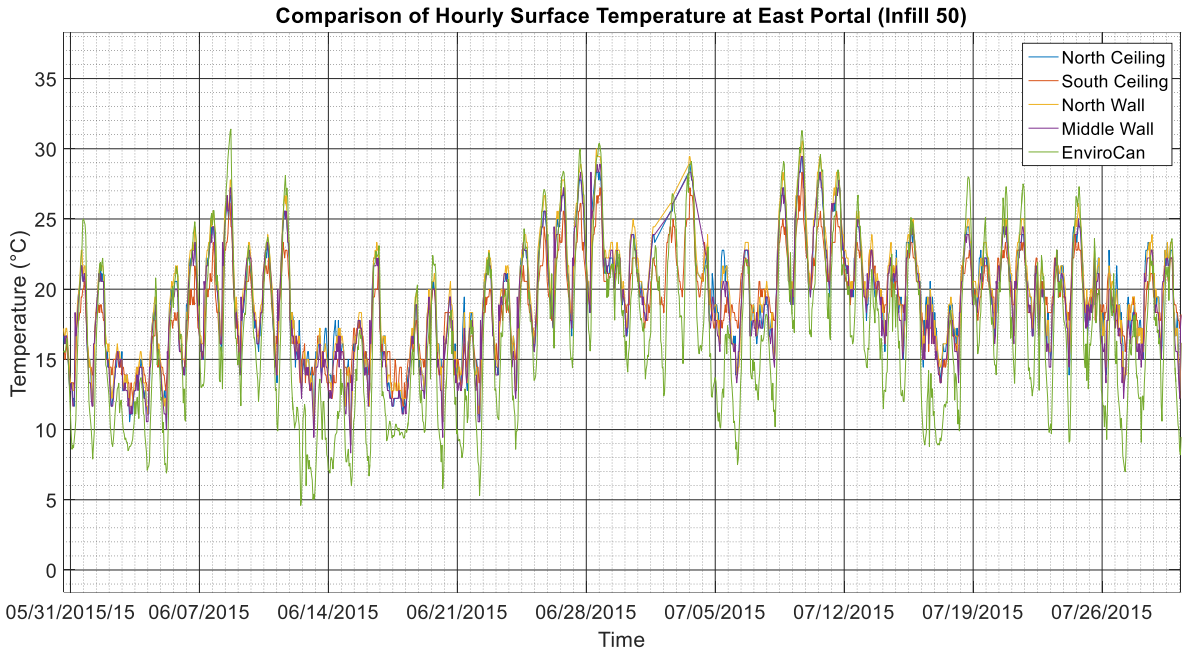

Figure 5.10. Comparison of Hourly Surface Temperature at East Portal from June 2015 to July 2015

5.1.2.2 *Longitudinal Temperature Profile*

The longitudinal temperature profile for the tunnel was analyzed using the North and South ceiling slab surface sensor data (see Figure 5.11 to Figure 5.16). The longitudinal temperature variation throughout the tunnel was generally uniform. Fluctuations in temperature are in rhythm or synchronous at the various locations in the tunnel. The largest difference in temperature was at the portal locations as expected (Infill 50). It can also be observed that the surface temperature in the North and South tunnels were relatively similar.

When comparing the maximum surface temperature difference between the portal (Infill 50) and mid tunnel location (Infill 28) with respect to time, a maximum difference of 8°C and 9.5°C was observed at the North and South ceiling sensor locations, respectively.

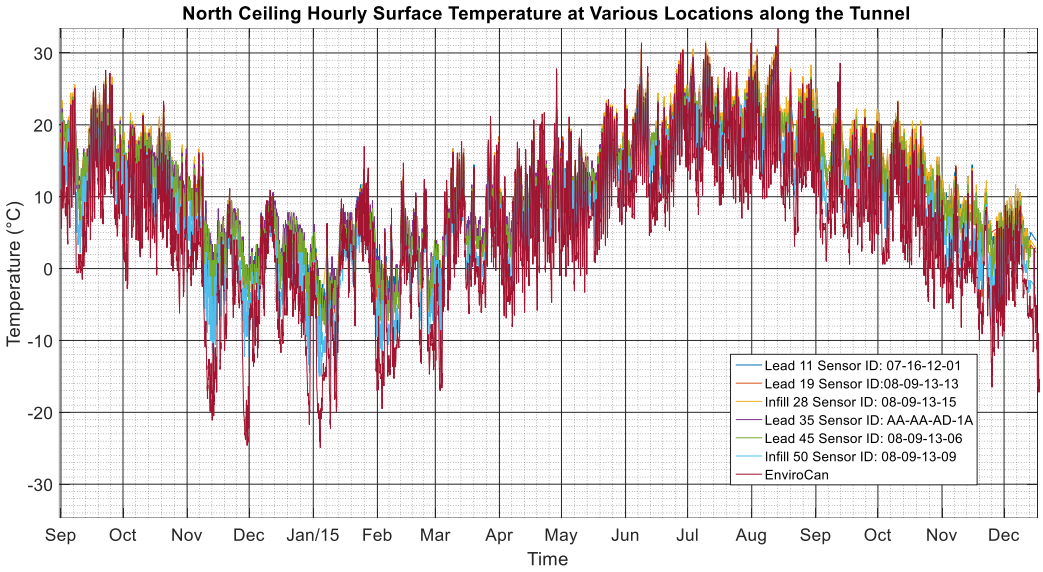

Figure 5.11. North Ceiling Hourly Surface Temperature at Various Locations along the Tunnel

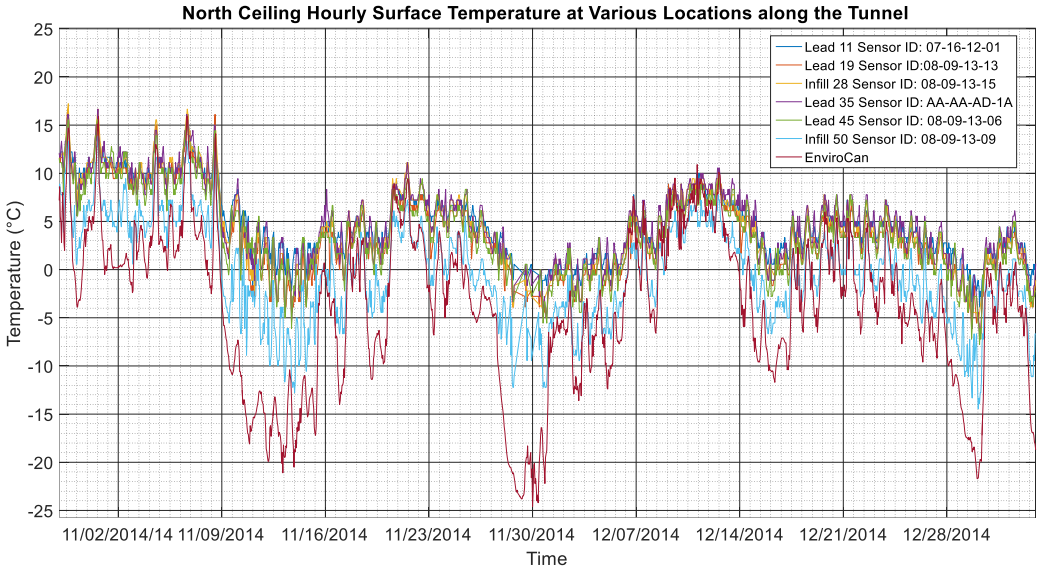

Figure 5.12. North Ceiling Hourly Surface Temperature from November 2014 to December 2014

In the winter, the tunnel surface temperature is generally higher than the Environment Canada temperature throughout. Temperature differences are up to approximately 12°C at peak negative temperatures.

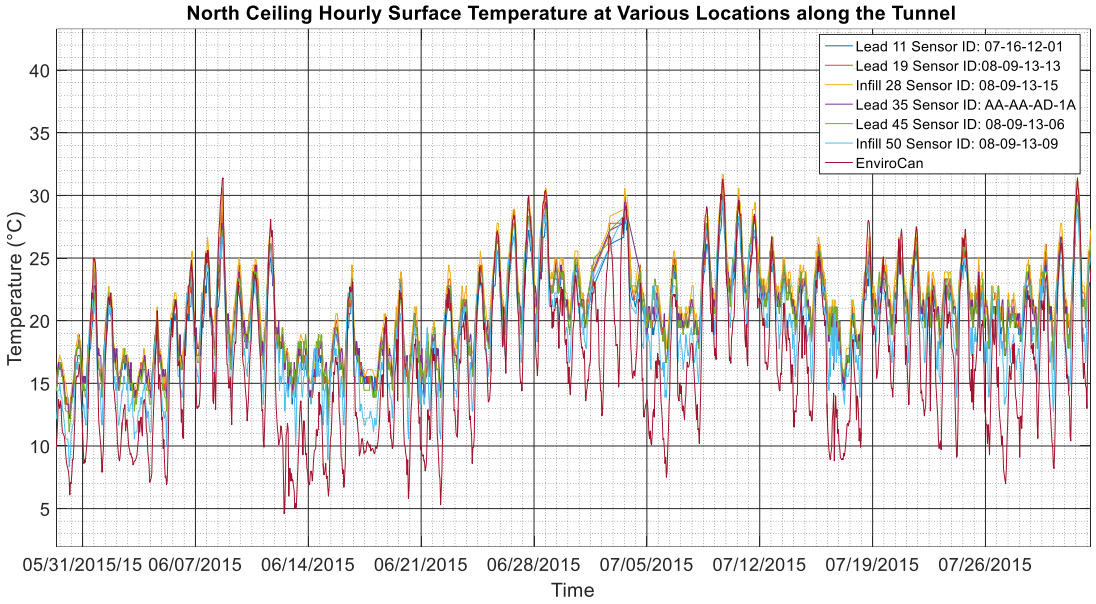

Figure 5.13. North Ceiling Hourly Surface Temperature from June 2015 to July 2015

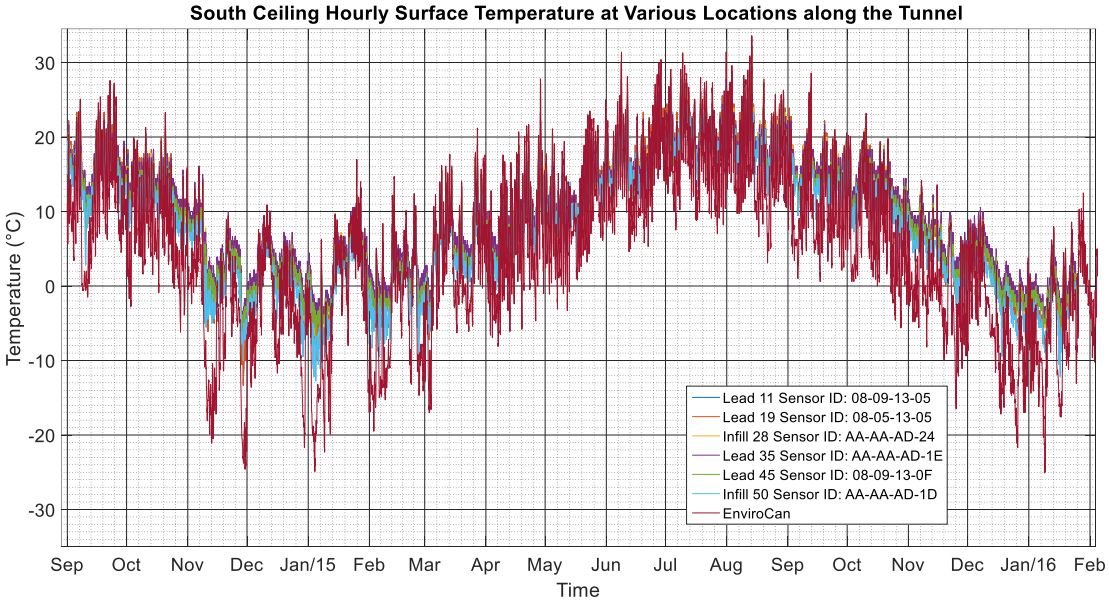

Figure 5.14. South Ceiling Hourly Surface Temperature at Various Locations along the Tunnel

In the summer, temperature difference between the tunnel and Environment Canada are less apparent. It remains evident that at peak drops in temperature, the tunnel temperature remains above Environment Canada although peak increases in temperature are similar.

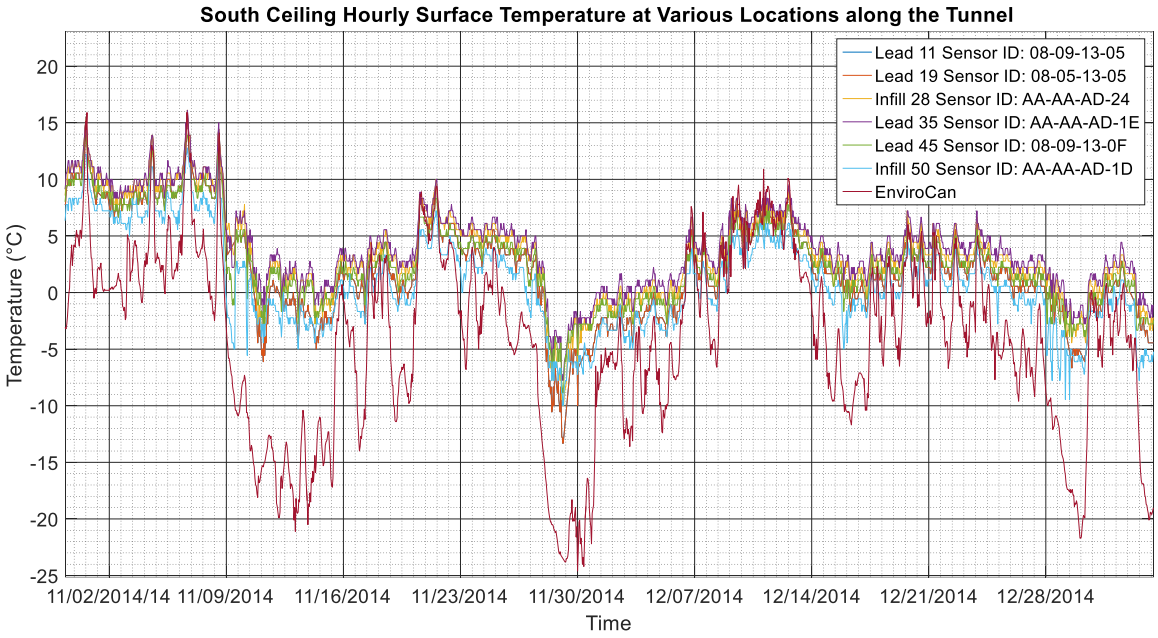

Figure 5.15. South Ceiling Hourly Surface Temperature from November 2014 to December 2014

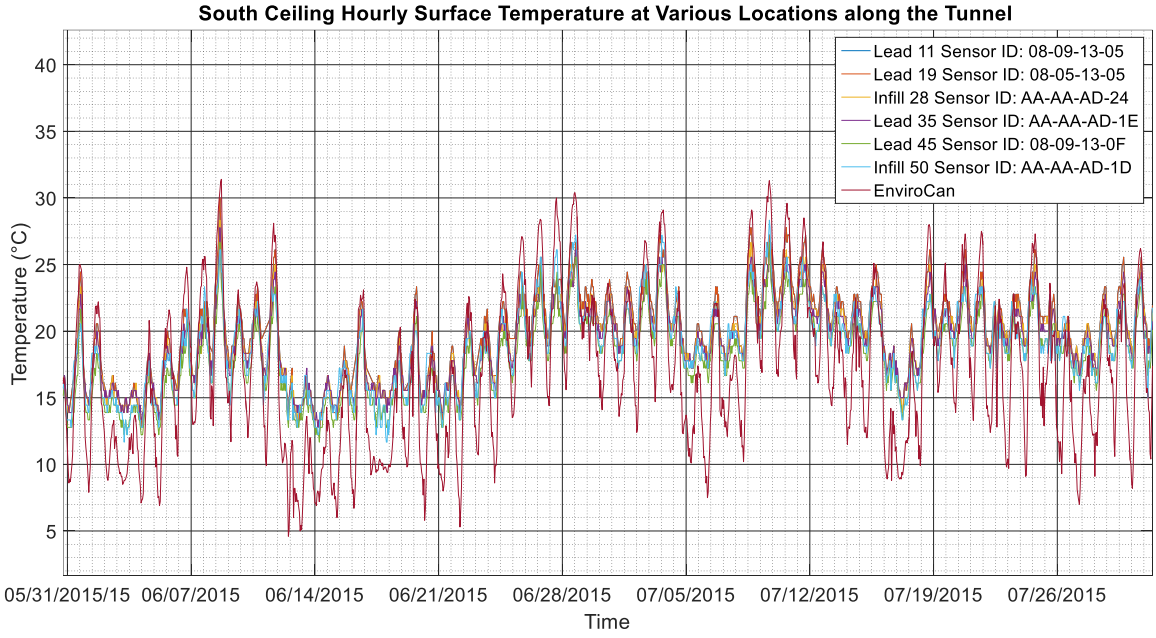

Figure 5.16. South Ceiling Hourly Surface Temperature from June 2015 to July 2015

Trends in the North and South ceiling mid-slab and dirt temperature record were also investigated (see Figure 5.17 to Figure 5.20). It can be observed that the dirt and mid slab temperature at various locations along the tunnel follows the same trend as the surface temperature. The most notable difference is that daily temperature cycles are not as noticeable in the dirt and mid-slab. A physical reason to account for the lack for daily temperature cycles in the data is the low conductivity of concrete along with the depth of the wall. Another, possible reason may be the resolution of the sensor. Temperature probes in the slab have a lower accuracy compared to the surface sensors (i.e. 1°C vs. 0.5°C) which may affect the results. It can also be observed that the temperature fluctuation in mid-slab and dirt temperature are more apparent at the East portal location (Infill 50) for both the North and South ceiling. A possible reason for this is the fact that the portals experiences temperatures closest to ambient temperature thus may experience higher fluctuations.

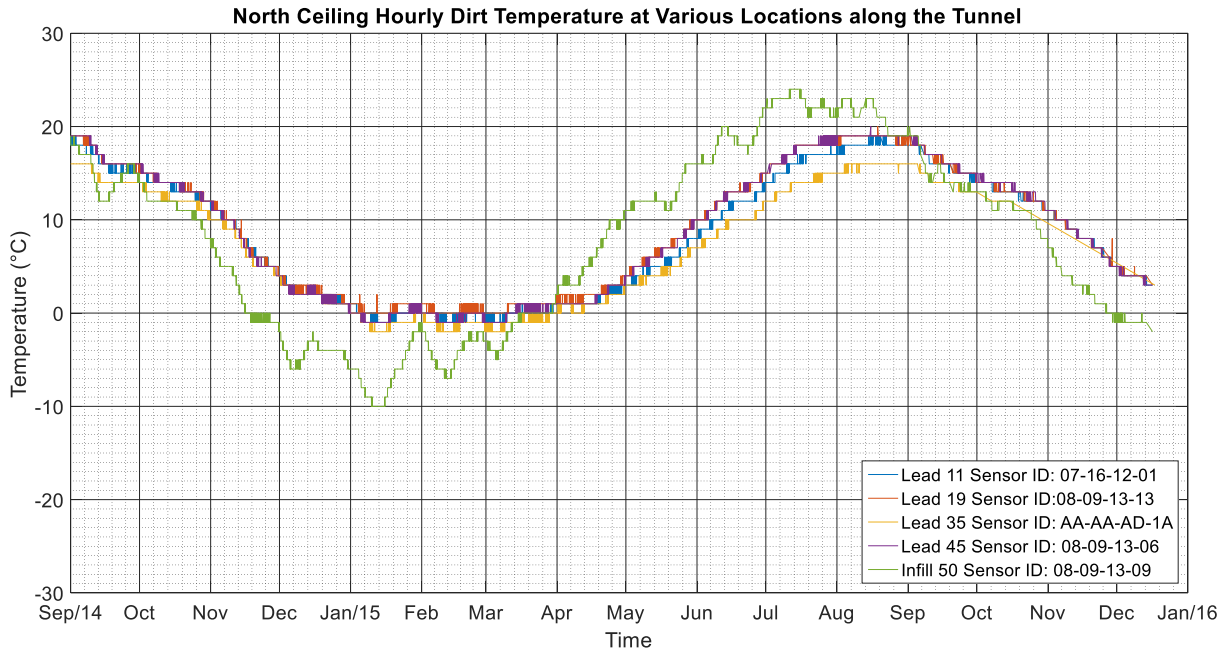

Figure 5.17. North Ceiling Hourly Dirt Temperature at Various Locations along the Tunnel

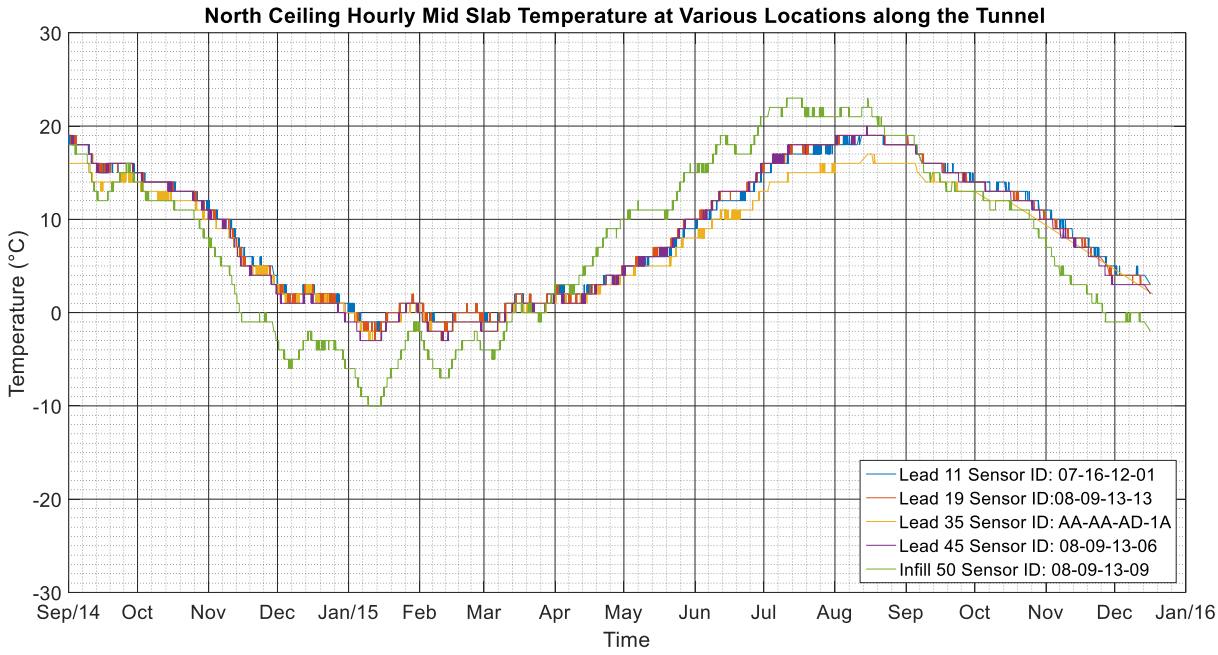

Figure 5.18. North Ceiling Hourly Mid Slab Temperature at Various Locations along the Tunnel

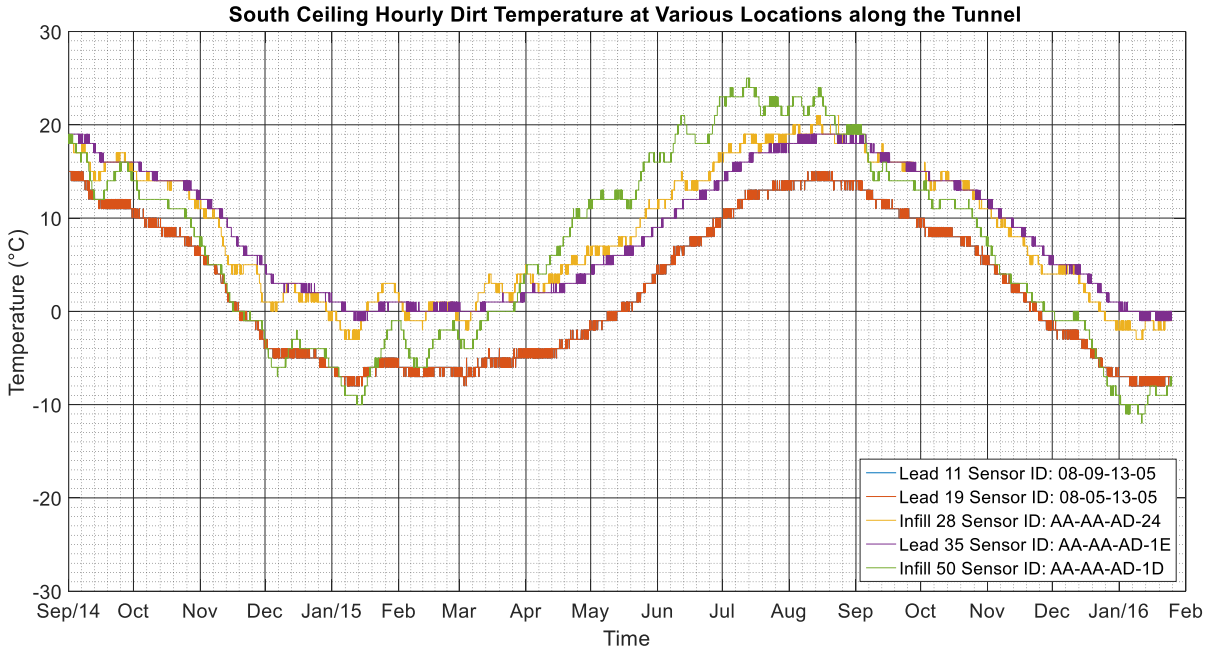

Figure 5.19. South Ceiling Hourly Dirt Temperature at Various Locations along the Tunnel

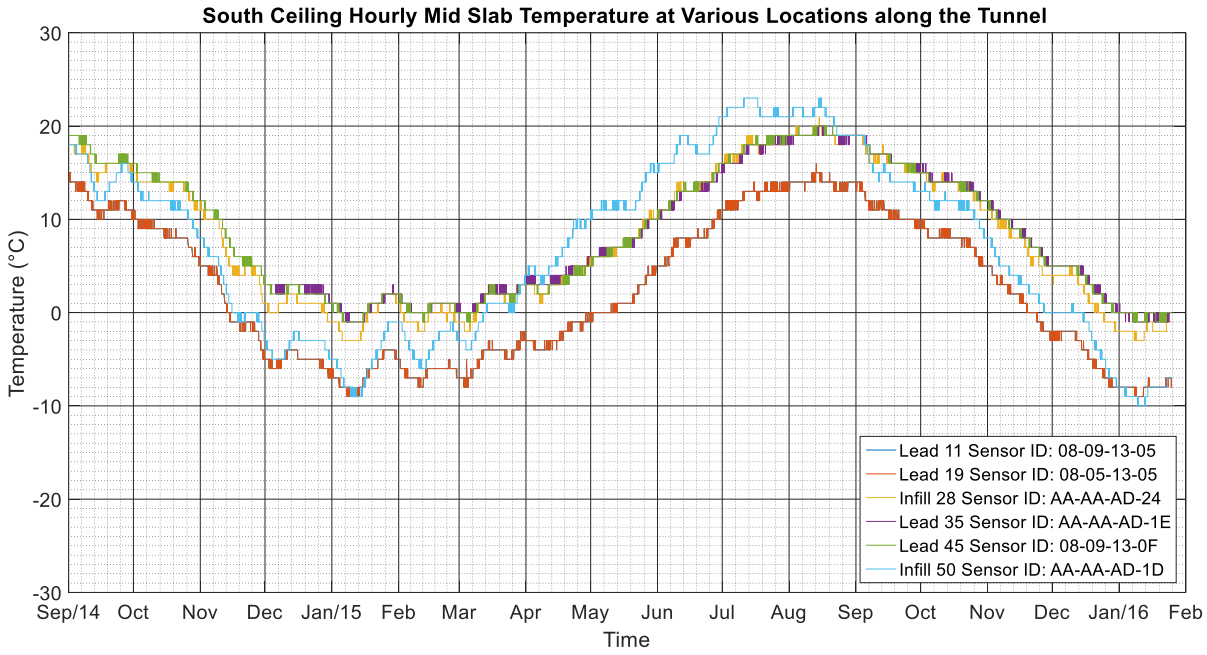

Figure 5.20. South Ceiling Hourly Mid Slab Temperature at Various Locations along the Tunnel

5.1.2.3 Lead 11 Sensor Temperature Comparison

Temperature data from Lead 11 of the tunnel was chosen to analyze the gradients in the exterior walls, ceiling slabs, and middle wall. See Figure 5.21, Figure 5.22, Figure 5.23, and Figure 5.24 for hourly temperatures at the North ceiling, South ceiling, South wall and middle wall respectively and the overall comparison of all Lead 11 sensors in Figure 5.25.

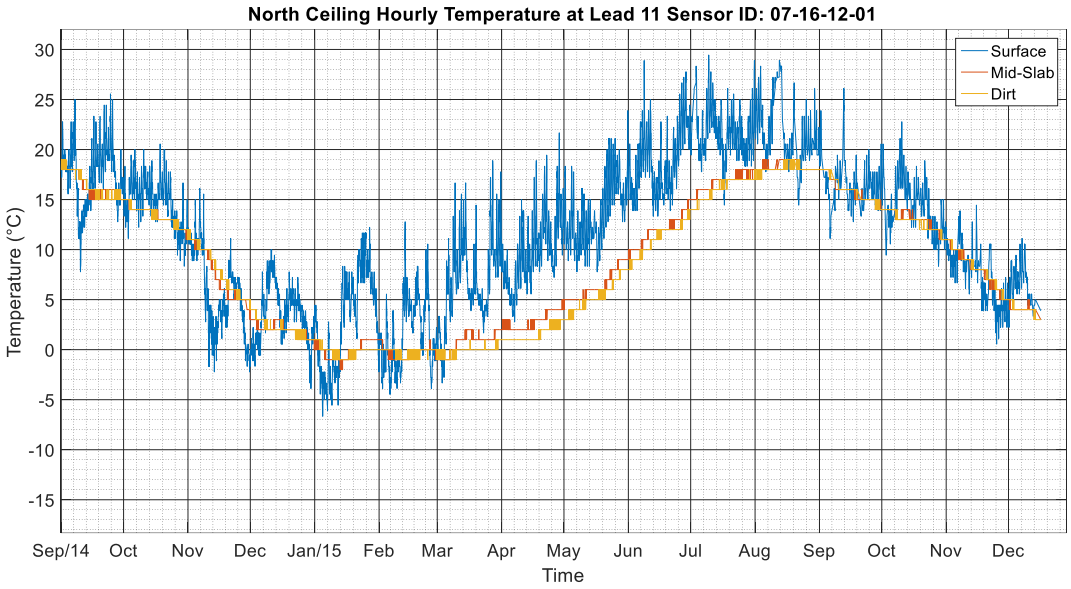

Figure 5.21. North Ceiling Hourly Temperature at Lead 11

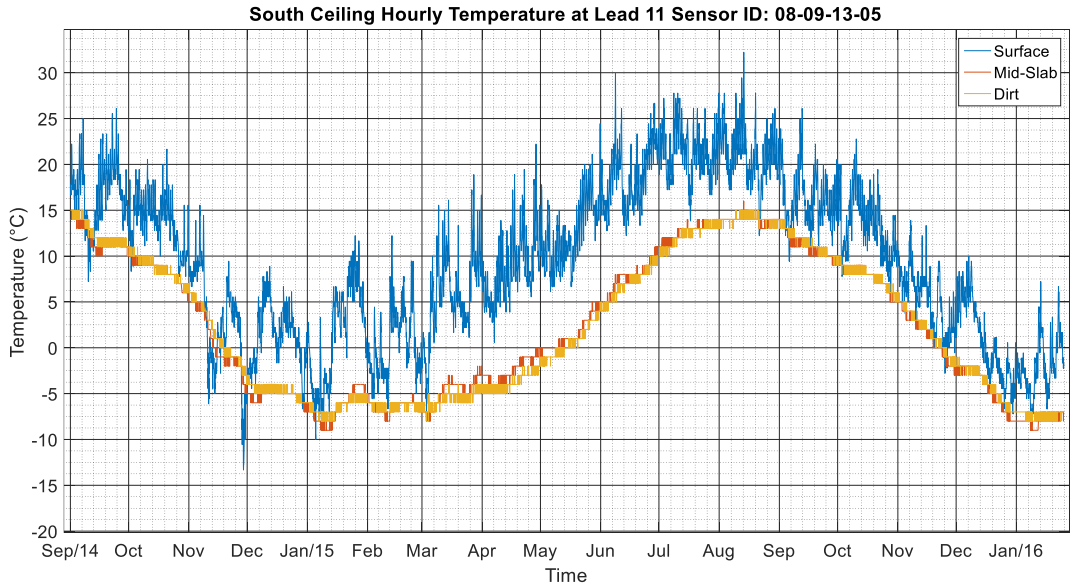

Figure 5.22. South Ceiling Hourly Temperature at Lead 11

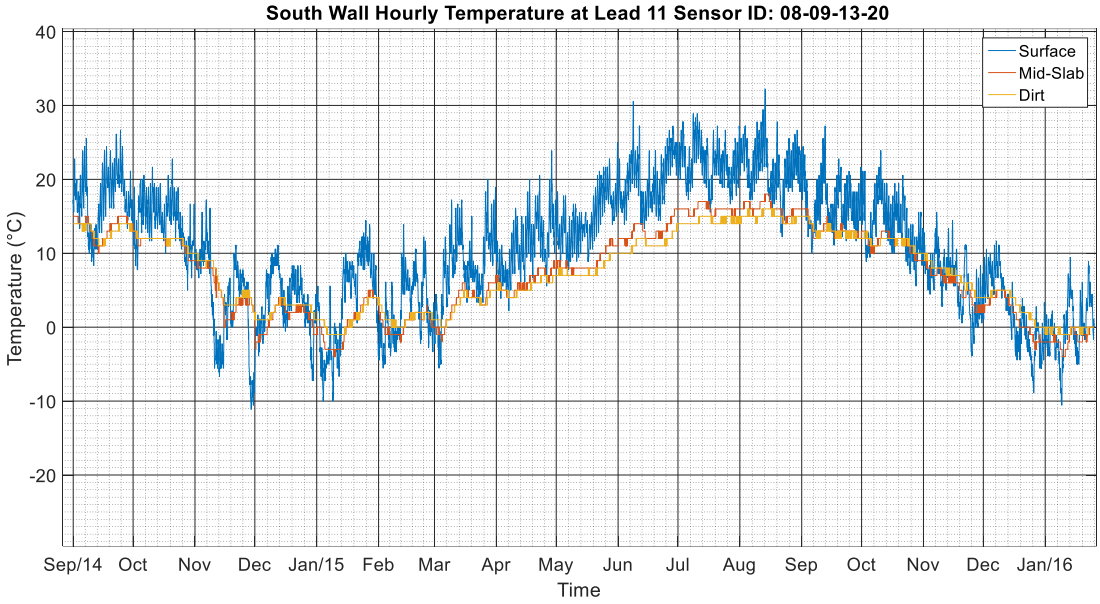

Figure 5.23. South Wall Hourly Temperature at Lead 11

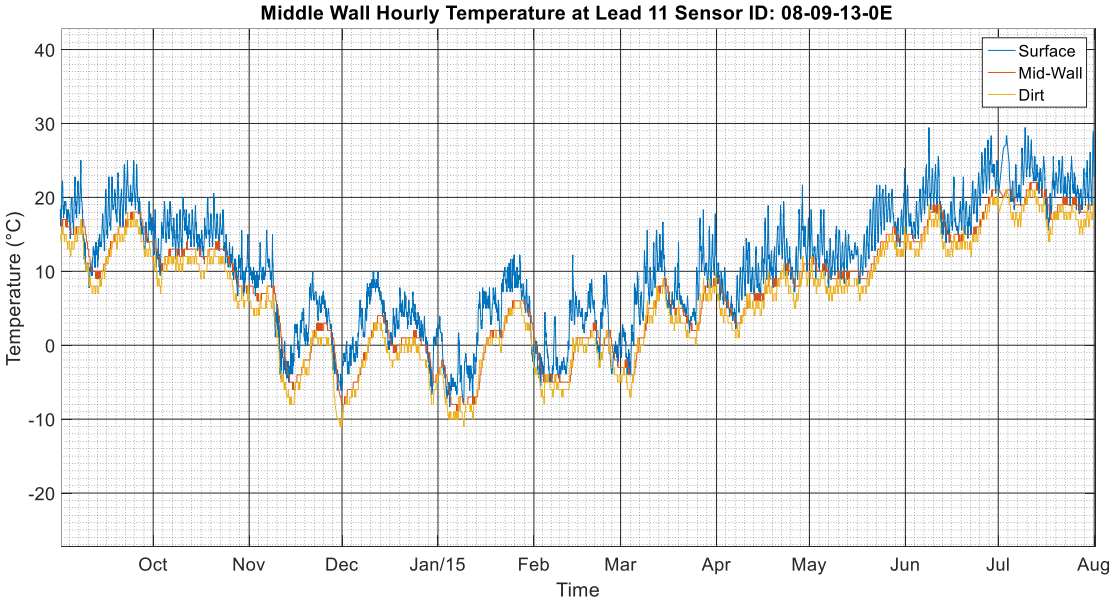

Figure 5.24. Middle Wall Hourly Temperature at Lead 11

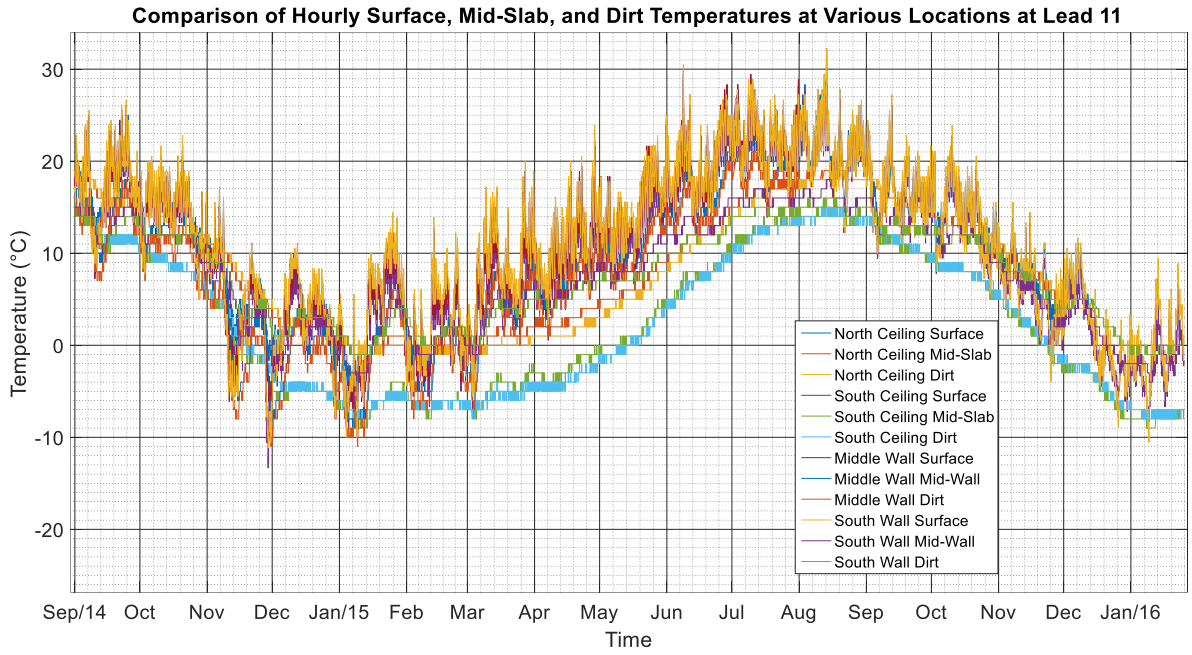

Figure 5.25. Comparison of Hourly Surface, Mid-Slab, and Dirt Temperatures at Various Locations at Lead 11

The North and South ceilings and South exterior wall all exhibit similar trend in temperature. This is expected since the ceiling and walls are exposed to the same ambient temperature conditions. The surface temperatures have greater fluctuations than the mid slab and dirt temperature, which is attributed to the low conductivity of the concrete. This also induces thermal lag which is evident between peak surface and slab temperatures. Furthermore, the mid slab and dirt temperature are similar for all cases.

It can be also observed that when there is a sharp decrease into subzero temperatures the mid slab and dirt temperature is higher than the surface temperature. Again, this is due to the thermal lag between the surface data and mid-slab/dirt data.

For the middle wall, it is observed that the difference between the surface temperatures and slab temperature are lower compared to the ceiling slabs and exterior wall. This is expected since both sides of the middle wall are exposed to similar surface temperature conditions.

5.1.2.4 Wall/Slab Temperature Gradient

The temperature gradients were considered for the exterior walls of the tunnel (North tunnel's North wall and South tunnel's South wall), North and South tunnel ceiling slabs, and middle wall. The selection of temperature sensors for mid slab and dirt was limited due to damage of the sensor, sensor malfunction, and/or errors in data transmission. Note that the temperature gradient refers to the difference between surface and dirt temperature. The surface to dirt gradient in the North ceiling, South ceiling, South wall, and middle wall for Lead 11 were considered for illustration (see Figure 5.26 to Figure 5.29).

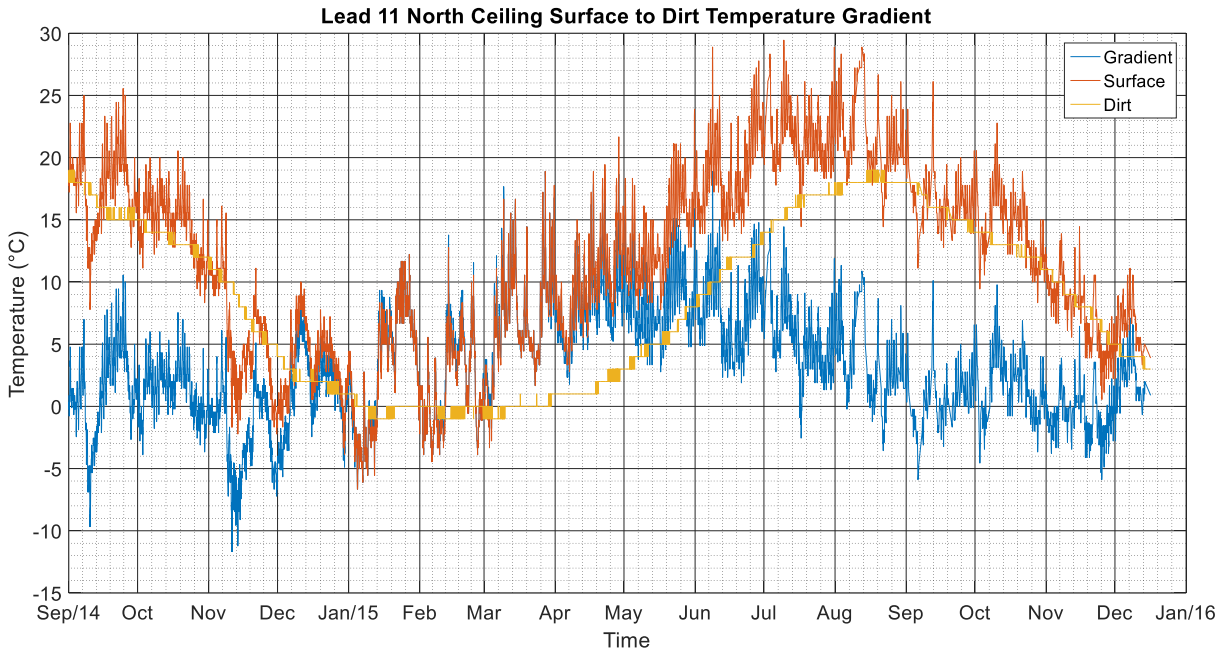

Figure 5.26. Lead 11 North Ceiling Surface to Dirt Temperature Gradient with Hourly Temperature

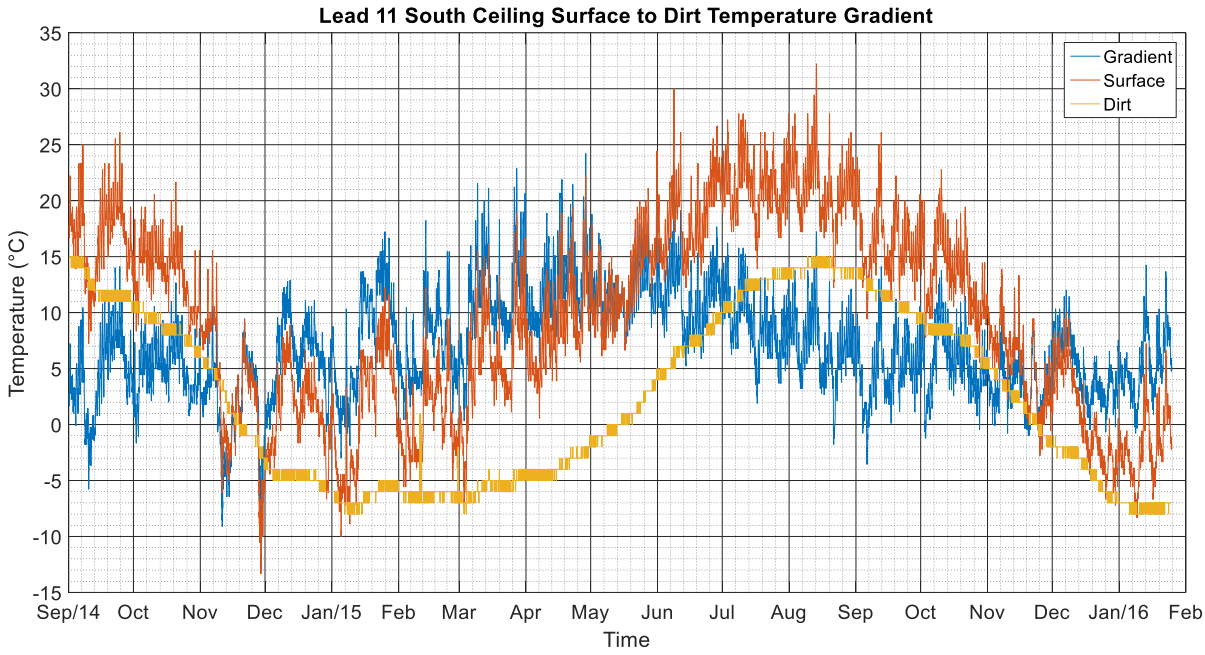

Figure 5.27. Lead 11 South Ceiling Surface to Dirt Temperature Gradient with Hourly Temperature

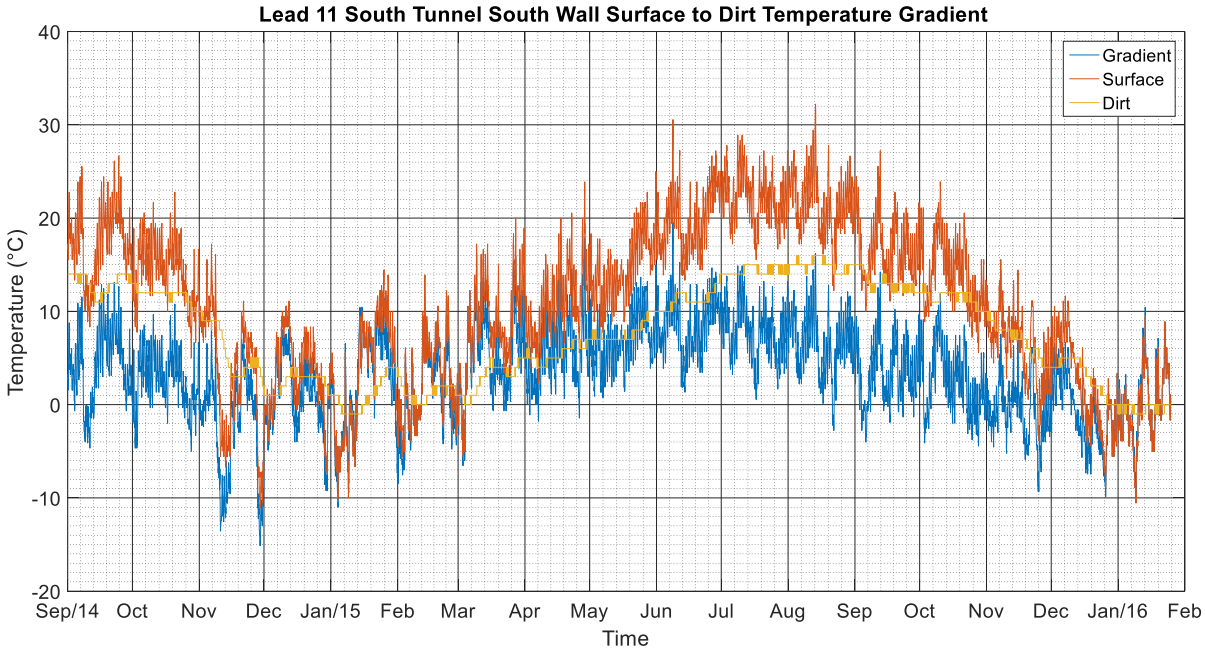

Figure 5.28. Lead 11 South Tunnel South Wall Surface to Dirt Temperature Gradient with Hourly Temperatures

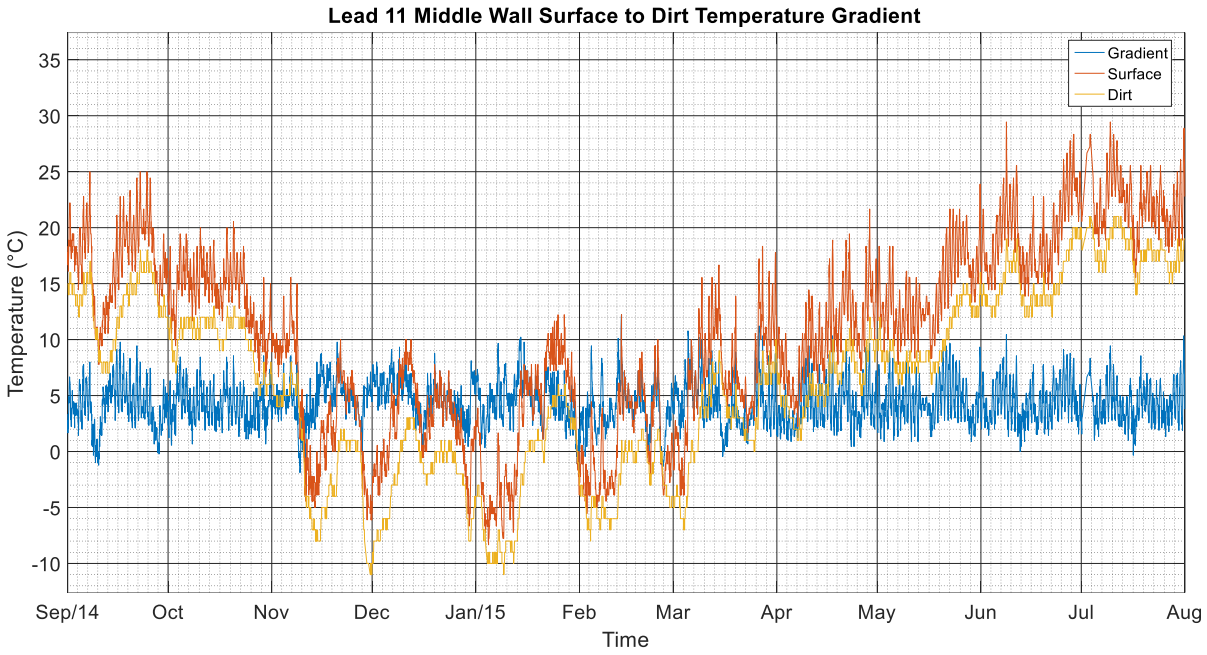

Figure 5.29. Lead 11 Middle Wall Surface to Dirt Temperature Gradient with Hourly Temperatures

It can be observed that the temperature difference between the mid-slab and dirt is generally insignificant as observed in Figure 5.21 to Figure 5.24, however the gradient between the surface and mid-slab is significant. Thus, in the analysis of gradient the surface to dirt was considered as opposed to the surface to mid-slab/wall gradient and the mid-slab to dirt gradients.

If surface temperature is positive, it is generally higher than the slab however when there is a sharp decrease in the surface temperature, the temperature in the slab may be higher than the surface temperature. A possible reason for this difference in temperature is that concrete has a low thermal conductivity so heat may not dissipate as fast in the slab compared to the surface. This effect translates into sharp spikes in the gradient response.

The change in surface temperature is generally proportional to the change in slab temperature. When the temperature is above zero the surface is typically warmer than the slab, however, when the temperature is below zero, the slab is warmer than the surface. It is important to note seasonal variations and diurnal variations should be distinguished. For instance, the slab/wall and dirt temperature sensors are not affected by short term temperature cycles (~10 days).

Since the longitudinal temperature is near uniform it would be expected that the temperature gradient in the ceiling slab and exterior walls should be similar throughout the tunnel with the

possible exception of the portal locations. It was observed that similar temperature gradients exist throughout the various locations in the tunnel.

The temperature gradient in the middle wall was also evaluated. Since the surface temperatures in the north and south tunnels are relatively similar it was expected that the temperature across the wall would be relativity similar. However, it was observed that the temperature at mid-wall was greater than the temperature at 100 mm into the wall from the South tunnel side. Possible reasons for this observation include damage to the sensor and error due to the low resolution of the temperature probes. Another observation for the middle wall is the fact that there is more pronounced temperature cycles in the mid slab and dirt compared to the ceiling slab.

5.1.3 Displacement Sensor Data

Displacement sensors were installed at the two movement joint locations in the tunnel. At Lead 12-13, a triaxial displacement sensor is located in the North tunnel, North wall and a linear displacement sensor is located in the South tunnel, South wall. At Lead 32-33, a triaxial displacement sensor is located in the North tunnel, North wall (Sensor ID: 13-12-27-42) and a linear displacement sensor is located in the North tunnel ceiling (Sensor ID: 14-04-30-01) as illustrated in Figure 5.30. Note that the displacement sensors have internal temperature sensors. The displacement sensor data at Lead 12-13 was not considered for analysis due to sensor malfunction for the time period considered in the analysis. The triaxial displacement and temperature sensor data for Lead 32-33 is plotted in Figure 5.31. Displacement in the X, Y, and Z directions correspond to the longitudinal, vertical, and transverse directions, respectively.

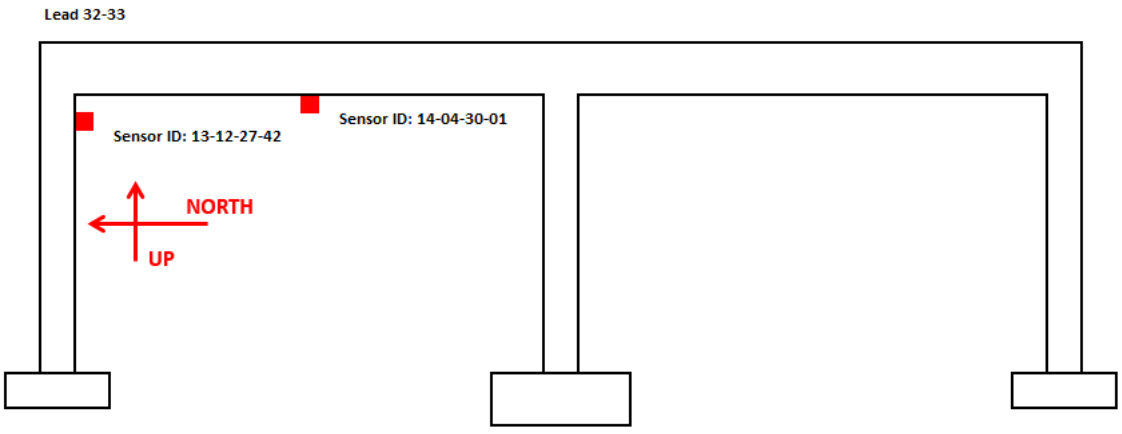

Figure 5.30. Profile view of approximate displacement sensor location at Lead 32-33 movement joint (adopted from CH2M drawings)

In Figure 5.31, the vertical and transverse displacement have minimum fluctuations over time when compared to temperature. Both vertical and transverse displacement seem to be in sync with the seasonal variations in temperature. For example, a decrease in displacement (contraction) is observed in subzero temperature. For longitudinal displacement, the opposite trend is observed. In subzero temperatures there is in overall increase in displacement due to contraction between adjacent sections. The longitudinal displacement has more fluctuations compared to the vertical and transverse displacement. Overall, displacement trends have less fluctuations when compared to the surface temperature record.

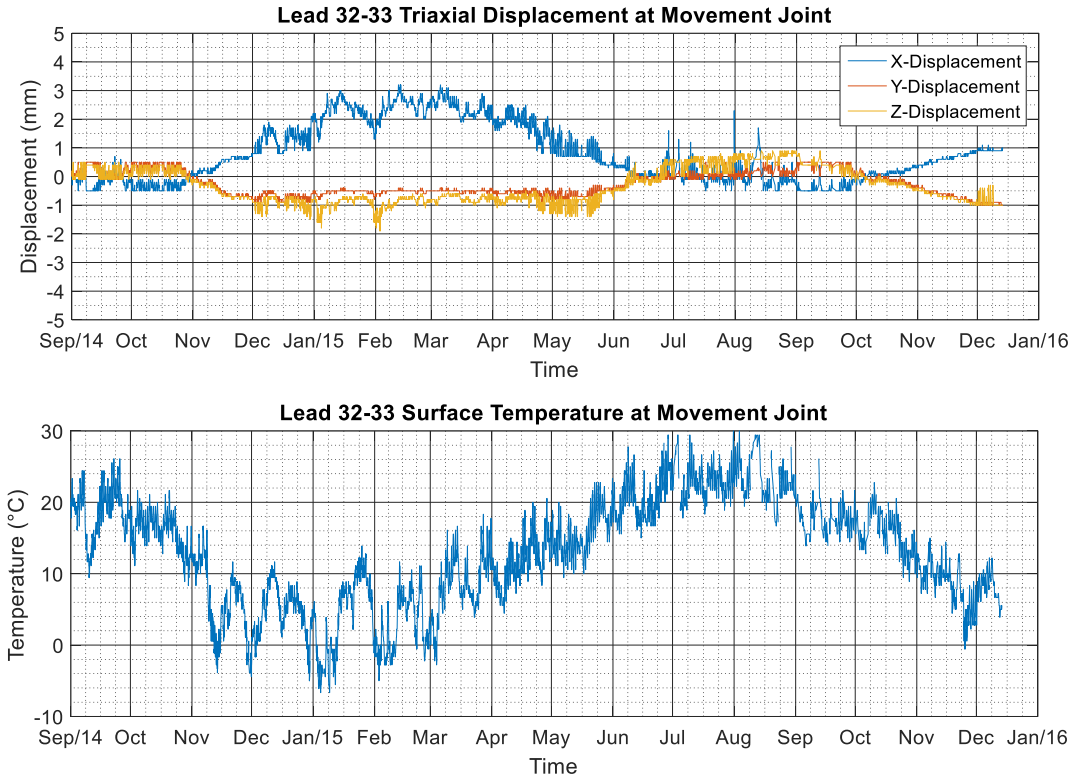

Figure 5.31. Lead 32-33 Triaxial Displacement and Surface Temperature at Movement Joint

In Figure 5.32, the triaxial and linear displacement sensor data at Lead 32-33 was plotted. It can be observed that displacement of the linear sensor was higher compared to the triaxial sensor but did follow the same trend. Note that these sensors are different and the readings for the linear displacement are based on 2″ displacement. The temperature data for the two sensors are

synchronous, however there are differences between the sensors of up to 6 mm at the peak which can be attributed to the difference in mechanism of the sensor.

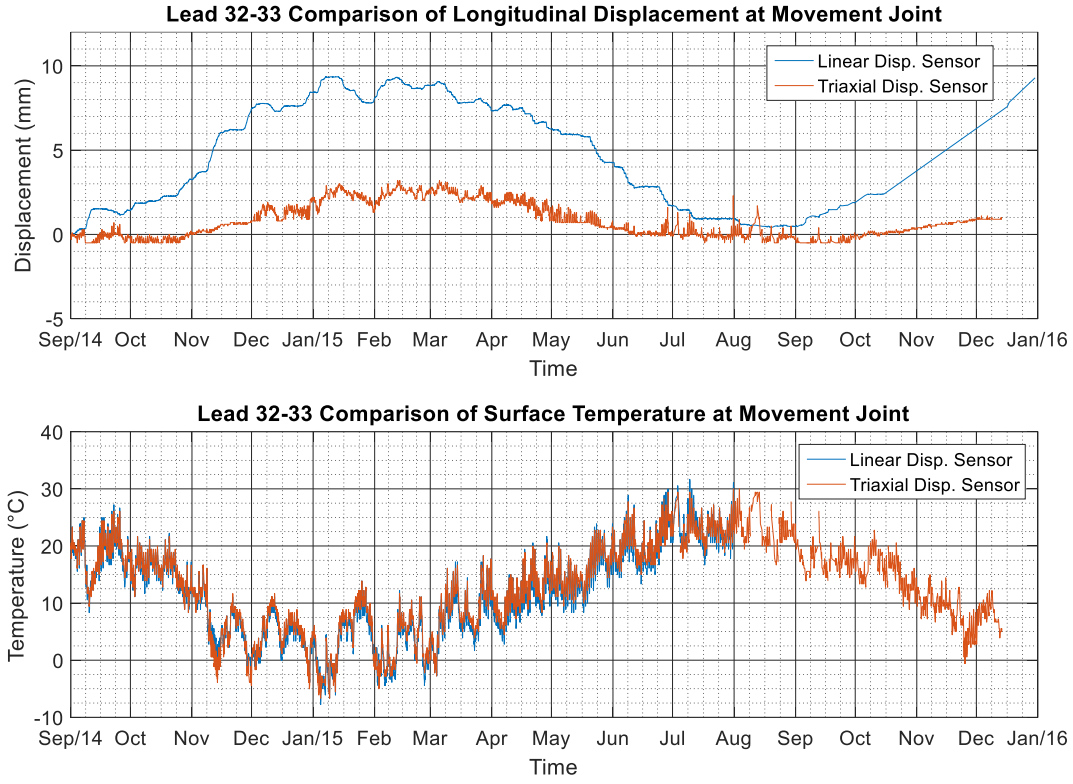

Figure 5.32. Comparison of Lead 32-33 Triaxial Displacement and Surface Temperature Data

5.2 Validation of Sensor Data

5.2.1 Tunnel Surface Temperature Measurement Comparison

A site visit was conducted in order to further investigate discrepancies observed in the temperature data. See Figure 5.33 for pictures of the South tunnel taken during the site visit. The main purpose of the visit was to determine if the discrepancies were due to sensor error or had a physical interpretation. Thus, on June 2 and 3, 2016, wall temperature measurements were taken in the tunnel at 10 am, 2 pm, and 12 am. A Flir E5 infrared camera was used to measure the temperature (see Figure 5.34). The resolution of the camera was 0.1°C and the accuracy was ±2°C.

Figure 5.33. South tunnel pictures taken during site visit

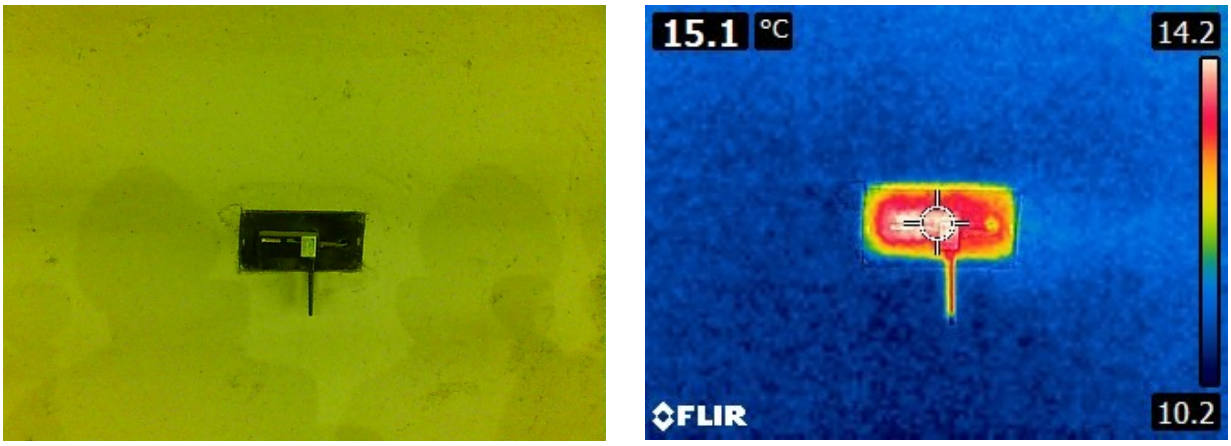

Figure 5.34. Optical (left) and infrared (left) images of temperature sensor housing using infrared camera

Figure 5.35 is a comparison of the wall temperature measurements with corresponding sensor data. Each data point represents an average of 2-3 measurements depending on location and time. For each set of measurements, i.e. North Tunnel 10 am, it took approximately 30 minutes to collect all measurements from the West to East portal or vice versa. Likewise, for the sensor data each point represents an average temperature reading from that particular Lead/Infill section. Sensors with notable damage/malfunction were not considered in the comparison plot. Figure 5.35 also includes the Environment Canada temperature readings from the Calgary International Airport station.

The recorded Environment Canada is a representation of the average temperature for the duration of the measurements, thus the temperature at 10 am, 2 pm, and 12 am were 19.2°C, 21.5°C, and 11.85°C, respectively. Based on the measurements, the internal ambient tunnel temperature is relatively constant overall. At 10 am and 2 pm, the internal temperature was lower than Environment Canada by up to approximately 8°C. On the other hand, at 12 am the internal temperature was up to 4°C higher than Environment Canada. The largest change in temperature is approximately 20 m into the tunnel from the portals, with the main reason being the solar radiation contribution. Another observed trend from the measurements is that the North tunnel is slightly warmer than the South tunnel overall nearing the East Portal and the South tunnel is slightly warmer than the North tunnel overall nearing the West Portal.

When comparing sensor data with the temperature measurements there is a discrepancy which is most evident at times 10 am and 2 pm. Overall, the trend is such that the temperature sensor readings are higher than the measurements. It was determined that the surface temperature sensor requires further calibrations such that the ambient temperature could be measured correctly.

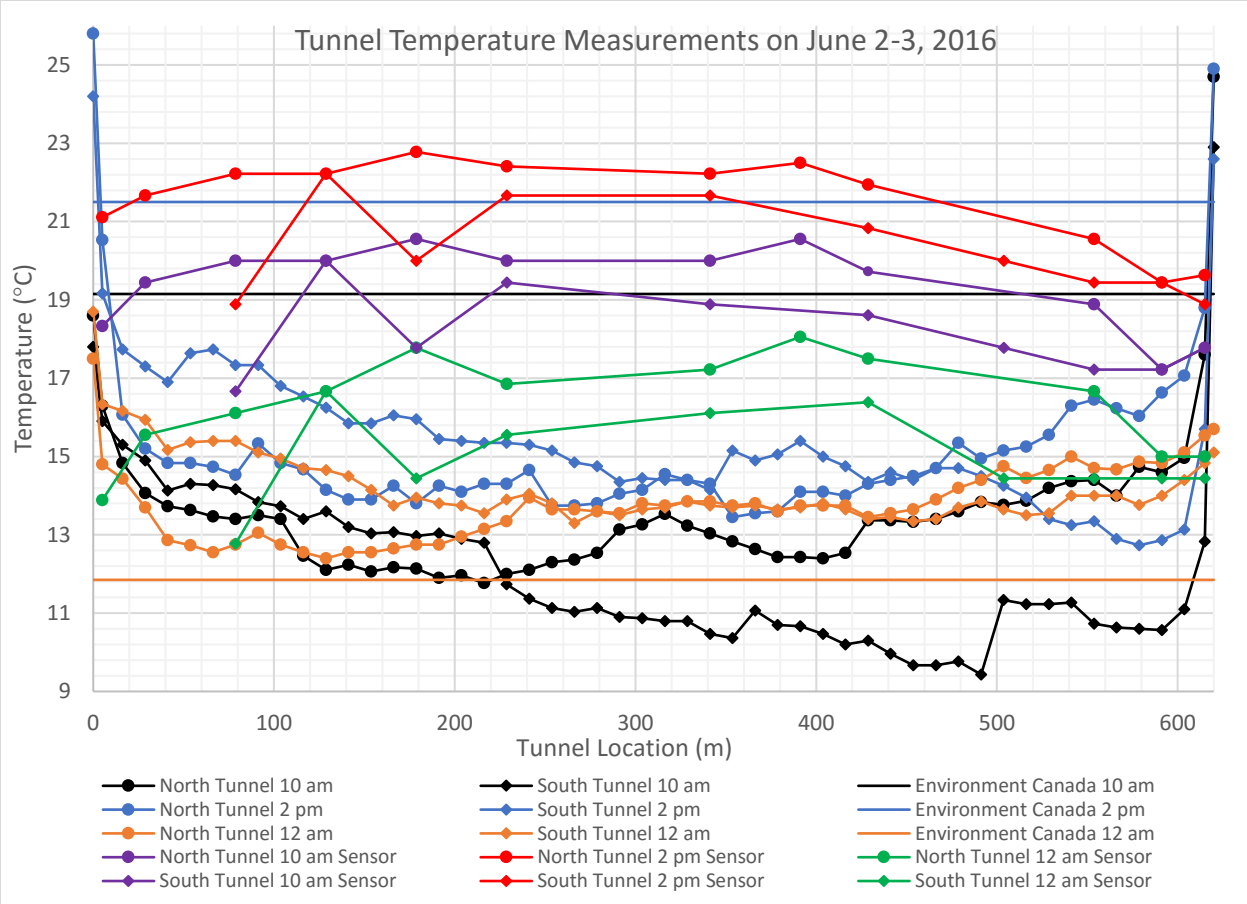

Figure 5.35. Tunnel temperature measurements on June 2-3, 2016

5.2.2 Comparison of Mid Slab and Dirt Sensor Data with Abaqus Modelling using Field Temperature Measurements as Input

In order to verify the mid slab and dirt sensor data, the temperature measurements taken on June 2, 2016 were used as input into the Abaqus model as surface temperature such that the interior node temperatures could be compared to sensor data. Temperature curves were created based on the measurement data for the north and south tunnel (see Figure 5.36 and Figure 5.37). In the figures, data from the west portal, east portal, Lead 11, Lead 19, Infill 28, Lead 35. Lead 45, Infill 50, and Environment Canada are presented. At the portal locations, it is evident that the temperatures were generally higher than the Environment Canada temperature throughout the day. At interior tunnel locations, the temperatures were relatively constant throughout the day resulting in flat curves. At measurement times 10 am and 2 pm the temperatures are lower than

Environment Canada however at 12 am the temperatures were slightly higher. Note that there is a significant difference between the East portal face and Infill 50 which is the interior tunnel wall adjacent to the portal face.

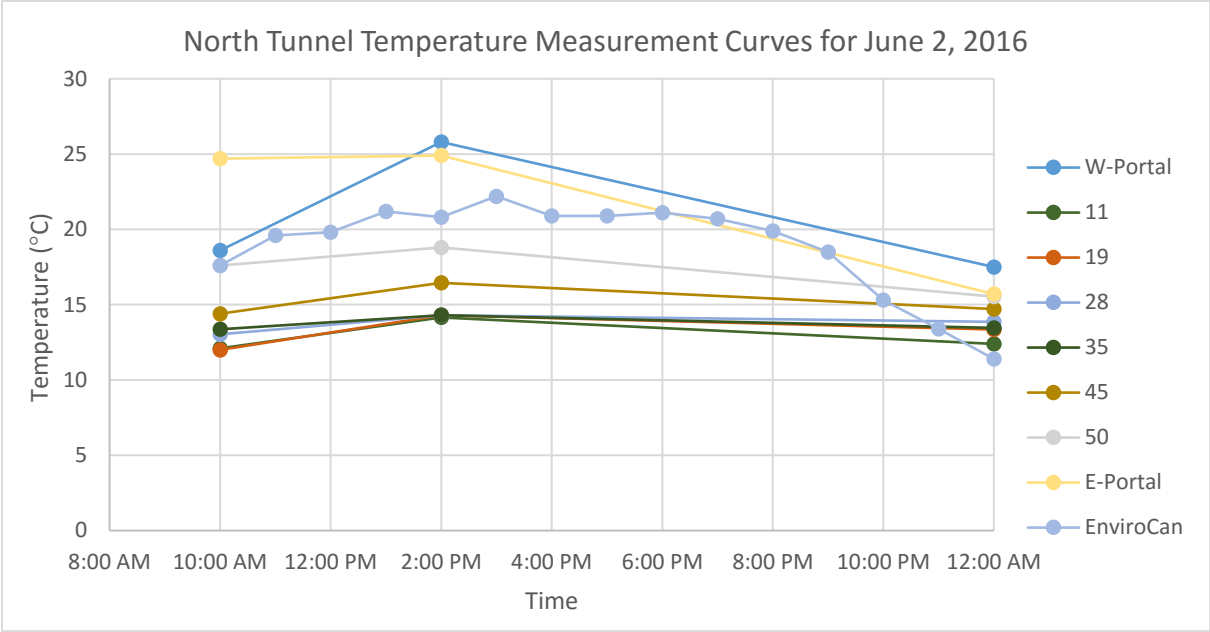

Figure 5.36. North Tunnel Temperature Measurement Curves for June 2, 2016

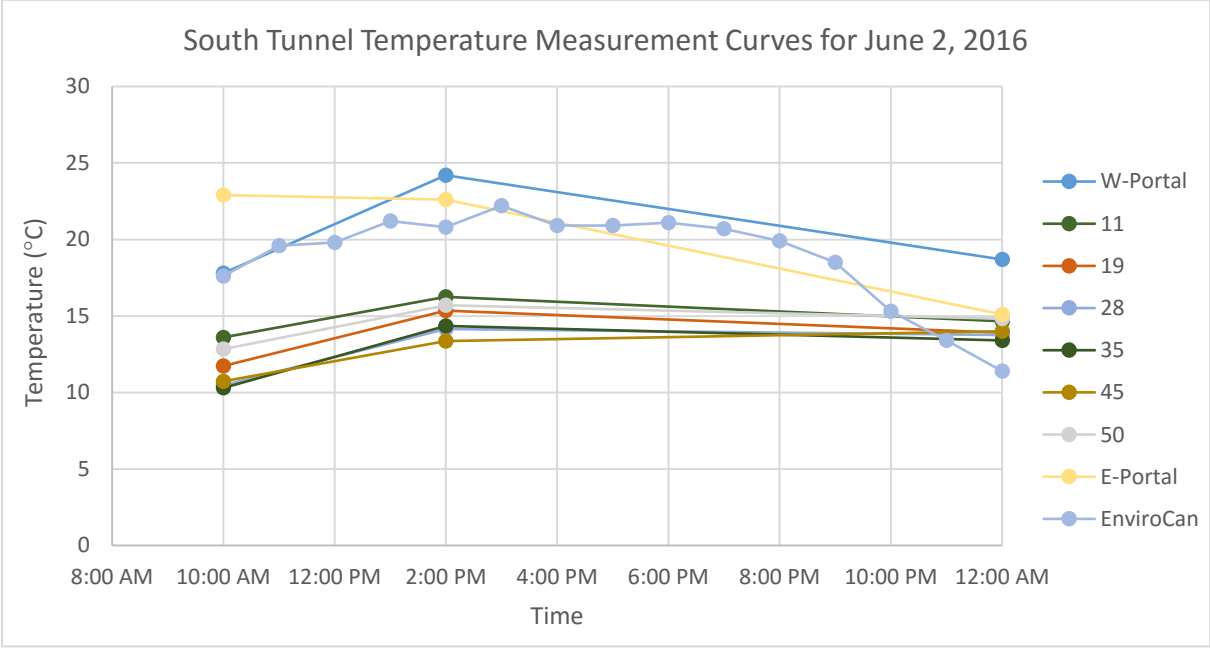

Figure 5.37. South Tunnel Temperature Measurement Curves for June 2, 2016

For analysis purposes, Lead 35 and Infill 50 North tunnel temperature measurement curves were chosen as input into the Abaqus model. At these locations, several sensors are available for comparison. Infill 50 was mainly chosen because there are no sensors directly on the portal wall face however it is the section adjacent to the portal face. Since the temperature record is short (14 hours) the output will be highly dependent on the initial temperature condition assigned to the model. Thus, initial temperatures of 15°C and 10°C were considered for the East portal and Lead 35 respectively based on assumption of the previously temperature state. Results from the model were plotted in Figure 5.38 and Figure 5.39. Node 1341 approximately corresponds to the mid slab sensor location and Node 345 approximately corresponds to the dirt sensor location.

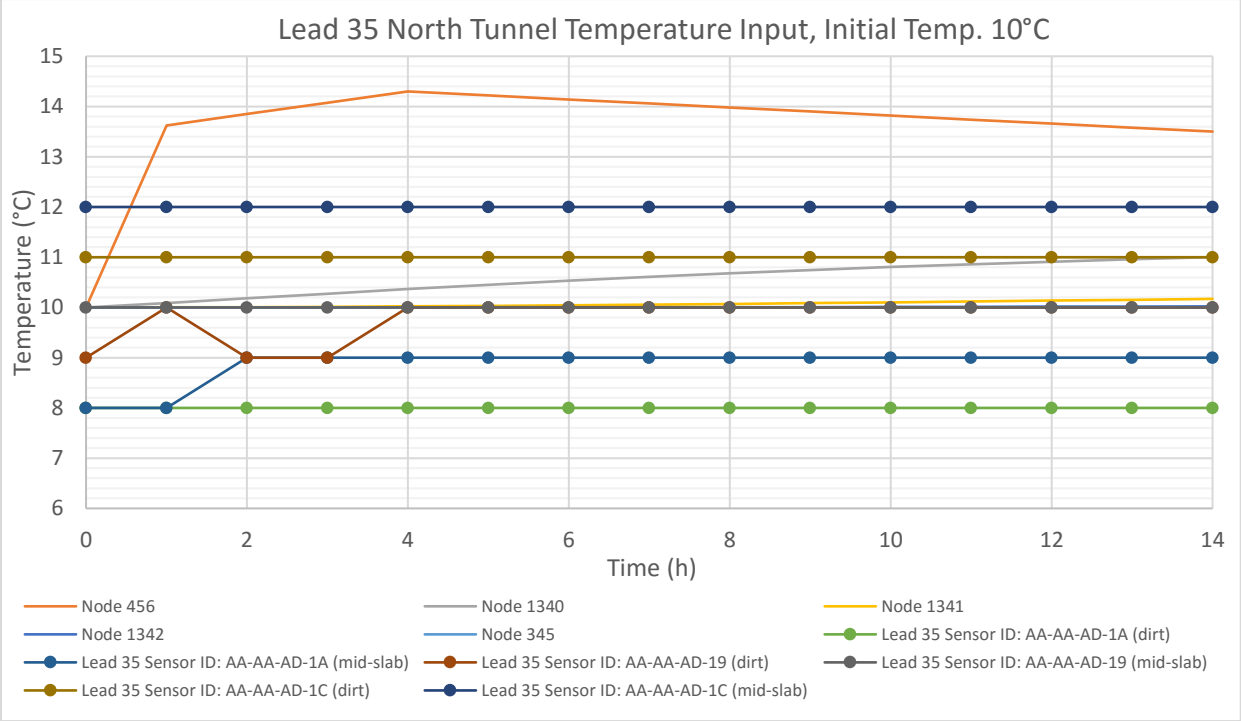

Figure 5.38. Lead 35 North Tunnel Temperature Input with Initial Temperature of 10°C

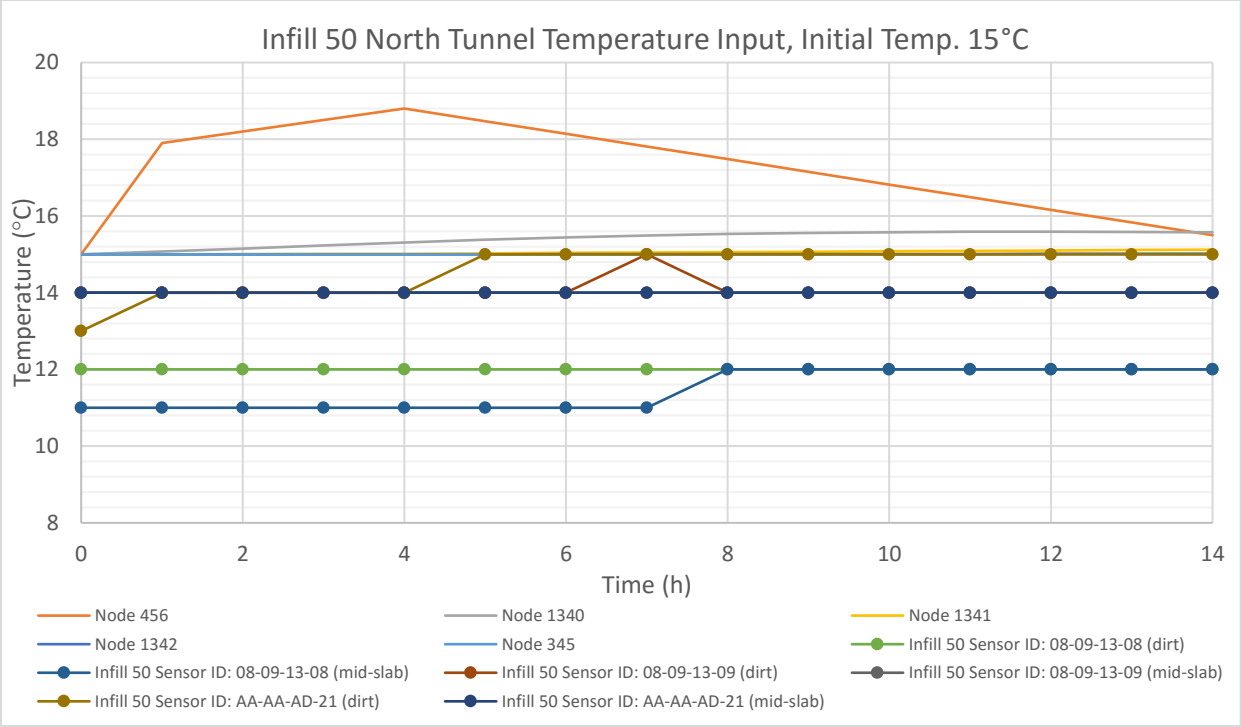

Figure 5.39. Infill 50 North Tunnel Temperature Input with Initial Temperature of 15°C

Note that time zero in the figures is 10 am. The mid-slab and dirt sensor data was constant throughout the time period with little to no fluctuations in temperature. There was also no significant differences between the mid slab and dirt temperatures. At Lead 35 and Infill 50, the maximum difference between sensors is 4°C and 3°C, which is acceptable considering the sensor accuracy. The interior nodal temperatures from the Abaqus model output slightly increased from the defined initial temperature. The increase is most evident at the first interior node (Node 1340) with an increase in temperature of approximately 1°C at Lead 35 and 0.5°C at Infill 50 at the end of the analysis.

5.2.3 Tunnel Slab Temperature Comparison with Numerical Model

Recall, that in the model the ambient temperature record from Environment Canada was applied to the surface of the tunnel to simulate temperature conditions at the portals. Since the tunnel portals are exposed to ambient temperature conditions, the slab temperatures collected from the mid slab and dirt sensors at the portal located could be compared to the numerical model results at the corresponding nodes in the cross section of the member. North and South ceiling sensor data at the East portal (Infill 50) and Lead 45, which is approximately 62.5 m from the east portal, were selected to compare with the model output of temperature distribution of the roof slab (see Figure 5.40).

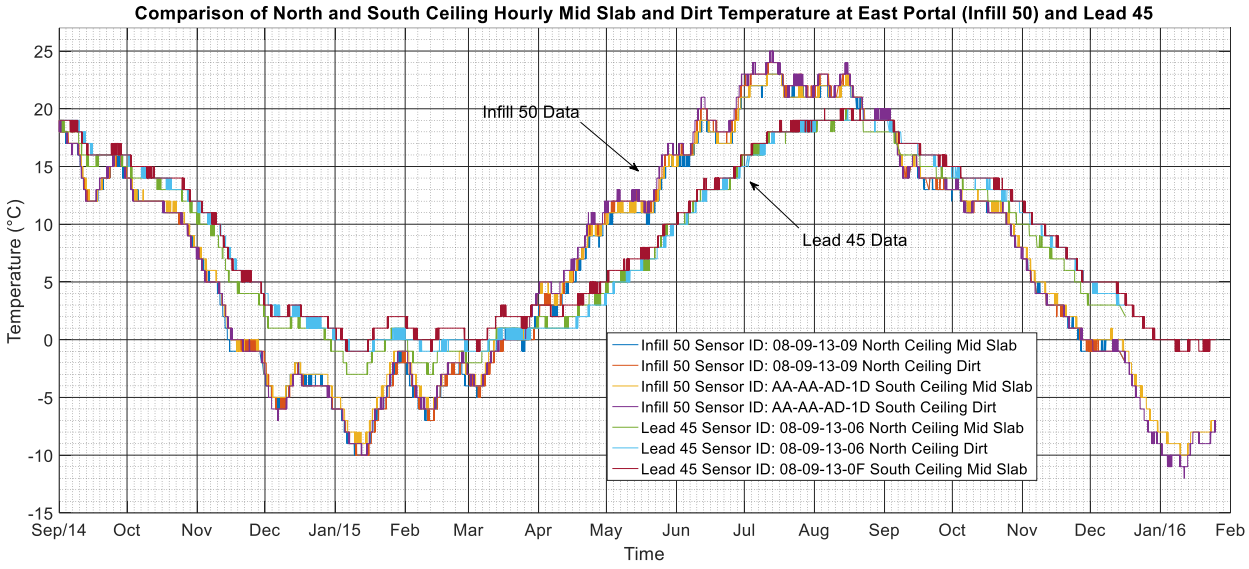

Figure 5.40. Comparison of North and South Hourly Mid Slab and Dirt Temperature at the East Portal (Infill 50) and Lead 45

When comparing the slab temperatures at the East portal and Lead 45, it is evident that there are greater fluctuations in temperatures at the portal. This can be attributed to the fact that the portal is exposed to ambient temperature conditions and the effects of solar radiations which will caused increased fluctuations. Also note that there is a time lag between peak temperatures at the East portal and Lead 45. A reason for this observation is the longitudinal ambient temperature differences from the portals to the interior tunnel. Recall, from the field measurements that the

largest changes in temperature occurred at up to 20 m from the portals. This effect on the surface temperature condition propagates to the slab temperatures.

The overall comparison of the East portal and Lead 45 slab sensor data along with the model output is illustrated in Figure 5.41. Furthermore, separate comparisons with the East portal and Lead 45 data with the model is illustrated in Figure 5.42 and Figure 5.43, respectively. Since the ambient temperature record from Environment Canada inputting into the model was from May 2013 to May 2016, the model output from September 2014 to January 2016 was extracted to align with the sensor data such that direct comparisons could be attained.

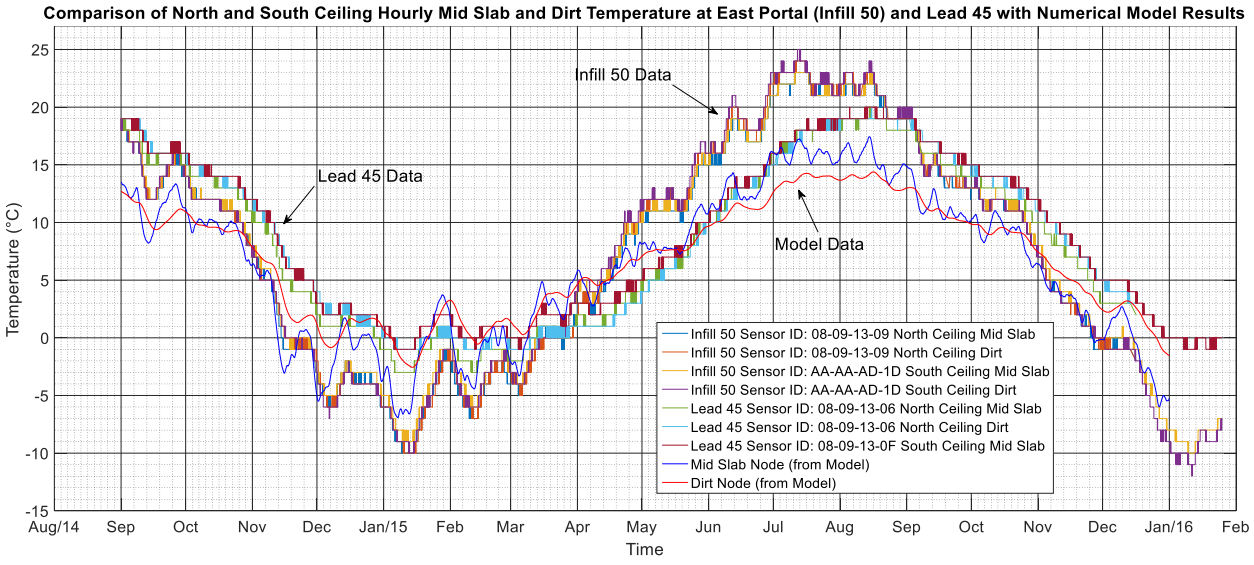

Figure 5.41. Comparison of North and South Hourly Mid Slab and Dirt Temperature at the East Portal (Infill 50) and Lead 45 with Numerical Model Results

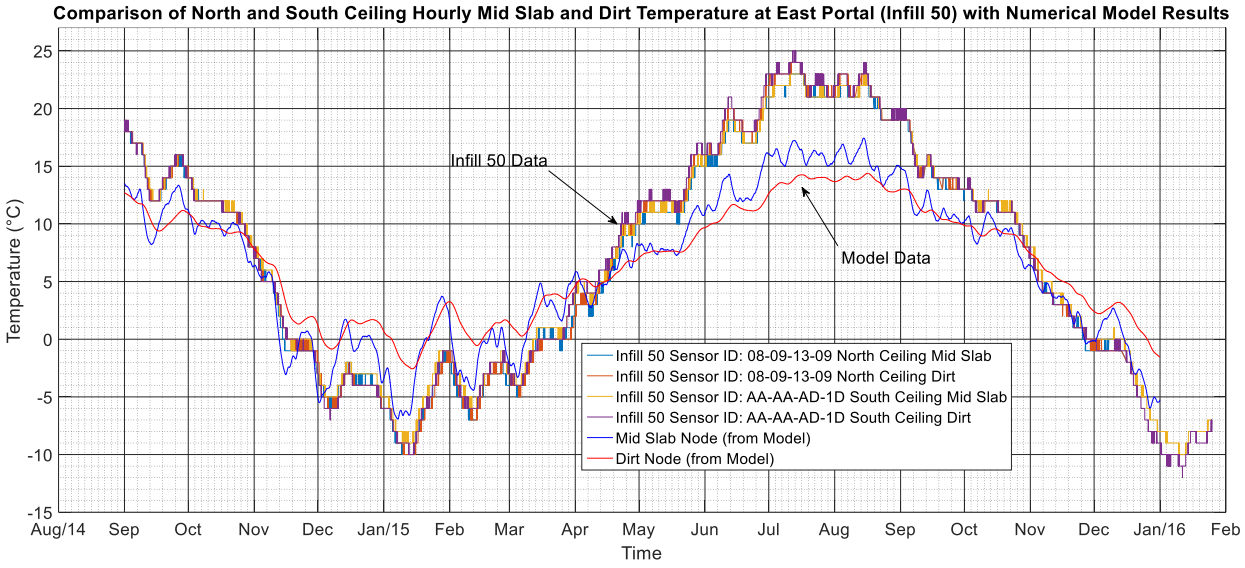

Figure 5.42. Comparison of North and South Hourly Mid Slab and Dirt Temperature at the East Portal (Infill 50) with Numerical Model Results

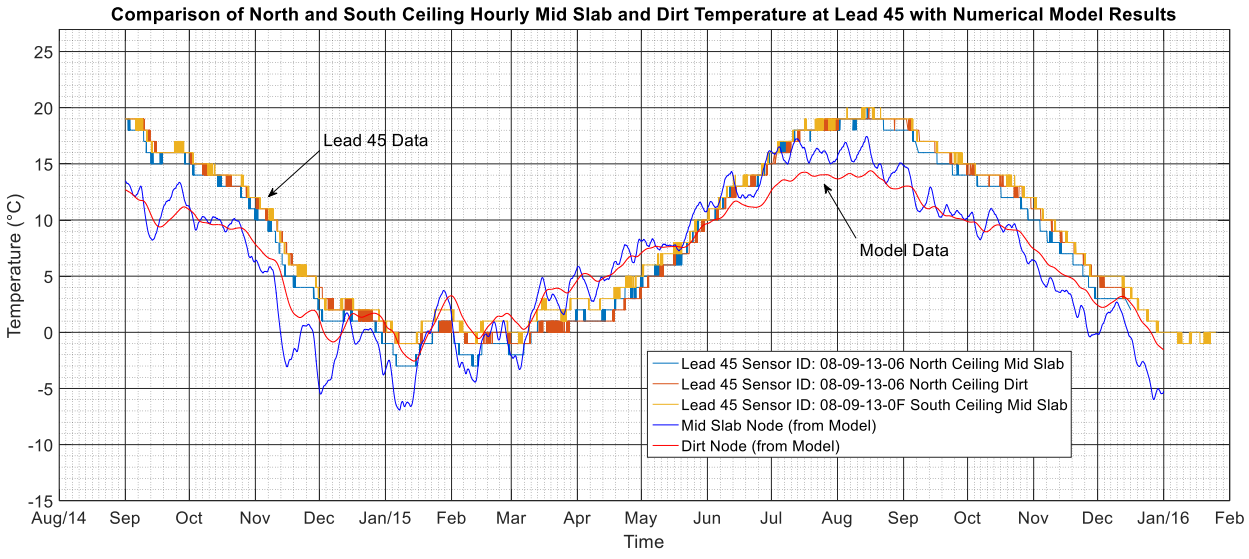

Figure 5.43. Comparison of North and South Hourly Mid Slab and Dirt Temperature at Lead 45 with Numerical Model Results

From Figure 5.41, it can be observed that the temperature fluctuations from the sensor data and model are synchronous. However, the discrepancy between the mid slab node and dirt node temperatures from the model are generally higher when compared with the sensor slab. These differences can be attributed to the thermal properties and boundary conditions considered in the model compared to in situ conditions. These properties were unknown but reasonable assumptions were made. In regards to the sensor data, the resolution of the temperature probes could also affect the results. For instance, using a higher resolution sensor could result in greater temperature fluctuations in the data.

The model results match relatively well with portal sensor data as observed in Figure 5.42. The peak maximum and minimum temperatures align between the model and sensor data and there is no lag time between peaks. The peak temperatures observed from July to August are higher the in sensor data compared to the model results. A potential reason for this occurrence is the effect of solar radiation at the portals which is highest during summer months. This effect was not considered in the model. When comparing the model with sensor data from Lead 45 in Figure 5.43, there is a noticeable lag between temperature curves which is expected due to longitudinal ambient temperature difference between the portal and interior tunnel which in turn affects the slab temperatures.

In the model, the soil temperature boundary condition was inputted as a constant based on the assumption that there is sufficient soil cover above the tunnel such that fluctuations in temperature would be negligible. Based on comparison of model and field data results in the figures above, the assumption is reasonable considering the model and field data outputs are comparable.

5.3 Discussion of Tunnel Data and Comparison to CSA S6 Design Code

5.3.1 Maximum and Minimum Tunnel Temperatures

The maximum and minimum temperatures in the North and South ceiling slab are summarized in Table 5.2. The maximum and minimum Environment Canada temperatures were also included in the table. The maximum and minimum temperatures occur at the surface as expected. There is no significant difference between the maximum and minimum temperatures in the mid-slab and dirt.

The maximum/minimum temperatures in the tunnel from all sensor data fits within the design temperature range (-38°C to 34°C) of the member recommended in CSA S6 for the geographical region. The comparison may be more correct if mid wall/slab temperature is considered or a weighted average of dirt, mid wall/slab, and surface temperature to represent the temperature of any given cross section.

Figure 5.44 illustrates the maximum and minimum temperatures along the tunnel for the North and South ceiling. In Figure 5.44, "NC" refers to North ceiling and "SC" refers to South ceiling. The maximum surface, mid-slab, and dirt temperatures in the North and South tunnel are relatively consistent. The minimum surface temperatures are relatively consistent with the exception of lead 11 where the difference is approximately 7°C. There is a discrepancy between minimum mid-slab and dirt temperatures of the North and South ceiling, with temperature differences of up to 5°C. For the time period analyzed, the maximum and minimum Environment Canada temperatures are 33.6°C and -25.1°C. When comparing these temperatures with the data in Figure 5.44, the maximum surface temperature the tunnel experiences is near the maximum Environment Canada temperature and this trend is observed throughout the tunnel. On the other hand, the minimum surface temperature in the tunnel is up to approximately 9°C higher than the minimum Environment Canada at the East portal.

Note that the results are influenced by the surface sensor data readings which are subject to further calibrations.

Table 5.2. Maximum and Minimum Temperatures in North and South Ceiling Slab from September 2014 to January 2016

Location			Max. Temperature (°C)	Min. Temperature (°C)
North Ceiling	Surface	Lead 11	29.4	-6.7
		Lead 19	31.1	-9.4
		Infill 28	31.7	-10.6
		Lead 35	30.0	-8.9
		Lead 45	30.0	-10.6
		Infill 50	30.0	-15.0
	Mid-Slab	Lead 11	19.0	-2.0
		Lead 19	19.0	-3.0
		Lead 35	17.0	-3.0
		Lead 45	20.0	-3.0
		Infill 50	23.0	-10.0
	Dirt	Lead 11	19.0	-1.0
		Lead 19	20.0	0.0
		Lead 35	16.0	-2.0
		Lead 45	20.0	-1.0
		Infill 50	24.0	-10.0
South Ceiling	Surface	Lead 11	32.2	-13.3
		Lead 19	32.2	-13.3
		Infill 28	30.6	-10.0
		Lead 35	29.4	-7.8
		Lead 45	28.3	-9.4
		Infill 50	28.3	-12.8
	Mid-Slab	Lead 11	16.0	-9.0
		Lead 19	16.0	-9.0
		Infill 28	21.0	-3.0
		Lead 35	20.0	-1.0
		Lead 45	20.0	-1.0
		Infill 50	23.0	-10.0
	Dirt	Lead 11	15.0	-8.0
		Lead 19	15.0	-8.0
		Infill 28	21.0	-3.0
		Lead 35	19.0	-1.0
		Infill 50	25.0	-12.0
Environment Canada	Calgary Int'l Airport		33.6	-25.1

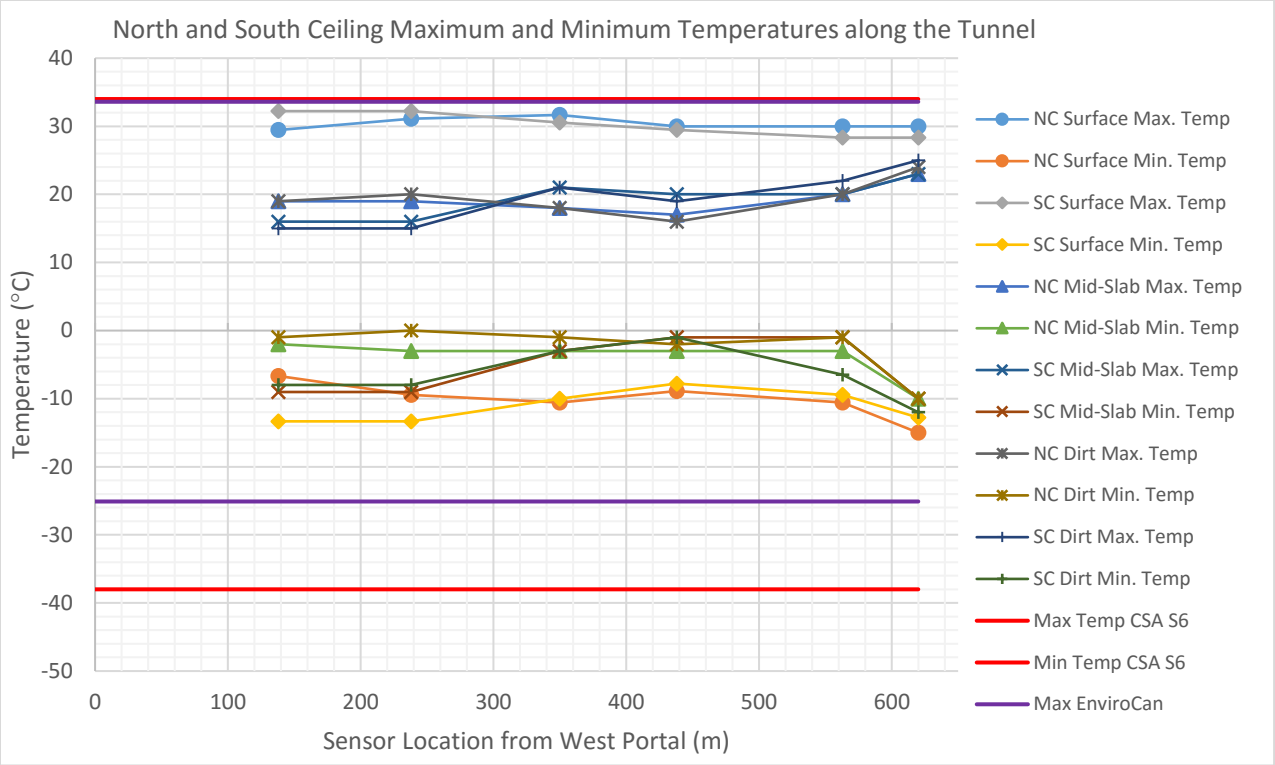

Figure 5.44. North and South Ceiling Maximum and Minimum Temperatures along the Tunnel

5.3.2 Temperature Gradient in the Tunnel

Histogram plots of the surface to dirt gradient as well as normal distribution curves were used to determine the mean and standard deviation of the gradient (see Figure 5.45 and Figure 5.48). The data generally fits the normal distribution curves well although for some plots the data is slightly skewed.

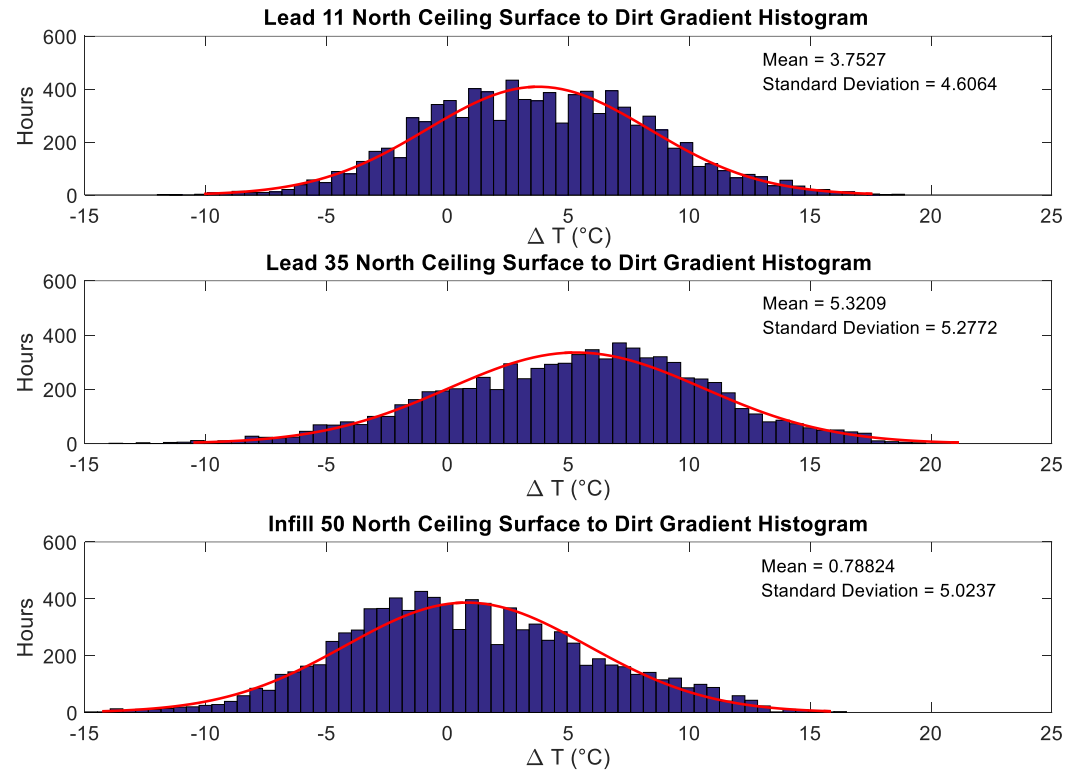

Figure 5.45. North Ceiling Surface to Dirt Gradient Histogram Plots with Normal Distribution

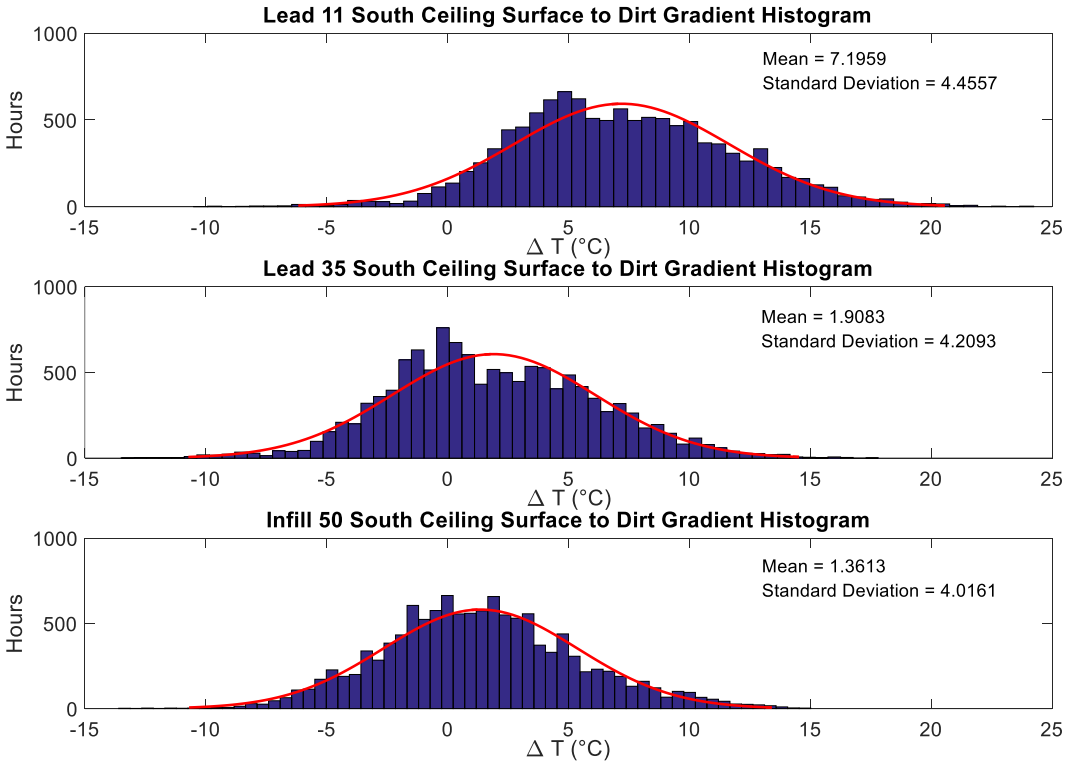

Figure 5.46. South Ceiling Surface to Dirt Histogram Plots with Normal Distribution

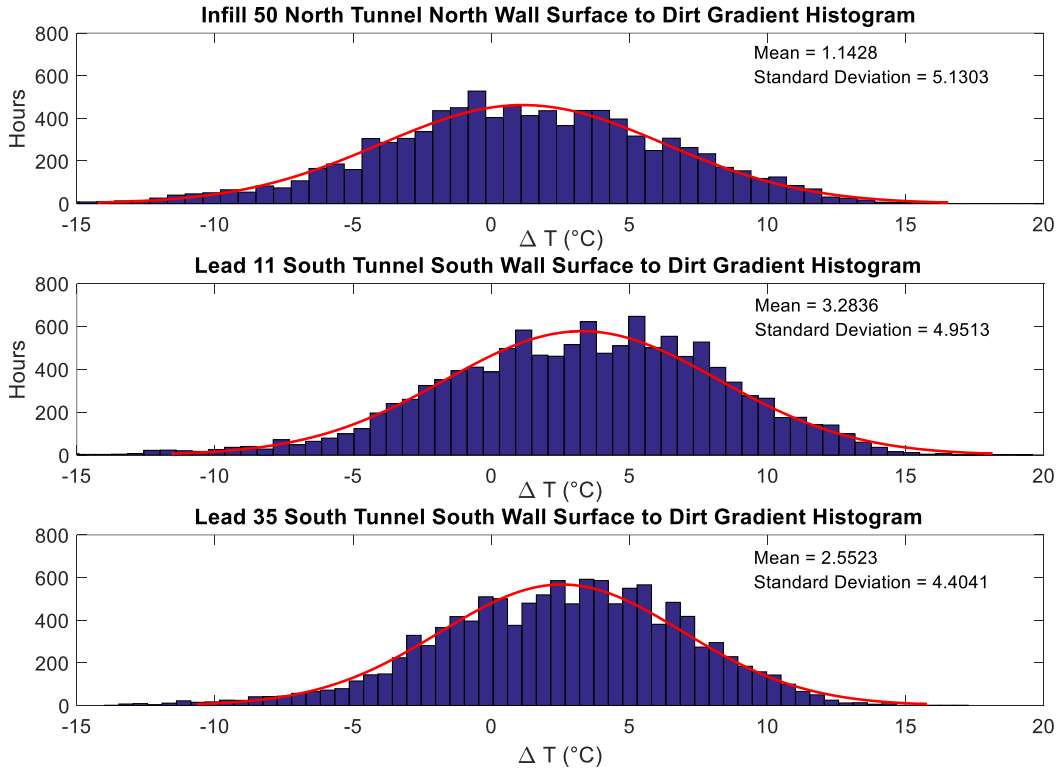

Figure 5.47. Exterior Tunnel Wall Surface to Dirt Histogram Plots with Normal Distribution

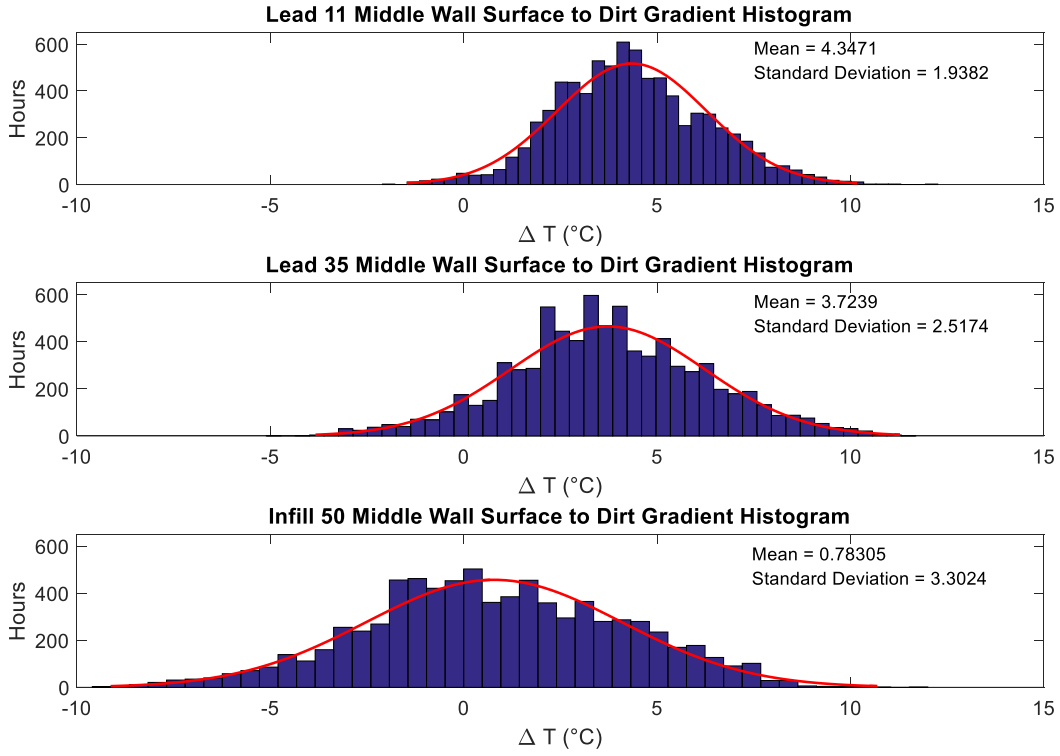

Figure 5.48. Middle Wall Surface to Dirt Histogram Plots with Normal Distribution

Table 5.3. Surface to Dirt Temperature Gradients using Normal Statistical Distribution

Location	Gradient	Mean, μ (°C)	Standard Deviation, σ (°C)	μ - 1 σ (°C)	μ + 1 σ (°C)	μ - 2 σ (°C)	μ + 2 σ (°C)	μ - 3 σ (°C)	μ + 3 σ (°C)
North Ceiling	Lead 11	3.75	4.61	-0.85	8.36	-5.46	12.97	-10.07	17.57
	Lead 35	5.32	5.28	0.04	10.60	-5.23	15.88	-10.51	21.15
	Infill 50	0.79	5.02	-4.24	5.81	-9.26	10.84	-14.28	15.86
South Ceiling	Lead 11	7.20	4.46	2.74	11.65	-1.72	16.11	-6.17	20.56
	Lead 35	1.91	4.21	-2.30	6.12	-6.51	10.33	-10.72	14.54
	Infill 50	1.36	4.02	-2.65	5.38	-6.67	9.39	-10.69	13.41
North Wall	Infill 50	1.14	5.13	-3.99	6.27	-9.12	11.40	-14.25	16.53
Middle Wall	Lead 11	4.35	1.94	2.41	6.29	0.47	8.22	-1.47	10.16
	Lead 35	3.72	2.52	1.21	6.24	-1.31	8.76	-3.83	11.28
	Infill 50	0.78	3.30	-2.52	4.09	-5.82	7.39	-9.12	10.69
South Wall	Lead 11	3.28	4.95	-1.67	8.23	-6.62	13.19	-11.57	18.14
	Lead 35	2.55	4.40	-1.85	6.96	-6.26	11.36	-10.66	15.76

Table 5.3 outlines the normal statistical distribution results from histogram plots above. The maximum/minimum gradients obtain from the data in the slab and exterior walls are higher/lower than the values in CSA S6-14 (±5°C temperature differential shall be considered for winter conditions and a +10°C temperature differential shall be considered for summer conditions), respectively. The maximum/minimum gradient in the middle wall is generally lower/higher compared to the exterior walls and ceiling slabs as expected. Note that the comparison of gradient values to the code is dependent on the chosen standard deviation. For instance, values in the third standard deviation may exceed code limits.

5.4 Discussion of Tunnel Data Analysis and Numerical Model Results

A heat transfer analysis was conducted in Abaqus in order to determine the time history of the temperature distribution through a typical tunnel cross section. Likewise, temperature sensors were installed in the tunnel such that temperature distributions in the tunnel could be analyzed. The temperature distribution time history outputs from the model and the data were then further analyzed in the form of temperature envelopes and statistical gradient analysis in order to evaluate design code provisions in CSA S6 regarding temperature loads.

When compared the temperature envelope data from the model with the data with the code there is agreeance in the fact that the temperature the tunnel experiences is within the design temperature limits in CSA S6. There were some noticeable difference between the sensor data and Environment Canada data. For instance, the minimum surface temperature that the tunnel experience, over the time period analyzed, was approximately -15°C even though at times the Environment Canada temperature would be in the -30°C. Further field investigation may be required to interpret this phenomenon.

A statistical analysis of the surface to dirt, surface to mid span, and mid span to dirt gradients were conducted from the model and sensor data. The main focus of the analysis was the surface to dirt gradient which was determined to govern the design. The model and sensor data, obtained similar conclusions that gradient values could significantly exceed the values described in CSA S6. A noticeable difference between the model and sensor data was the fact that the mean gradient values were higher for the sensor data compared to the mode, where the mean gradient was consistently near 0°C. The difference could be attributed to the assumptions made in the model. Another possibility is the fact that surface temperature sensor had the tendency to output higher values than expected, which was determined from the field measurements.

Since only a 2D heat transfer analysis was conducted due to limitations and complexity, temperature distributions in the longitudinal tunnel direction and 3D displacements which were captured in field data (sensors and infrared camera) could not be compared with modelling results.

Chapter 6: Conclusions and Recommendations

6.1 Conclusions

The main purpose of the study was to investigate the temperature field of the Calgary Airport Trail Tunnel using numerical modelling temperature and sensor data. In the numerical model, a long term ambient temperature record from Environment Canada was implemented to simulate realistic site conditions such that time histories of the temperature distributions and stress distributions could be outputted. Temperature and displacement sensor data from the Airport Trail was analyzed for the time period of September 2014 to January 2016. The results of the data analysis were then compared to design temperature clauses found in CHBDC CSA S6, which was the code considered in the design of the tunnel. Displacement data at a movement joint was analyzed to evaluate the movement of the structure due to thermal loading and the location of movement joints in the tunnel. The main findings are summarized below:

The maximum/minimum surface temperatures in the tunnel is within the design temperature range (-38°C to 34°C) recommended in CSA S6 for the geographical region. This conclusion was drawn from the modelling results for the time period considered in the analysis. The sensor data analysis results agreed with this finding however further calibrations are required. Note that the purpose of the design temperature is to consider the effect of the temperature range on longitudinal expansion in bridges. For tunnels, the temperature differs longitudinally, especially at the portals, which will in turn induce movement in the longitudinal direction. In this thesis, the model only considered 2D temperature distribution, thus, the additional effect of longitudinal temperature differences should also be considered in order to evaluate the appropriate design temperature.

The maximum/minimum temperature gradient effects exceeded values in CSA S6 (±5°C temperature differential for winter conditions and a +10°C temperature differential for summer conditions for a member depth equal to or greater than 1 m) when the extreme values are considered. Again, this conclusion was drawn from the modelling results for the time period considered in the analysis and the sensor data analysis results agreed with this finding however further calibrations are required. It was determined that the extreme gradients the tunnel experience may be significant since the corresponding stresses in the structure can exceed the

tensile capacity of concrete. The critical gradients corresponded to the maximum and minimum temperature differential between surface and dirt. These critical gradients can be approximated using a bilinear curve for simplicity.

Displacements at the Lead 32-33 movement joint were insignificant and inconclusive. A maximum displacement of approximately 3 mm occurred in the longitudinal tunnel direction between peak maximum and minimum temperatures for the triaxial displacement sensor. 3D modelling and/or a comprehensive displacement sensors system are required to evaluate expected displacements and the location of the movement joints.

6.2 Recommendations and Future Work

Following are recommendations for the monitoring system:

- Since the highest longitudinal temperature differences are expected near the portals install more sensors at the first 50 m from the portal as well as the portal face. The longitudinal temperature gradient near the portal will produce longitudinal displacements at movement joints thus place displacement sensors in this region.
- Since air flow is a governing factoring of heat transfer in the tunnel and thus temperature changes, installing wind velocity sensors would help better predict heat flow patterns as input for modelling purposes
- The largest temperature gradient through the wall/slab depth occurs at the first 250-300 mm from the surface so installing temperature probes in this region would more accurately capture the gradient
- The effects of the cast-in place concrete stresses and deformation and creep and shrinkage of the concrete will affect the subsequent stress state of the tunnel under ambient temperature loading. These factors should be quantified
- Also, since the initial state/condition of the structure affects the proceeded thermal response, use the temperature sensors to capture the heat of hydration effects

Following are recommendations for future work:

- Consider three dimensional heat flow studies in order to model longitudinal temperature distribution in tunnel. This would require accurate knowledge of wind speed conditions

along with the solar radiation input to accurately model the thermal environment. Once an accurate 3D temperature distribution time history is obtained, the displacements at movement and construction joint locations could be evaluated. A study on how the longitudinal distance between joints affects the displacements could also be performed

- Consider how construction sequence and methods affect the structural response due to ambient temperature loading. For instance, what would the effect of creep and differential shrinkage, early cracking due to heat of hydration, and initial cracks in the structure on the thermal response
- Study the effect of soil interaction and structure foundation type on the thermal response. This could be done by including the foundation i.e. footing, piles, etc.… in the model along with varying the soil conditions
- Further studies are required in order to establish a framework of guidelines for a generalized tunnel in regards to temperature load. Using similar methodology presented in this thesis, several variables can be investigated to determine their effects on temperature distribution and effects. These variables include tunnel geometry, portal orientation (in relation to the position of the sun), tunnel material, foundation type, and movement/construction joint locations.

References

Lai, Jinxing. 2012. "Experimental Study on Air Temperature Field for Cold-Region Tunnel in Qinghai-Tibet Plateau: A Case Study." *G. Lee (Ed.): Advances in Computational Environment Science, AISC 142*, p.265-271.

Li, Wenbo, Yimin Wu, Helin Fu, and Jiabing Zhang. 2015. "Long-Term Continuous in-Situ Monitoring of Tunnel Lining Surface Temperature in Cold Region and its Application." *International Journal of Heat and Technology* Vol.33 (No.2), p.39-44.

Mi, Junfeng, He Song, and Chaoliang Ye. 2014. "The Analysis of Temperature Field Distribution in Houanshan Tunnel."International Conference on Civil Engineering, Energy and Environment

Ding, You-liang and Gao-xin Wang. 2013. "Estimating Extreme Temperature Differences in Steel Box Girder using Long-Term Measurement Data ." p.2537-2545.

Elbadry, Mamdouh M. and Amin Ghali. 1983. "Temperature Variations in Concrete Bridges ." *Journal of Structural Engineering* Vol.109 (No.10), p.2355-2374.

El-Metwally, Salah E., Hamed S. Askar, Ahmed M. Yousef, and Essam H. El-Tayeb. 2015. "Analysis of RC Flat Slab System for Thermal Loads ." *International Journal of Engineering and Innovative Technology (IJEIT)* Vol.4 (No.12), p.62-73.

Larsson, Carl and Gustav Svensson. 2013. "Realistic Modeling of Thermal Effects in Concrete Bridges." Masters, Lunds Universitet.

Prasanna, W. G. J. and A. P. Subhashini. 2010. "Cracking due to Temperature Gradient in Concrete ." Kandy, Sri Lanka, International Conference on Sustainable Built Environment, 13-14 December 2010.

Priestley, M. J. Nigel. 1978. "Design of Concrete Bridges for Temperature Gradients ." *ACI Journal*, p.209-217.

Priestley, M. J. Nigel. 1984. "Long Term Observations of Concrete Structures: Analysis of Temperature Gradient Effects ." *Matériaux Et Constructions* Vol.18 (No.106), p.309-316.

Roberts-Wollman, Carin L., John E. Breen, and Jason Cawrse. 2002. "Measurements of Thermal Gradients and their Effects on Segmental Concrete Bridge ." *Journal of Bridge Engineering* Vol.7 (No.3), p.166-174.

Saetta, Anna, Roberto Scotta, and Renato Vitaliani. 1995. "Stress Analysis of Concrete Structures Subjected to Variable Thermal Loads ." *Journal of Structural Engineering* Vol.121 (No.3): p.446-457.

Thurston, S. J., M. J. Nigel Priestley, and N. Cooke. 1980. "Thermal Analysis of Thick Concrete Sections ." *ACI Journal*, p.347-356.

Tong, M., L. G. Tham, F. T. K. Au, and P. K. K. Lee. 2001. "Numerical modelling for temperature distribution in steel bridges" *Computers and Structures 79*, p.583-593.

Vecchio, F. J., N. Agostino, and B. Angelakos. 1993. "Reinforced Concrete Slabs Subjected to Thermal Load ." *Canadian Journal of Civil Engineering 20*, p.741-753.

Vecchio, F. J. and J. A. Sato. 1990. "Thermal Gradient Effects in Reinforced Concrete Frame Structures ." *ACI Structural Journal* Vol.87 (No.3), p.262-275.

Léger, P., J. Venturelli, and S. S. Bhattacharjee. 1993. "Seasonal Temperature and Stress Distributions in Concrete Gravity Dams. Part 1: Modelling." *Canadian Journal of Civil Engineering* Vol.20, p. 999-1017.

Léger, P., J. Venturelli, and S. S. Bhattacharjee. 1993. "Seasonal Temperature and Stress Distributions in Concrete Gravity Dams. Part 2: Behaviour." *Canadian Journal of Civil Engineering* Vol.20, p.1018-1029.

Nofziger, D. L. 2003. "Soil Temperature Variations with Time and Depth." http://soilphysics.okstate.edu/software/SoilTemperature/document.pdf. (Accessed July 22, 2016).

Toogood, J. A. 1976. "Deep Soil Temperature at Edmonton." *Canadian Journal of Soil Science* Vol.56, p.505-506.

Hyeong, Jun Kim. 2007. "Thermal Effects on Modular Maglev Steel Guideways." Doctor of Philosophy, University of Texas at Austin.

Steinemann, U., F. Zumsteg, and P. Wildi. 2004. "Measurements of Air Flow, Temperature Differences and Pressure Differences in Road Tunnels." Graz, Austria, International Conference Tunnel Safety and Ventilation

Emerson, M. 1976. *Extreme Values of Bridge Temperatures for Bridge Design Purposes*. Road Research Laboratory Crowthorne, England, TRRL Report 744.

Radolli, M., and Green, R. 1975. *"Thermal Stresses in Concrete Bridge Superstructures Under Summer Conditions."* TRB, Transportation Research Record 547.

Emanuel, J.H., and Hulsey, J.L. 1978. "*Temperature Distributions in Composite Bridges"*, ASCE Journal of Structural Engineering, Vol. 104, No. STI, January, pp. 65–78.

Bosshart, H. 1970. "*Temperaturspannungen in Spannbetonbrucken.*" Symposium, Design of Concrete Structures for Creep, Shrinkage and Temperature Changes, International Association for Bridge and Structural Engineering, Vol. 6, Zurich, Switzerland, pp. 73–80.

Ostapenko, A. 1976. "*Rio-Niteroi Bridge: Thermal Field Studies.*" TRB, Transportation Research Record 607.

Al-Hussein, Mohamed, J. J. Roger Cheng, Mark Ackerman, Mustafa Gul, Haitao Yu, Hamid Zaman, Gurjeet Singh, Rupak Mutsuddy, and Ahmed Alrifai. 2012. *Evaluation of Energy Efficient Wall Systems for Mid-Rise Wood Frame Buildings*. University of Alberta.

Ghali, Amin, Adam Neville, and Tom G. Brown. 2009. *Structural Analysis. A Unified Classical and Matrix Approach*. 6th edition ed. New York, NY: Taylor & Francis.

Fu, Feng. 2015. *Advanced Modelling Techniques in Structural Design*. United Kingdom: John Wiley & Sons, Ltd.

Lee, Yun, Myoung-Sung Choi, Seong-Tae Yi, and Jin-Keun Kim. 2009. "Experimental Study on the Convective Heat Transfer Coefficient of Early-Age Concrete." *Cement & Concrete Composites* Vol. 31: p. 60-71.

Azarnejad, Azita, Andrew Boucher, and Joost Bolderheji. "Calgary Airport Trail Tunnel." Winnipeg, Manitoba, Annual Conference of the Transportation Association of Canada, 2013.

Dassault Systèmes Simulia Corp. “Abaqus 6.13 User’s Manual”

Fraunhofer-Gesellschaft. “WUFI-Pro 5.3 User’s Manual”

Canadian Highway Bridge Design Code (CHBDC) CAN/CSA S6-14. December 2014

Canadian Highway Bridge Design Code (CHBDC) CAN/CSA S6-06. October 2011

Commentary on Canadian Highway Bridge Design Code (CHBDC) CAN/CSA S6-14. December 2014

Commentary on Canadian Highway Bridge Design Code (CHBDC) CAN/CSA S6-06. October 2011

AASHTO LRFD Bridge Design Specifications. Sixth Edition. 2012

EN 1991-1-5 (2003) (English): Eurocode 1: Actions on structures - Part 1-5: General actions - Thermal actions [Authority: The European Union Per Regulation 305/2011, Directive 98/34/EC, Directive 2004/18/EC]

American Concrete Institute (ACI) 207.1R-96 Mass Concrete

Technical Manual for Design and Construction of Road Tunnels – Civil Elements. U.S. Department of Transportation Federal Highway Administration. Publication No. FHWA-NHI-10-034. December 2009

Concrete Design Handbook. CSA A23.3-04. Third Edition

Resensys LLC. “SenSpot™ Displacement Meter Data Sheet”

Resensys LLC. “SenSpot™ Humidity/Temperature Data Sheet”

Resensys LLC. “SeniMax™ Data Sheet”

Microchip Technology Inc. “TC1047/TC1047A Precision Temperature-to-Voltage Converter Data Sheet.”

Honeywell International Inc. “Magnetic Displacement Sensors HMC1501/1512 Data Sheet.” Form #900246 Rev C. December 2010

Associate Engineering. 2016. “Calgary International Airport Trail Tunnel Calgary, AB.” https://www.ae.ca/files/splash/2014_yyctunnel.jpg (Accessed August 20, 2016)

Engineering Toolbox. 2016. “Air properties.” http://www.engineeringtoolbox.com/air-properties-d_156.html (Accessed July 14, 2016).

Engineering Toolbox. 2016. “Thermal Conductivity of some common Materials and Gases.” http://www.engineeringtoolbox.com/thermal-conductivity-d_429.html (Accessed July 14, 2016).

Engineering Toolbox. 2016. “Specific Heat Capacity of common Substances.” http://www.engineeringtoolbox.com/specific-heat-capacity-d_391.html (Accessed July 14, 2016).

Engineering Toolbox. 2016. “Concrete Properties.” http://www.engineeringtoolbox.com/concrete-properties-d_1223.html (Accessed July 14, 2016).

Engineering Toolbox. 2016. “Emissivity Coefficients of some common Materials.” http://www.engineeringtoolbox.com/emissivity-coefficients-d_447.html (Accessed July 14, 2016).

Engineering Toolbox. 2016. “Absorbed Solar Radiation.” http://www.engineeringtoolbox.com/solar-radiation-absorbed-materials-d_1568.html (Accessed July 14, 2016)

Infrared Services Inc. 2016. “Emissivity Values for Common Materials.” http://www.infrared-thermography.com/material-1.htm (Accessed July 14, 2016)

CH2M Hill, 2015. “The City of Calgary’s Airport Trail Tunnel and the Calgary Airport Authority’s Runway Projects Win National Engineering Award.” https://www.ch2m.com/newsroom/news/calgary-airport-tunnel-award-of-excellence (Accessed March 3, 2016)

Appendix A: WUFI Pro Model Verification

Introduction to WUFI Pro Software

WUFI Pro is a software used to perform one-dimensional hydrothermal calculations typically on building component cross-sections. Software inputs include built-in moisture, driving rain, solar radiation, long-wave radiation, capillary transport, and condensation (WUFI-Pro 5.3 User's Manual).

WUFI Pro was used to simulate the temperature distribution in the tunnel walls in order to validate the output from the Abaqus model.

Model Steps

The following steps were considered in the WUFI model. The objective of the WUFI model was to valid the Abaqus model. The baseline concrete properties used in the Abaqus model will be input into the WUFI model and the output will be compared.

Geometry

The concrete slab was assigned a 1.25 m thickness. The roof slabs of the tunnel has a fireproof coating however the thickness of these coatings was assumed to be negligible thus not considered in the model. A 1 m thick layer of soil was also considered

Material

Concrete (C35/45) from the WUFI material database was assigned to the wall. A density of 2400 kg/m^3, specific heat of 900 J/kg K, and thermal conductivity of 1.5 W/m K were assigned as the thermal properties of the concrete. For the soil layer, a density of 2000 kg/m^3, specific heat of 1140 J/kg K, and thermal conductivity of 0.75 W/m K were assigned, which were the properties considered in the Abaqus model. Temperature dependency of the properties was neglected.

Grid and Monitoring Positions

A medium mesh grid was assigned to the wall and soil (see Figure A1). Five monitoring positions were assigned that correspond to the nodal temperatures extracted from the Abaqus

model. The soil layer contained monitoring positions at the middle of the layer and exterior surface.

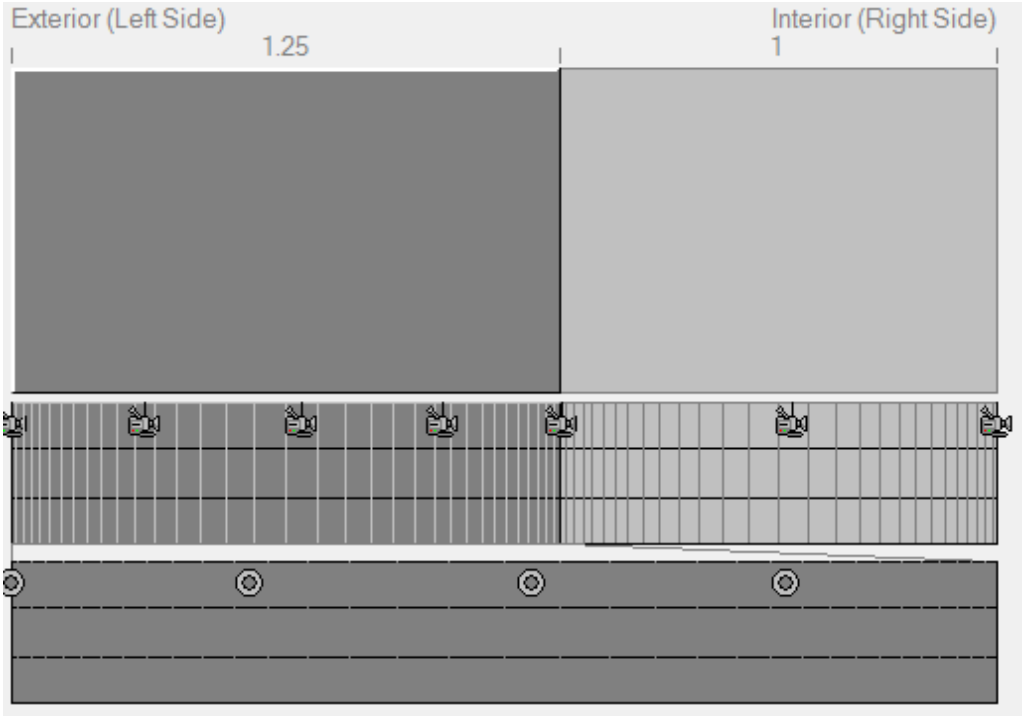

Figure A1. Concrete wall and soil grid and monitoring positions

Initial Conditions

The initial temperature for the component was set to 15 °C however according to literature the initial temperature conditions should not affect the simulation results since the temperature profile adapts to the ambient boundary conditions within a few hours so it is not necessary to specify elaborate initial temperature for long term analysis (Al-Hussein et al., 2012). The moisture (relative humidity) was neglected in the analysis. With the typical conditions in road tunnels, the influence of the relativity humidity to the density of air is less than 1% and not relevant (Steinemann, 2004). The heat resistance of the exterior and interior (dirt) walls were specified as 0.05 m^2K/W and 0 m^2K/W, respectively. The value for the exterior wall was based on a convection coefficient of 20 W/m^2K on the surface and the interior wall value represents a condition of zero heat flux. The effect of solar radiation and long wave radiation were not considered for the validation.

Surface/Climate Input

For the exterior wall, the exterior surface was assigned the Environment Canada temperature record at CIA for year 2014. In the analysis only the temperature record from September 1, 2014 to January 1, 2015 was considered (see Figure A2). The interior surface (or dirt surface) was assigned a constant temperature of 7.5°C (see Figure A3). Note that a time lag on the interior surface temperature was not considered.

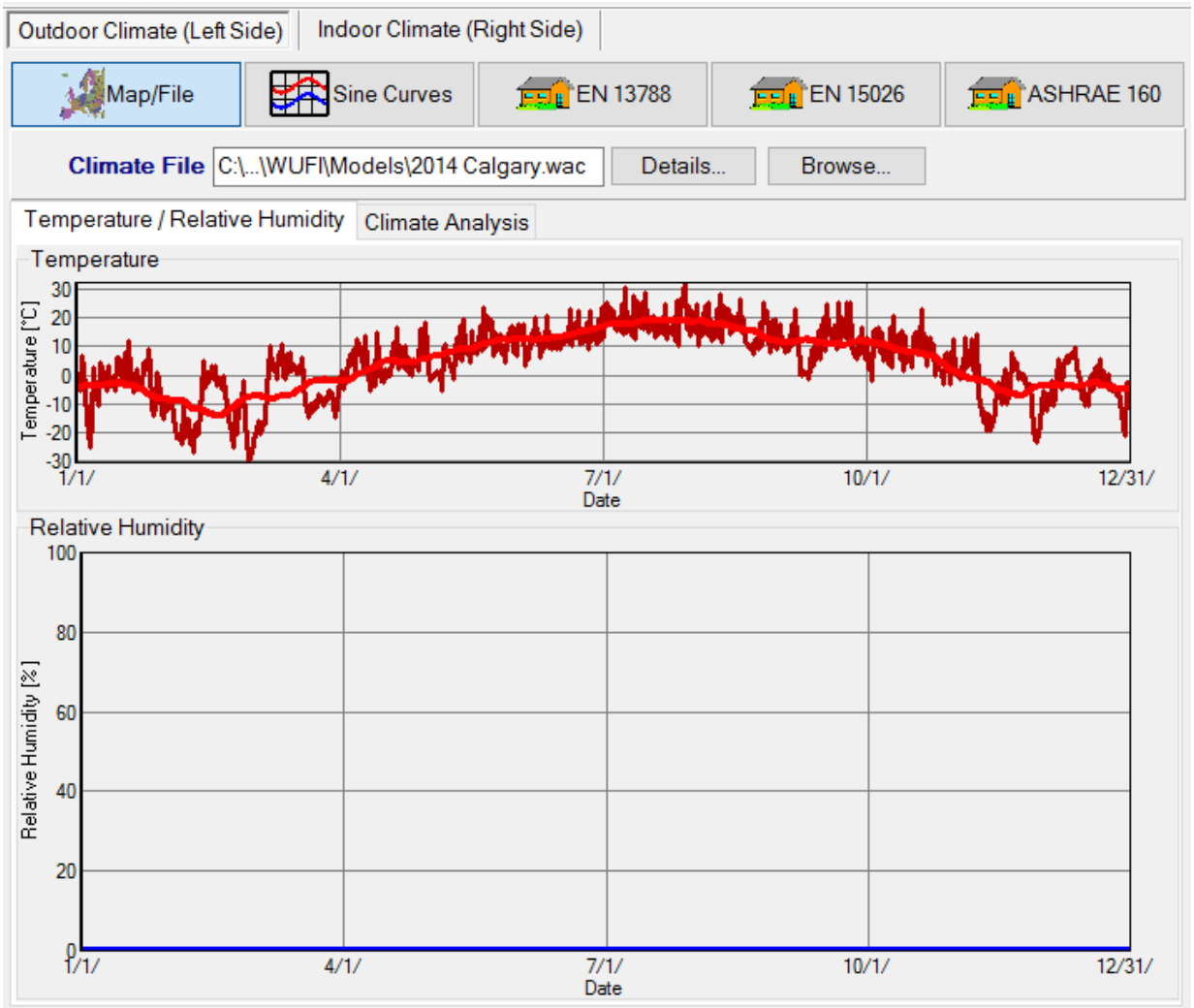

Figure A2. Exterior wall climate

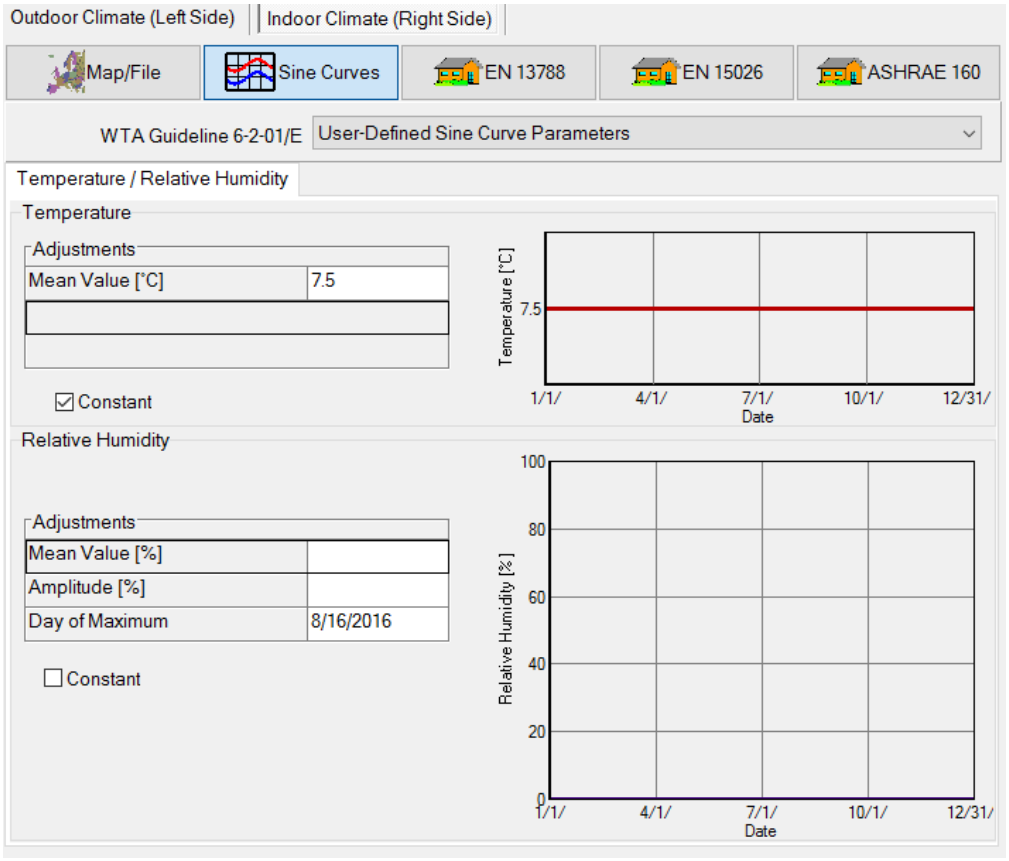

Figure A3. Interior wall climate

Computational Parameters

The calculation period was set to 2929 hours to match the time period of the data set and the mode of calculation was limited to heat transport (i.e. moisture transport was neglected).

Film Simulations and Wall Temperature

See Figure A4 and Figure A5 for the temperature film simulation results as well as the temperature records from WUFI, respectively.

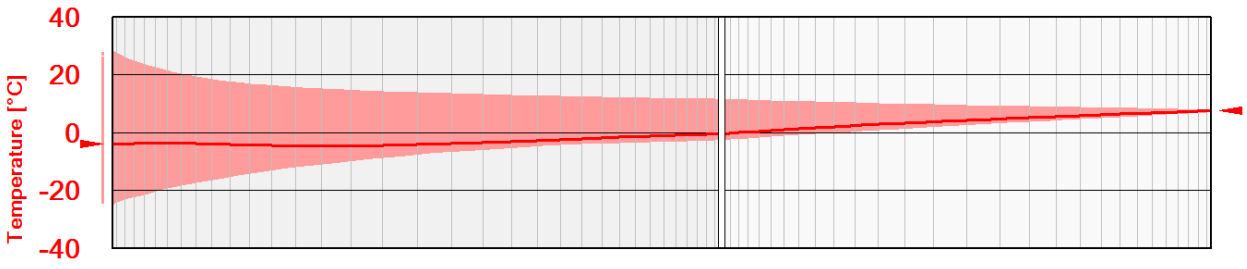

Figure A4. Temperature Film Simulation Results for Roof Slab

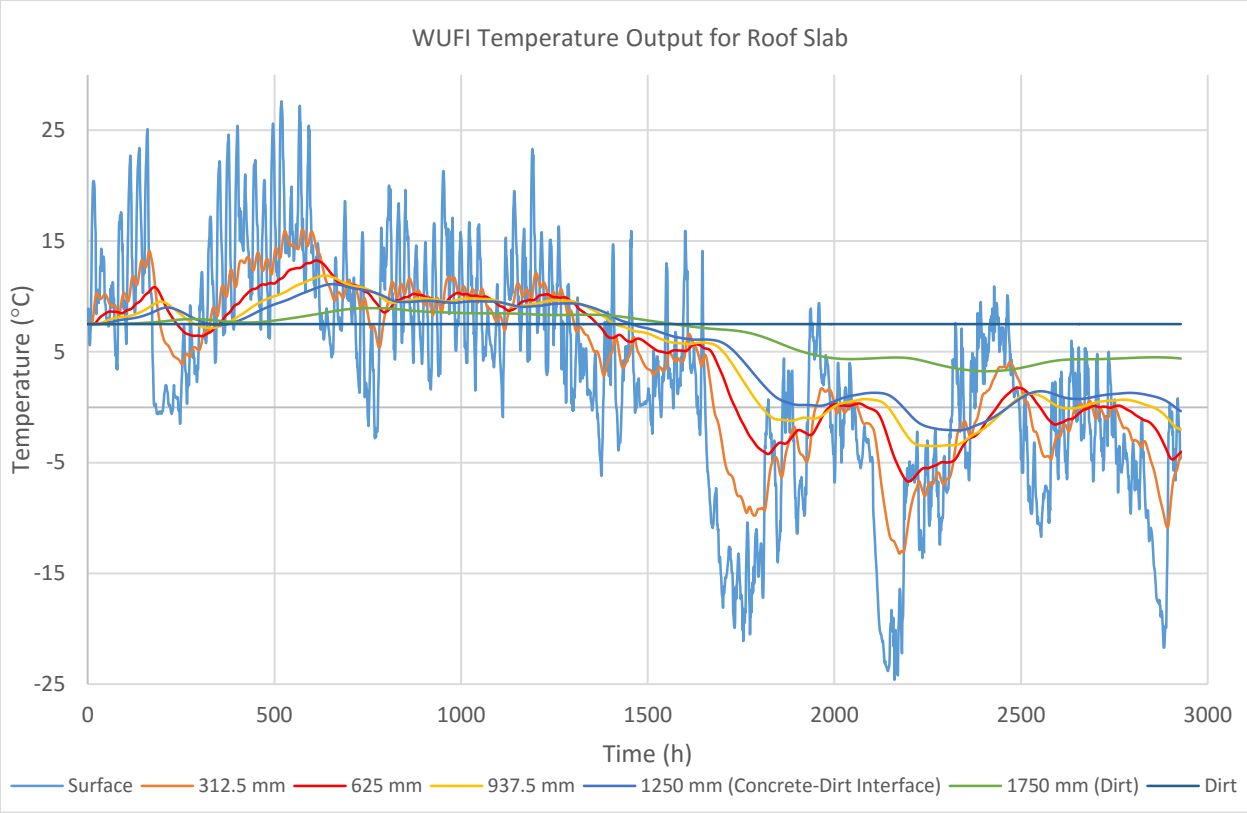

Figure A5. Roof Slab Temperature Distribution Output

Discussions

The film simulation in WUFI illustrated the heat distribution through the slab over time. For the exterior slab, the temperature fluctuations were higher at the interior surface than the dirt surface as expected. Due the low thermal conductivity of the concrete it was expected that the surface would be more affected by diurnal variations in temperature compared to the mid-wall region. From the film simulation, it could be observed that the diurnal variations would have an effect on the concrete wall to a depth approximately 0.3 m from the surface. In addition, note that the temperature distribution was non-linear which was expected for a concrete wall.

The film simulation could be used to determine the maximum temperature gradient in the wall by determining the maximum difference at any given instance in time. The enveloped temperatures as displayed in Figure A4 could be used to determine the gradient however the approach may be too conservative as time is ignored. The gradients obtained could then be compared to current design codes.

The temperature records outputted from WUFI in Figure A5 can be compared to the Abaqus model for the baseline case. The temperature difference between the WUFI and Abaqus model are displayed in Figure A6 with convection neglected. The results are comparable and within reason. The largest discrepancy were in surface temperature with a maximum absolute difference of 1.3°C. In Figure A6, differences between models are compared when the convective boundary condition is added to the models. There are slightly higher discrepancies in temperature most noticeable at the surface with temperature differences up to 2.5°C, however, still within reason. Overall, discrepancies can be accredited to varying model input method and numerical analysis techniques in each software.

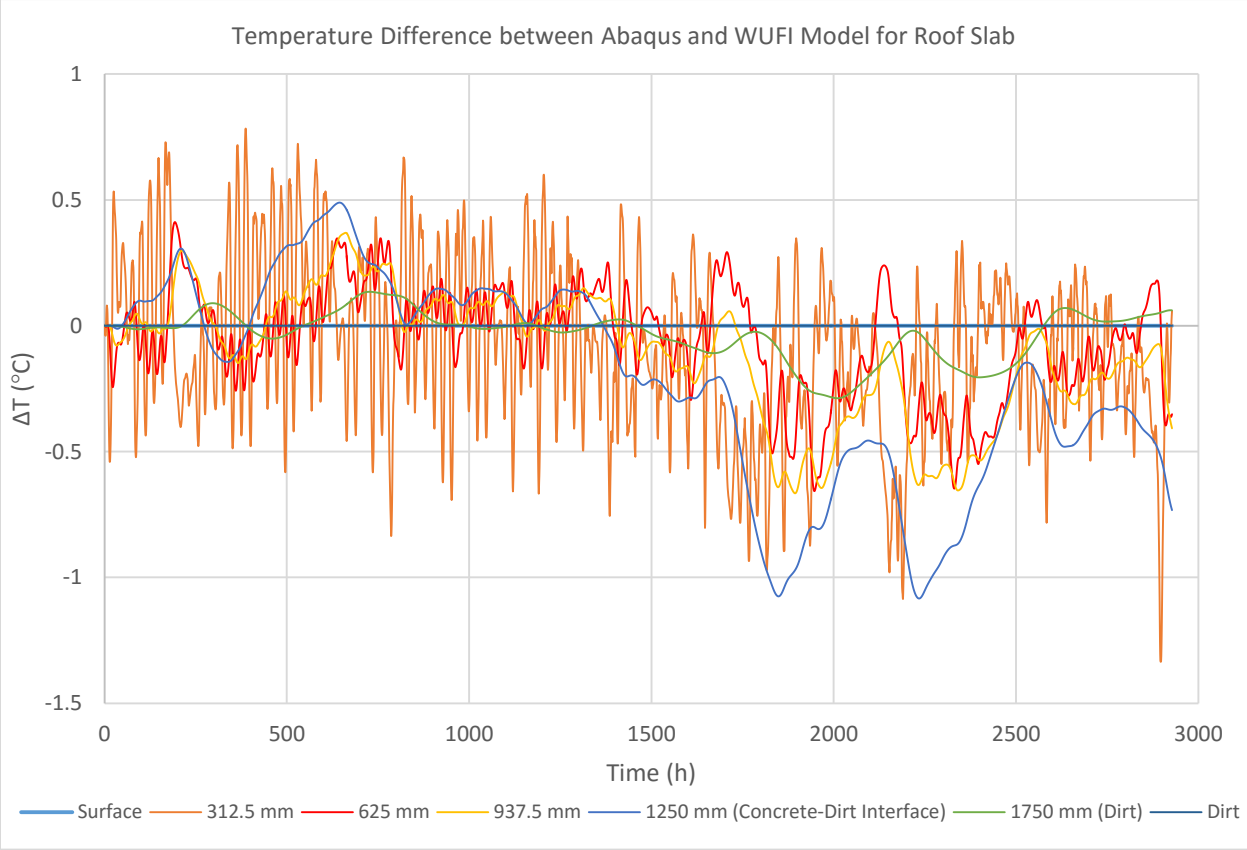

Figure A6. Temperature difference between WUFI and Abaqus model for roof slab

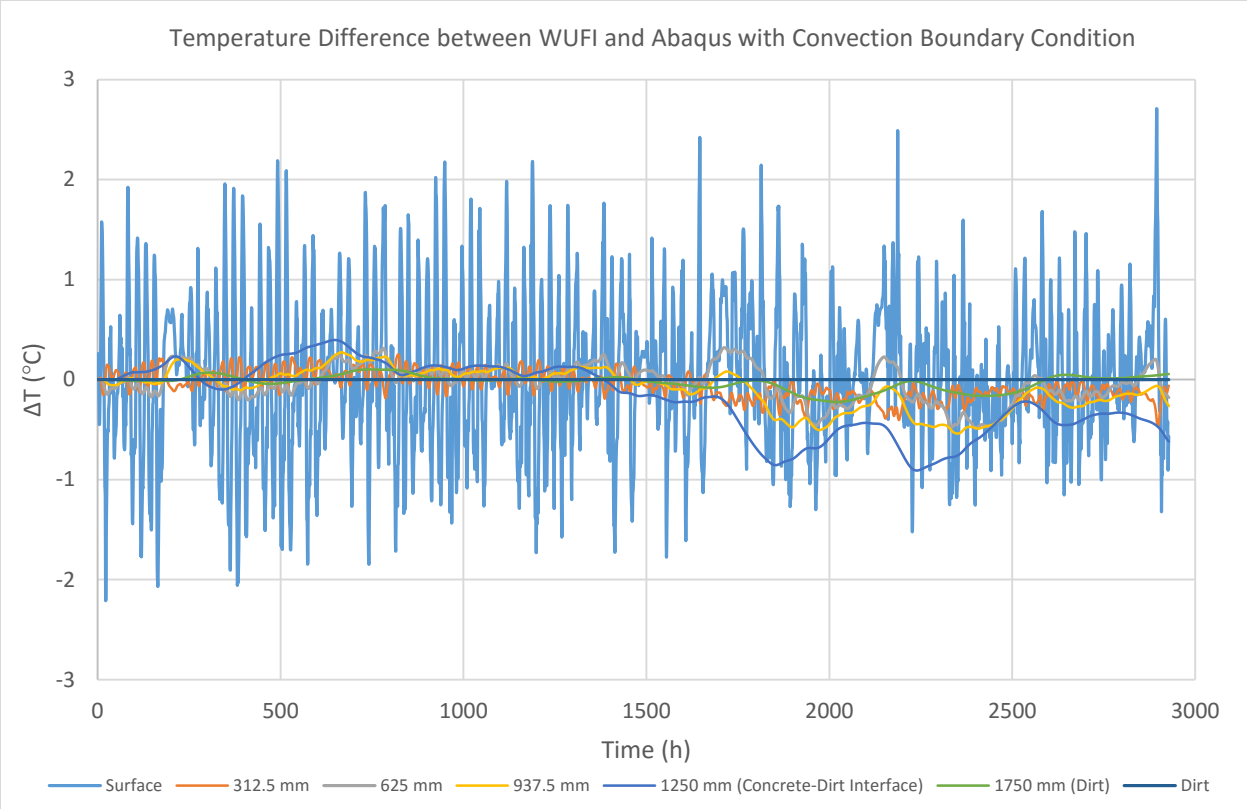

Figure A7. Temperature difference between WUFI and Abaqus models for roof slab with convection boundary condition